Bifurcation Analysis of Homogeneous-Heterogeneous Combustion

A Dissertation

Presented to

the Faculty of the Department of Chemical and Biomolecular Engineering

University of Houston

In Partial Fulfillment

of the Requirements for the Degree

Doctor of Philosophy

in Chemical Engineering

by

Imran Alam

August 2016

Bifurcation Analysis of Homogeneous-Heterogeneous Combustion

Imran Alam

Approved:

Chair of the Committee
Vemuri Balakotaiah, Professor,
Chemical and Biomolecular Engineering
University of Houston

Committee Members:

Dan Luss, Professor,
Chemical and Biomolecular Engineering,
University of Houston

Giles Auchmuty, Professor,
Mathematics,
University of Houston

Lars Grabow, Assistant Professor,
Chemical and Biomolecular Engineering,
University of Houston

Igor Schreiber, Professor,
Chemical Engineering,
University of Chemistry and Technology,
Prague, Czech Republic

Suresh Khator, Associate Dean,
Cullen College of Engineering

Michael P. Harold, Professor and Chair,
Chemical and Biomolecular Engineering

Acknowledgement

First and foremost, I want to express my deep gratitude to my advisor Professor Vemuri Balakotaiah for years of support and guidance. Prof. Balakotaiah helped me tremendously with almost every part of this work. He was always very generous with his time, and I learnt a lot during my innumerable discussions with him. The courses he taught were very well-organized and proved quite useful for my research. I am also grateful to David West of SABIC Global Technologies for starting this project, giving me the opportunity to contribute to it and for offering his wise insights. With his fresh perspectives tempered by years of industrial experience and his ability to see the big picture, he helped make this research more practically relevant.

I am thankful to the committee members, Dr. Dan Luss and Dr. Lars Grabow for many discussions and comments throughout the course of this work. My debt to Dr. Grabow goes beyond academic matters. I was influenced by his unassuming and considerate character and his excellent communication skills. I am very thankful to Professors Igor Schreiber and Giles Auchmuty, for taking the time off their busy schedule to read my thesis and offer valuable comments. I would like to acknowledge SABIC Global Technologies for the financial support. I am also thankful to the Graduate Coordinator, Miranda Vernon-Harrison, the staff of the Department of Chemical and Biomolecular Engineering, especially My-Dung Lieu, Nicolette Solano, Patricia Cooks, Pamela Moses and Yolanda Thomas for their tireless administrative help.

I want to thank all my past and present teachers and colleagues for their help and support. I am especially thankful to Tian Gu for our many interesting conversations over lunch and coffee. I am thankful to Zhe Sun for sharing an office with me and Rama

Krishna Dadi for being my housemate for a year. I thank them both for our many walks. I would also like to thank senior members of the lab: Bijesh Shakya who helped me tremendously when I was starting as a graduate student, Arun Kota for his friendship and much help with day to day matters and Ram Ratnakar who gave me a lot of advice throughout my stay in Houston. Saurabh Joshi and Santhosh Gundlapally were invaluable during my job search. I also appreciate my time with co-workers Richa Raj, Priyank Maheshwari and Wei-Lun Ting.

My time at Houston during this work became much more enjoyable because of friends. I would like to acknowledge Joe Berg, Hoang Nguyen, Sophia Thang, Ngozi Onwuama, Angelynn Alvarez and Aliece Porterfield. Especially I want to thank my best friend Vatsal Dwivedi for our many long conversations, mostly over phone, the subjects of which ran the gamut from the technical to the philosophical. Many teachers helped infuse me with a scientific temper and therefore, I will restrict myself here to only a few. I want to thank Dr. David Blecher and Dr. William Ott of the math department at UH for their excellent courses. The way they made me feel welcome in their courses and the patience with which they answered all my questions helped deepen my interest in mathematics. I am very grateful to Professor A. R. Roy of the Mathematics department at IIT Kharagpur for igniting my appreciation of mathematics that continues to enhance the quality of my life.

Finally, I want to express my love and gratitude to my parents, brother and sister for their constant support and encouragement.

Bifurcation Analysis of Homogeneous-Heterogeneous Combustion

An Abstract

of a

Dissertation

Presented to

the Faculty of the Department of Chemical and Biomolecular Engineering

University of Houston

In Partial Fulfillment

of the Requirements for the Degree

Doctor of Philosophy

in Chemical Engineering

by

Imran Alam

August 2016

Abstract

We present theory and comprehensive bifurcation analysis of thermally coupled homogeneous-heterogeneous combustion of propane and methane in short monolith, fibermat or gauze type reactors with a focus on the dependence of the ignition, extinction, hysteresis, double and boundary limit loci on the various design and operating parameters. We analyze the impact of inlet fuel mole fraction, inlet temperature, residence time and channel hydraulic radius on the relative position of the homogeneous and catalytic ignition and extinction points and identify the parameter regions in which either catalytic or homogeneous reaction dominates. We also identify the regions in which catalytic ignition leads either to an intermediate branch on which the homogeneous reaction rate is negligible or directly to a high conversion and temperature state thereby facilitating homogeneous ignition. For the case of methane oxidation, we examine both the lean and rich feeds with the operating pressure as the bifurcation variable and compare the predicted results with available experimental data and numerical simulations using detailed CFD models.

We then study the impact of the Lewis number, Le_f (thermal diffusivity of the reaction mixture to the molecular diffusivity of the limiting reactant) and the Peclet numbers on the maximum temperature attained for coupled homogeneous-heterogeneous combustion process in a parallel plate reactor using one, two and three-dimensional models. For the case of 1-D models, we find that the maximum temperature never exceeds the adiabatic value for physically consistent boundary conditions. For 2-D models, we find that for Le_f<1, the hot spot temperature can exceed the adiabatic value, it is always located on the wall and its distance from the inlet and magnitude increase with

increasing radial Peclet number. However, for Le_f>1, contrary to some literature claims, the peak temperature never exceeds the adiabatic value, though the temperature can be non-monotontic across the channel. We show that 3-D solutions can bifurcate either from 1-D or 2-D solutions irrespective of the value of the Lewis number. The implications of these observations for catalyst and process design in systems in which both homogeneous and catalytic reactions occur are discussed.

Table of Contents

List of Figures

List of Tables

Chapter 1

Introduction

1.1 Introduction and literature review:

Catalytic partial (complete) oxidation of hydrocarbons is of interest for the production of intermediate chemicals (power generation). In recent years, processes such as production of syngas from methane partial oxidation, oxidative dehydrogenation of ethane, and the conversion of methane to C_2^+ hydrocarbons have been perceived as attractive alternatives for basic chemical production (for example see [1-4]). Complete oxidation (combustion) of hydrocarbons with low emissions of NO_x and other pollutants is also of interest in power generation. However, the high operating temperatures, short residence times and highly exothermic nature of the oxidation processes pose a formidable engineering challenge, and without appropriate theoretical understanding, undesirable situations like runaways and side reactions might undermine the purpose of operation. Models describing these systems typically involve both catalytic and homogeneous reactions. These models must account for the effects of transport processes as well as the complex chemistry in an idealized manner in order to be amenable to theoretical and computational analysis while avoiding too much simplification. An article by Pfefferle [5] reviews the various models and parameter ranges

in which they are valid for such systems. It is well-known that catalytic reaction systems exhibit complex behavior such as multiple steady states and hysteresis. It is therefore intuitively obvious that the coupling between catalytic and homogeneous chemistry should lead to even more complicated behavior. A comprehensive analysis of this system requires study of observables like solid/gas temperatures or conversion of reactants (or yield of intermediate products) with respect to changes in the system parameters such as inlet mole fraction of fuel, operating pressure, space/inlet velocity, diameter of the monolith channel and so forth.

Because of its obvious industrial relevance, there have been numerous experimental and computational studies on homogeneous-heterogeneous combustion in the past three decades. The work of Song et al. ([6], [7] and [8]) analyzed a stagnation flow model using the methods of singularity theory. Later work of Vlachos et al. [9] used more detailed microkinetic models to understand homogeneous combustion near isothermal and adiabatic surfaces. There has also been a large amount of work using computational fluid dynamic (CFD) models to study catalytic combustion ([10-11]). Deutschmann et al. [12] investigated 1-D CFD models to understand transitions from catalytic to homogeneous combustion of propane on Pt foils using detailed homogeneous-heterogeneous chemistry. Later work of Deutschmann and coworkers ([13-14]) addressed catalytic combustion and partial oxidation of methane with 2-D and 3-D models. These papers also discuss the dependence of light-off behavior on system parameters. Karagiannidis et al. [15, 16] use 2-D CFD simulations in a plane channel reactor and obtain combustion stability diagrams for propane and methane microreactors with more detailed chemistry. Pizza et al. [17, 18] studied

flame dynamics in fuel-lean hydrogen/air flames and studied the effect of heterogeneous reactions on the suppression of the combustion instabilities. Stefanidis and Vlachos [19] solve 2-D CFD models for propane oxidation taking heat losses into account with global chemistry. They analyze the interplay between catalytic and homogeneous chemistry by describing how a catalyst-induced gas phase stabilization results at high inlet velocities due to synergistic thermal effects between the phases. The work of Chattopadhyay and Veser [20] studied heterogeneous-homogeneous interactions in Pt-coated microchannels with detailed surface and gas chemistries using a 2-D boundary layer model and investigated ignition behavior. These approaches, however, do not provide an exhaustive picture of the different possible bifurcation behaviors in the multi-dimensional parameter space. CFD models are not convenient for bifurcation analysis and detailed exploration of the parameter space but are useful to study specific types of solutions or reactor systems in more detail. Microkinetic modeling of a combustion system can involve hundreds of reactions making computation of bifurcations or high order singularities very challenging. This subverts their practicability in providing a detailed understanding of the system in the multi-dimensional parameter space. The work of Song et al. [6-8] studies bifurcations with global reaction kinetics, but the stagnation flow system used in their work is not realistic for industrial settings. In the present thesis, we circumvent this by basing our studies on practical models that describe short monolith, fibermat or gauze type reactors where flow is parallel to the catalyst surfaces.

1.2 Bifurcation Analysis on Chemically Reacting Systems

Bifurcation studies in Chemical Reaction Engineering can be traced back to the papers of Van Heerden (1953) and Bilous and Amundson (1955). A substantially large literature on bifurcations in Chemical Engineering has subsequently accumulated. A wide range of interesting behaviors such as multiple steady states, oscillations and chaos have been studied both theoretically and experimentally. Several books as well as review articles have summarized these developments. We list a few of these here, noting that the literature is too vast to mention all such works here and omissions are inevitable. Aris (1975), Schmitz (1975), Hlaváček (1986) and Luss (1985) are important works we found useful. The reactors most commonly studied in these works are the CSTR (the seminal paper Uppal, Ray and Poore, 1974, many articles of Balakotaiah and Luss, especially Balakotaiah and Luss, 1983, 1984, 1985, Farr, et al., 1986) and the tubular reactor (several papers of Amundson and coworkers and of Hlavacek and coworkers; the important article of Jensen and Ray, 1982). In addition, in the Chemistry and Biochemistry literatures, the Brusselator system has been extensively studied. The classic textbook by Nicolis and Prigogine (1977) which discusses this system, among other interesting phenomena, has been cited more than 8000 times. The numerical techniques pertinent to bifurcation calculations have been discussed in many excellent articles and books, some of them written by Chemical Engineers (e.g. the books of Kubíček and Marek (2012) and Marek and Schreiber

(1995)) aside from many books written for the mathematical audience (e.g. the book of Allgower and Georg (2012)).

There is considerable interest in understanding bifurcation phenomena because it answers important questions like how many solutions (or steady-states) exist in different operating regions, and how the system behaves with changes in various parameters. A recent review article [Balakotaiah and West, 2014] presents a good survey of the state of the art in this field. The alternatives to the bifurcation approach to modeling and simulation are large-scale numerical computation for the entire system and asymptotic analysis. In contrast to full numerical study and asymptotics, a bifurcation study helps provide insights about the physics by classifying the parameter space into different regions and aids further numerical explorations; however a purely numerical approach without theoretical guidance usually fails to provide much insight for complex systems. The singularity theory approach that we employ in this thesis derives its power from being able to give global information about the system from a local analysis because of the use of a very powerful theory of unfolding of singularities and construction of phase diagrams in the space of design or operating parameters.

Thus this thesis aims to study the bifurcation behavior of models that combine the thermal coupling between the catalytic and homogeneous reactions. This problem has been known to be of great practical importance for quite some time but is not yet well-studied. A clear picture of essential features of the process as the parameters are changed is still not available. One major goal of this thesis is to determine an approximate phase diagram of the thermally coupled combustion process in the space of various design and operating parameters (e.g. inlet fuel mole fraction, inlet tem-

perature, channel dimensions, operating pressure and space velocity). Even coarse phase diagrams that identify the parameter regions in which either the homogeneous or catalytic reaction dominates can provide not only physical insight but are also useful in designing laboratory scale experiments that may lead to a better understanding of the interactions between catalytic and homogeneous chemistry during the oxidation of hydrocarbons. There is an obvious trade-off in how detailed a model one wants to analyze and how fully one can analyze it with existing mathematical and computational prowess. If an understanding of essential features is desired, then we believe that a deep understanding of relatively simple systems, like the ones studied in the present work, can go a long way.

1.3 Homogeneous-Heterogeneous Reaction Systems

The term homogeneous-heterogeneous reaction systems is used to mean that catalytic and homogeneous reactions occur in tandem in the system. This is not unique to combustion, but can be widely observed in many other practically relevant systems. Important examples are catalysis (e.g. gasification of coal) and microelectronics (e.g. chemical vapor decomposition) besides catalytic partial oxidation and catalytic combustion. Homogeneous-heterogeneous systems are often very nonlinear and it is challenging to design these processes. The optimization of these processes depends on choosing various operating and design parameters in appropriate ranges, as the process behavior can be very drastically different depending on the choices of these parameters owing to the nonlinearities. This also makes the control of these systems a complex problem. Bifurcation analysis proves indispensable before tackling these

engineering challenges. When aided with experiments, bifurcation analysis can be useful for fitting kinetic parameters (e.g. Harold and Luss 1987) and this is especially relevant for systems such as catalytic partial oxidations where appropriate reaction kinetics for modeling amenable for engineering is still uncertain. In fact, bifurcation analysis can serve as the essential first step to design appropriate experiments for such systems.

Amundson and coworkers analyzed bifurcation features for combustion of carbon utilizing a boundary layer model in several papers in the early 1980s (e.g. Sotirchos and Amundson, 1984 a, b). The existence of several steady states was established and the stability of these steady states was investigated for the aforementioned system. Homogeneous-Heterogeneous reaction systems were studied by Nielson and Villadsen (1985) for a falling film where absorption followed by catalytic reaction occurs alongside homogeneous reactions. Later work of Song et al (1991 a, b, c) used Singularity theory methods to study bifurcations in homogeneous-heterogeneous combustion of hydrocarbons, but their attention was restricted to stagnation flow type systems.

To our knowledge, no comprehensive bifurcation studies have been performed even for the simplest homogeneous-heterogeneous systems. Systematic studies of high-dimensional singularities are almost non-existent. This gap in the literature can be attributed to the difficulties arising from strong nonlinearity and multiple parameters in the system. Such systems have more than one phase and the transport processes are coupled with both homogeneous and catalytic reactions which makes the modeling complicated. A further issue is the lack of kinetic data amenable to bifurcation analysis. Although recent microkinetic models for both catalytic and homogeneous

reaction systems have been proposed using a variety of theoretical and experimental techniques, a large number (several hundreds) of microkinetic steps alongside strong thermal nonlinearities is quite complicated for detailed bifurcation analysis, especially when the bifurcation behavior for much simpler systems is also not clearly understood.

The present thesis is structured as follows. We first give details of the development of models that incorporate essential physics and chemistry, are structurally stable (i.e. robust to perturbations) and are well-suited for bifurcation analysis. Next, we consider propane oxidation with stoichiometric feed and investigate the possible bifurcation phenomena, presenting a complete bifurcation analysis in short monolith or gauze type reactors, illustrating the impact of inlet fuel mole fraction, residence time and channel hydraulic diameter on the various ignitions and extinctions. The important practical case of methane oxidation is also examined for the case of both lean and rich feeds with the operating pressure as the bifurcation variable and the predicted results are compared with available results in the literature. We then proceed to address questions on the presence of hot spots in these reacting systems and the formation of transport limited patterns in the following two chapters. We also show the derivation of low-dimensional reactor models that are useful for bifurcation analysis using Liapunov-Schmidt reduction and singular perturbation theory. In the last chapter, we summarize the results and conclude by pointing out some possible extensions to this work.

Chapter 2

Mathematical Models

2.1 Introduction

In order to describe the family of useful models and how they are related to each other, we start with a 2-D model valid for reactors with a single homogeneous and catalytic reactions. We denote the fluid phase cup-mixing mole fraction of the j-th species by y_j and the temperature by T. Two reactants A and B representing the fuel and oxygen, respectively have been considered.

In the following, we outline the mathematical model for a system consisting of flow between parallel plate reactors in which homogeneous reaction occurs in the fluid phase and the catalytic reaction on the wall. For simplicity, we have assumed that the velocity profile does not change with axial position and the pressure drop is negligible. (However the dependence of the velocity profile on the transverse coordinate is given by the function $\widehat{f}(y')$ multiplying the average velocity $\overline{u}$). Thus we do not need to solve the equations for momentum balance separately. With this assumption, the mathematical model for parallel plates with plate spacing $2a$ is given by

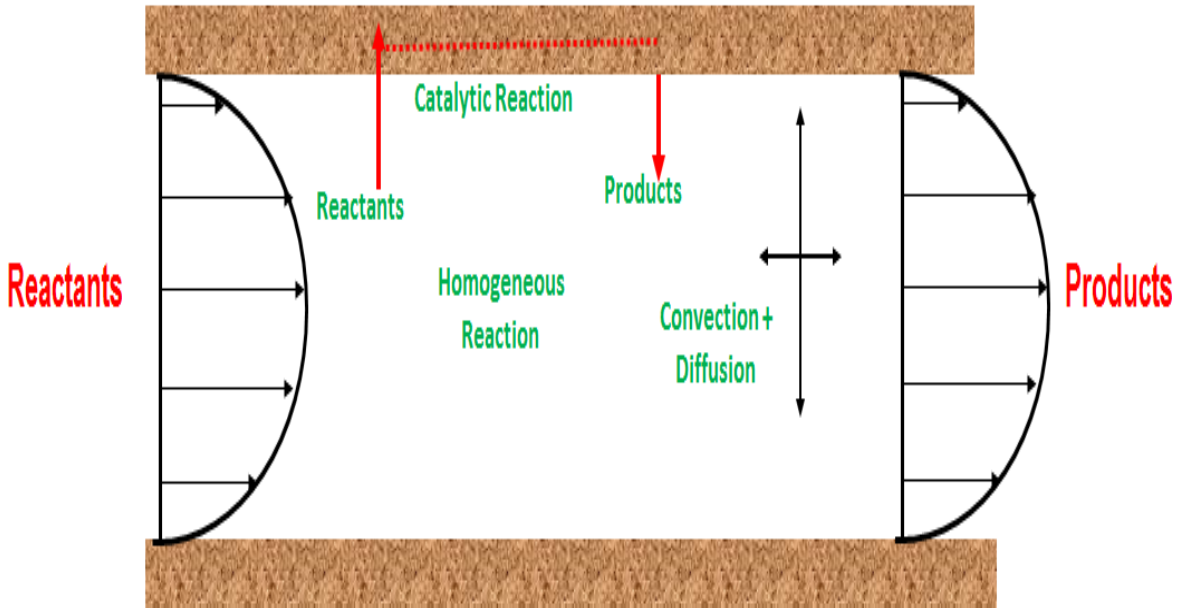

Figure 2-1: Schematic diagram of flow between parallel plates with a homogeneous reaction in the fluid phase and a catalytic reaction on the wall

$$\frac{\overline{u}}{\epsilon_f}\widehat{f}(y')\frac{\partial y_A}{\partial x'} = D_{m,A}\left(\frac{\partial^2 y_A}{\partial x'^2}+\frac{\partial^2 y_A}{\partial y'^2}\right)-\frac{r_h(y_A,y_B,T)}{C_0}, \tag{2.1}$$

$$\frac{\overline{u}}{\epsilon_f}\widehat{f}(y')\frac{\partial y_B}{\partial x'} = D_{m,B}\left(\frac{\partial^2 y_B}{\partial x'^2}+\frac{\partial^2 y_B}{\partial y'^2}\right)-\nu\frac{r_h(y_A,y_B,T)}{C_0} \quad \text{and} \tag{2.2}$$

$$\frac{\overline{u}}{\epsilon_f}\widehat{f}(y')\frac{\partial T}{\partial x'} = \frac{k_f}{\rho_f C_{pf}}\left(\frac{\partial^2 T}{\partial x'^2}+\frac{\partial^2 T}{\partial y'^2}\right)+\frac{(-\Delta H)C_0}{\rho_f C_{pf}}\frac{r_h(y_A,y_B,T)}{C_0} \tag{2.3}$$

$$= \alpha_f\left(\frac{\partial^2 T}{\partial x'^2}+\frac{\partial^2 T}{\partial y'^2}\right)+\Delta T^*_{ad}\frac{r_h(y_A,y_B,T)}{C_0}; \tag{2.4}$$

$$0 < x' < L,\ 0 < y' < a$$

with the inlet and boundary conditions given by

$$D_{m,A}\frac{\partial y_A}{\partial x'} = \frac{\overline{u}}{\epsilon_f}\widehat{f}(y')(y_A - y_{A,in}), \tag{2.5}$$

$$D_{m,B}\frac{\partial y_A}{\partial x'} = \frac{\overline{u}}{\epsilon_f}\widehat{f}(y')(y_A - y_{A,in}) \tag{2.6}$$

$$\alpha_f\frac{\partial T}{\partial x'} = \frac{\overline{u}}{\epsilon_f}\widehat{f}(y')(T - T_{in}) at x' = 0 \tag{2.7}$$

$$\frac{\partial y_A}{\partial x'} = \frac{\partial y_B}{\partial x'} = \frac{\partial T}{\partial x'} = 0 \text{ at } x' = L \tag{2.8}$$

$$-D_{m,A}\frac{\partial y_A}{\partial y'} = 0 \tag{2.9}$$

$$-D_{m,B}\frac{\partial y_B}{\partial y'} = 0 \tag{2.10}$$

$$\alpha_f\frac{\partial T}{\partial y'} = 0 \text{ at } y' = 0 \text{ and} \tag{2.11}$$

$$-D_{m,A}\frac{\partial y_A}{\partial y'} = \frac{r_c(y_A, y_B, T)}{C_0} \tag{2.12}$$

$$-D_{m,B}\frac{\partial y_B}{\partial y'} = \nu\frac{r_c(y_A, y_B, T)}{C_0} \tag{2.13}$$

$$\alpha_f\frac{\partial T}{\partial y'} = \Delta T^*_{ad}\frac{r_c(y_A, y_B, T)}{C_0} \text{ at } y' = a. \tag{2.14}$$

Here, r_c and r_h denote the catalytic and the homogeneous reaction rates, respectively, C_0 is a reference concentration and ΔT^*_{ad} is a reference adiabatic temperature rise corresponding to combustion of 100 mole percent of the fuel. Let us introduce the

following non-dimensional variables and parameters

$$\begin{aligned} x &= \frac{x'}{L},\ y = \frac{y'}{a},\ \theta = \frac{T}{\Delta T^*_{ad}}, \\ \tau &= \frac{L}{\overline{u}},\ f(y) = \widehat{f}(y'/a) \\ Le_f &= \frac{k_f}{\rho_f C_{pf} D_{m,A}},\ Pe_{m,A} = \frac{\overline{u}L}{D_{m,A}},\ \ P_A = \frac{a^2\overline{u}}{D_{m,A}L}, \qquad (2.15) \\ Pe_{m,B} &= \frac{\overline{u}L}{D_{m,B}},\ \ P_B = \frac{a^2\overline{u}}{D_{m,B}L}, Pe_h = \frac{\overline{u}L}{\alpha} \text{ and } P_h = \frac{a^2\overline{u}}{\alpha L} \qquad (2.16) \end{aligned}$$

and express the model in the following dimensionless form:

$$\begin{aligned} f(y)\frac{\partial y_A}{\partial x} &= \epsilon_f \left(\frac{1}{Pe_{m,A}} \frac{\partial^2 y_A}{\partial x^2} + \frac{1}{P_A} \frac{\partial^2 y_A}{\partial y^2} \right) - \tau \epsilon_f \frac{r_h(y_A, y_B, \theta)}{C_0}, \qquad (2.17) \\ f(y)\frac{\partial y_B}{\partial x} &= \epsilon_f \left(\frac{1}{Pe_{m,B}} \frac{\partial^2 y_B}{\partial x^2} + \frac{1}{P_B} \frac{\partial^2 y_B}{\partial y^2} \right) - \nu \tau \epsilon_f \frac{r_h(y_A, y_B, \theta)}{C_0} \text{ and} \qquad (2.18) \\ f(y)\frac{\partial \theta}{\partial x} &= \epsilon_f \left(\frac{1}{Pe_h} \frac{\partial^2 \theta}{\partial x^2} + \frac{Le_f}{P_A} \frac{\partial^2 \theta}{\partial y^2} \right) + \tau \epsilon_f \frac{r_h(y_A, y_B, \theta)}{C_0}; \qquad (2.19) \\ 0 &< x < 1, 0 < y < 1. \end{aligned}$$

$$\begin{aligned} \frac{\epsilon_f}{Pe_{m,A}} \frac{\partial y_A}{\partial x} &= f(y)(y_A - y_{A,in}), \\ \frac{\epsilon_f}{Pe_{m,B}} \frac{\partial y_B}{\partial x} &= f(y)(y_B - y_{B,in}) \text{ and} \qquad (2.20) \\ \frac{\epsilon_f}{Pe_h} \frac{\partial \theta}{\partial x} &= f(y)(\theta - \theta_{in}) \quad \text{at } x = 0, \qquad (2.21) \end{aligned}$$

$$\frac{\partial y_A}{\partial x} = \frac{\partial y_B}{\partial x} = \frac{\partial \theta}{\partial x} = 0 \text{ at } x = 1 \text{ and} \qquad (2.22)$$

$$\begin{aligned} \frac{\partial y_A}{\partial y} &= 0, \\ \frac{\partial y_B}{\partial y} &= 0 \text{ and} \\ \frac{\partial \theta}{\partial y} &= 0 \text{ at } y = 0 \end{aligned} \tag{2.23}$$

and

$$\frac{\partial y_A}{\partial y} + \frac{P_A \tau}{\epsilon_f} \frac{\epsilon_s r_c(y_A, y_B, \theta)}{C_0} = 0, \tag{2.24}$$

$$\frac{\partial y_B}{\partial y} + \nu \frac{P_B \tau}{\epsilon_f} \frac{\epsilon_s r_c(y_A, y_B, \theta)}{C_0} = 0 \text{ and} \tag{2.25}$$

$$\frac{\partial \theta}{\partial y} - \frac{P_h \tau}{\epsilon_f} \frac{\epsilon_s r_c(y_A, y_B, \theta)}{C_0} = 0 \text{ at } y = 1. \tag{2.26}$$

This full 2-D model contains several important parameters. Of these, the axial Peclet numbers, $Pe_{m,A}, Pe_{m,B}$ and Pe_h serve as measures of strength of the axial gradients. For the short monolith or gauze type reactors, the value of these axial Peclet numbers is of order 1.[Remark: 3-D elliptic models that include azimuthal gradients are practically impossible to analyze with the current computational power as the mesh size needed to determine all the asymmetric solutions that may exist is extremely small.]

2.1.1 Limiting Models

We formulate below three limiting cases of the above general model. These limiting models isolate the effect of spatial gradients in the transverse and axial direction and provide insight on the phenomena observed in the general 2-D model whose behavior can be bounded by those of the following models.

Short Channel Model:

When the length of the channel is very small compared to the spacing between the plates (as in the case of gauze or short monolith reactors), we can neglect the axial gradients and average the aforementioned 2-D model in the axial direction. This leads to a model similar to the "short monolith model" that has been widely studied for systems with catalytic reactions [Balakotaiah, Gupta and West, 2000]. This model is given by

$$f(y)(y_A - y_{A,in}) = \epsilon_f \frac{1}{P_A}\frac{d^2 y_A}{dy^2} - \tau\epsilon_f \frac{r_h(y_A, y_B, \theta)}{C_0}, \tag{2.27}$$

$$f(y)(y_B - y_{B,in}) = \epsilon_f \frac{1}{P_B}\frac{d^2 y_B}{dy^2} - \nu\tau\epsilon_f \frac{r_h(y_A, y_B, \theta)}{C_0} \text{ and} \tag{2.28}$$

$$f(y)(\theta - \theta_{in}) = \epsilon_f \frac{Le_f}{P_A}\frac{d^2 \theta}{dy^2} + \tau\epsilon_f \frac{r_h(y_A, y_B, \theta)}{C_0}. \tag{2.29}$$

$$0 < y < 1.$$

and the same transverse boundary conditions (in y) as the full model. The usefulness of this model lies in the fact that it simplifies the flow terms and focuses mainly on the transverse variations. It has been shown in previous work [see Gupta et al [5]]. that this model has the same bifurcation features as the full 3-D model for catalytic reactions. Changing the form of $f(y)$ in our calculations did not lead to much qualitative differences in our results and therefore, for simplicity, we chose to consider $f(y) = 1$ in subsequent calculations.

By integrating in y, this model can be reduced to a 0-D two mode model, where the transverse gradients are accounted for by use of heat and mass transfer coefficients

to express fluxes involved. We obtain

$$y_A - y_{A,in} = k_{c,A} a_v \tau \left(y_A - y_{A,s}\right) - \tau \epsilon_f \frac{r_h(y_A, y_B, \theta)}{C_0}, \tag{2.30}$$

$$y_B - y_{B,in} = k_{c,B} a_v \tau \left(y_B - y_{B,s}\right) - \nu \tau \epsilon_f \frac{r_h(y_A, y_B, \theta)}{C_0} \text{ and} \tag{2.31}$$

$$\theta - \theta_{in} = h a_v \tau \left(\theta - \theta_s\right) + \tau \epsilon_f \frac{r_h(y_A, y_B, \theta)}{C_0}. \tag{2.32}$$

At the wall, we employ the definitions of the heat and mass transfer coefficients to obtain the following equations

$$k_{c,A} a_v \left(y_A - y_{A,s}\right) - \epsilon_s \frac{r_c(y_A, y_B, \theta_s)}{C_0} = 0, \tag{2.33}$$

$$k_{c,B} a_v \left(y_B - y_{B,s}\right) - \nu \epsilon_s \frac{r_c(y_A, y_B, \theta_s)}{C_0} = 0 \text{ and} \tag{2.34}$$

$$h a_v \left(\theta - \theta_s\right) + \epsilon_s \frac{r_c(y_A, y_B, \theta_s)}{C_0} = 0. \tag{2.35}$$

Both forms of the short channel model are analyzed in detail in chapter 3 of this thesis.

Analysis of the 1-D model with transverse gradients leads to bifurcation diagrams of S and double-S shapes (along with the trivial bifurcation diagrams with no multiplicity). Mathematically these correspond to the unfolding of the singularity $x^5 - \lambda = 0$ where x and λ are the state variable and the bifurcation variable, respectively. We refer the reader to the next chapter and the textbook of Golubitsky and Schaeffer (1985) for further details. We have calculated the complete phase diagram for this system which includes the hysteresis locus, the boundary limit locus and the double limit locus for propane oxidation in the plane of residence time and inlet mole

fractions of propane. Further details on these calculations alongwith their physical interpretations can be found in Chapter 3.

1-D Model with Axial Gradients:

When the spacing between the channels is very small (i.e. in the limit of $P \rightarrow 0$), we can ignore the transverse gradients and consider only the axial variations. This limiting case is described by the following 1-D model:

$$\frac{dy_A}{dx} = \frac{\epsilon_f}{Pe_{m,A}}\frac{d^2y_A}{dx^2} - \tau\epsilon_f\frac{r_h(y_A, y_B, \theta)}{C_0} - \tau\epsilon_s\frac{r_c(y_A, y_B, \theta_s)}{C_0}, \tag{2.36}$$

$$\frac{dy_B}{dx} = \frac{\epsilon_f}{Pe_{m,B}}\frac{d^2y_B}{dx^2} - \nu\left(\tau\epsilon_f\frac{r_h(y_A, y_B, \theta)}{C_0} - \tau\epsilon_s\frac{r_c(y_A, y_B, \theta_s)}{C_0}\right) \text{ and} \tag{2.37}$$

$$\frac{d\theta}{dx} = \frac{Le_f\epsilon_f}{Pe_{m,A}}\frac{d^2\theta}{dx^2} + \left(\tau\epsilon_f\frac{r_h(y_A, y_B, \theta)}{C_0} - \tau\epsilon_s\frac{r_c(y_A, y_B, \theta_s)}{C_0}\right); 0 < x < 1. \tag{2.38}$$

The boundary conditions at the inlet and exit are the same as that for the general 2D model shown above.

Adiabatic Invariants:

The above steady-state 1D model can be solved by using the shooting method combined with arclength continuation. This is greatly aided by the presence of adiabatic invariants, reducing the computational effort. We discuss this approach here as this is an important numerical technique useful for many calculations presented in this thesis. We can see immediately from the balance equations that the following

two equations are valid:

$$\frac{d(\nu y_A - y_B)}{dx} = \frac{\nu\epsilon_f}{Pe_{m,A}}\frac{d^2y_A}{dx^2} - \frac{\epsilon_f}{Pe_{m,B}}\frac{d^2y_B}{dx^2} \text{ and} \tag{2.39}$$

$$\frac{d(y_A + \theta)}{dx} = \frac{\epsilon_f}{Pe_{m,A}}\frac{d^2y_A}{dx^2} + \frac{Le_f\epsilon_f}{Pe_{m,A}}\frac{d^2y_B}{dx^2}. \tag{2.40}$$

Now, let us define the axial fluxes of the mole fractions of species A and B and the nondimensional temperature, θ, respectively as

$$\begin{aligned} J_A &= y_A - \frac{\epsilon_f}{Pe_{m,A}}\frac{dy_A}{dx}, \\ J_B &= y_B - \frac{\epsilon_f}{Pe_{m,B}}\frac{dy_B}{dx} \text{ and} \\ J_\theta &= \theta - \frac{Le_f\epsilon_f}{Pe_{m,A}}\frac{d\theta}{dx}. \end{aligned}$$

The balance equations can be rewritten as a system of six first order differential equations comprising of the above equations along with

$$\frac{dJ_A}{dx} = -\tau\epsilon_f\frac{r_h(y_A, y_B, \theta)}{C_0} - \tau\epsilon_s\frac{r_c(y_A, y_B, \theta_s)}{C_0}, \tag{2.41}$$

$$\frac{dJ_B}{dx} = -\nu\left(\tau\epsilon_f\frac{r_h(y_A, y_B, \theta)}{C_0} - \tau\epsilon_s\frac{r_c(y_A, y_B, \theta_s)}{C_0}\right) \text{ and} \tag{2.42}$$

$$\frac{dJ_\theta}{dx} = \tau\epsilon_f\frac{r_h(y_A, y_B, \theta)}{C_0} - \tau\epsilon_s\frac{r_c(y_A, y_B, \theta_s)}{C_0}, \ 0 < x < 1. \tag{2.43}$$

with the boundary conditions given by

$$J_A = y_{A,in},$$

$$J_B = y_{B,in} \text{ and}$$

$$J_\theta = \theta_{in} \text{ at } x = 0 \text{ and} \tag{2.44}$$

$$\frac{dy_A}{dx} = \frac{dy_B}{dx} = \frac{d\theta}{dx} \text{ at } x = 1.$$

We can now express the equations (2.39) and (2.40) as

$$\begin{aligned} \nu \frac{dJ_A}{dx} - \frac{dJ_B}{dx} &= 0 \text{ and} \\ \frac{dJ_A}{dx} + \frac{dJ_\theta}{dx} &= 0. \end{aligned}$$

These equations let us eliminate two of the six differential equations. If we denote the exit values of the variables by subscript *ex,* the integration of these equations leads to the invariants

$$\begin{aligned} \nu y_{A,in} - y_{B,in} &= \nu J_{A,ex} - J_{B,ex} = \nu y_{A,ex} - y_{B,ex} \text{ and} \\ y_{A,in} + \theta_{in} &= J_{A,ex} + J_{\theta,ex} = y_{A,ex} + \theta_{ex}. \end{aligned}$$

Using these invariants, the shooting procedure is greatly simplified. We now need to guess only one variable at one of the boundaries and the other variables can be expressed in terms of that variable. We choose to guess $y_{A,ex}$ and integrate the system backwards. We demand that the inlet condition $J_A = y_{A,in}$ is satisfied at $x = 0$ and in order to accomplish this, the shooting variable $y_{A,ex}$ is refined by a Newton iteration. Upon solution of the system for a particular value of θ_{in}, we employ the arclength continuation to find another set of θ_{in} and $y_{A,ex}$ for which the shooting procedure is

repeated. It is interesting to note that in this limiting case, the coupled homogeneous-catalytic reaction system is completely characterized by one variable which can be chosen to be the fluid exit temperature. This is the hallmark of a *one state variable bifurcation problem* in the vocabulary of Bifurcation Theory (see Golubitsky and Schaeffer, 1985).

2.2 Summary and comments on other models

Aside from the 2D model and its 1D limiting cases with axial or transverse gradients only, several other models are popular in chemical engineering literature. The present thesis focuses on models for short monolith or gauze reactors, for which 1D model with transverse gradients only or its lumped variant are good models. We would further like to make the following remarks (which are substantiated in references [52-62]) about the hierarchy of models to describe homogeneous-catalytic combustion so that our choice of model can be justified:

(i) The simplest of the models, namely the one dimensional pseudo-homogeneous plug flow model is structurally unstable and does not show ignition/extinction but only parametric sensitivity (ii) The pseudo-homogeneous model with no axial gradients (which is included as a special case of our model when interphase gradients are negligible) is robust but is good only for very small axial length scales and hydraulic diameters (micro-channels) [Remark: Structural stability or robustness here implies that the bifurcation and/or qualitative features do not change when the model is perturbed by including spatial gradients or other phenomena as long as the perturbations are small, see [Balakotaiah, 1996]] (iii) The 2-D boundary layer models

(of parabolic type) that ignore axial diffusion (conduction) are structurally unstable, index infinity differential-algebraic system (and are not initial value problems). Further, as explained in the literature articles [Gupta et al 2001, Gupta and Balakotaiah 2001], most computational codes do not consider the Gibbs' phenomenon (which does not disappear even for arbitrarily small mesh size and leads to incorrect fluxes and temperature overshoot at the point of ignition) and compute only a single solution. The same comment applies to 3-D boundary layer models (iv) 2-D elliptic models that include axial diffusion (conduction) but use Dirichlet boundary conditions at the inlet to the channel represent the physics incorrectly and lead to thermodynamic inconsistencies (e.g. fixing the inlet composition and temperature but including conduction/diffusion for $x > 0$ but not for $x \leq 0$ can lead to temperatures above adiabatic value even for long residence times, violating thermodynamic constraints) (v) 2-D elliptic models that use Danckwerts' boundary conditions are physically consistent but are difficult to analyze for large values of the axial Peclet numbers (or longer length scales in the flow direction) as the mesh size needed to eliminate spurious solutions may be exponentially small (see for example, Dommeti and Balakotaiah, 2000). However, when axial length scales are small, they reduce to a one-dimensional model with transverse gradients or its lumped two-mode version that uses heat and mass transfer coefficients. These models are analyzed in the next chapter. This lumped two-mode model is the simplest, non-trivial and physically consistent model that gives a coarse map of the various bifurcations [Remark: 3-D elliptic models that include azimuthal gradients are also practically impossible to analyze with the current computational power as the mesh size needed to determine all the asymmetric solutions that may

exist is extremely small, see Gupta et al, 2002). Thus, we expect the one-dimensional model with transverse gradients or the lumped two-mode model to retain most of the qualitative features of the 2-D elliptic models (at least for small values of the axial Peclet numbers) except azimuthally asymmetric solutions.

Chapter 3

Bifurcation Analysis for Oxidation of Propane

3.1 Introduction

We present a comprehensive bifurcation analysis for the total oxidation of propane in this chapter. As outlined in Chapter 1, catalytic combustion technologies, of which the subject of the present chapter is a prototype, have been widely studied due to their promise of meeting future energy demands and production of intermediate chemicals. As explained in Chapter 1, the models describing catalytic combustion and catalytic partial oxidations typically involve both catalytic and homogeneous reactions. Although homogeneous ignition in catalytic combustion has been investigated in various settings such as stagnation point flows, external boundary layer flows and two-dimensional channel flows (for a good overview of the subject see Hayes and Kolaczkowski, 1998), most of these studies have been direct numerical studies relying on CFD packages. Multiple ignitions and extinctions are possible for such thermally coupled systems, and a direct numerical study can obscure the essential features as multiple reactions and space dimensions may detract from the underlying physics.

The present chapter is structured as follows. We first give details of the development of a simple but nontrivial model that incorporates all the essential physics and chemistry and that is well-suited for bifurcation analysis. Next, we consider propane oxidation with stoichiometric feed and investigate the possible bifurcation phenomena for three limiting cases in which either the homogeneous reaction only occurs or catalytic reaction only occurs or both reactions are present but no interphase gradients exist. The insight obtained from these limiting cases is used to present a complete bifurcation analysis of propane oxidation in short monolith or gauze type reactors and the impact of inlet fuel mole fraction, residence time and channel hydraulic diameter on the various ignitions and extinctions. In the last section, we summarize the results and point out some possible extensions to this work.

3.2 Model development

Since the bifurcation analysis of a full three-dimensional model of homogeneous-catalytic reaction system with convection and diffusion in both phases coupled with detailed kinetics is much too difficult to be of any practical use (and also numerically very expensive, if not impractical), we consider here a one-dimensional model with radial gradients and its lumped version. This model is valid for short monolith reactors where the effects of reactor length are negligible. The reason such reactors are appropriate models for the combustion systems we are studying is because these processes are very highly exothermic with high operating temperatures. This necessitates low residence times (10^{-4} to 10^{-1} s), otherwise undesirable runaways to very high temperatures are possible and side reactions may compromise the operation. The model

considered is an extension of the so called "Short Monolith Reactor Model" developed by Balakotaiah, Gupta and West (2000) and is applicable to systems such as short monolith reactors, ceramic foam reactors, fibermat and gauze reactors in which the length scale in the flow direction is small compared to the transverse length scale of the reactor (The model is also applicable to a thin layer of packed-bed of catalyst sandwiched between inert layers or the so called 'shallow packed-bed catalytic reactor'. Also the transverse length scale in a monolith is the channel hydraulic diameter). Also, the short length scale in the flow direction allows us to ignore any axial gradients within the system (but the state variables can be different from feed values). Thus, we have several short monoliths in sequence making up a typical industrial monolith that is used in after-treatment systems. As shown in references [55-59], multi-mode models of the type used here can be derived rigorously by spatial averaging of the 2D/3-D governing equations by taking advantage of the disparate length or time scales, and the reduced order lumped model considered here retains a significant wealth of information and most of the qualitative bifurcation features of the full model.

We use two versions of the short monolith model in this chapter: a one-dimensional model described by a boundary value problem (described in Chapter 2) and a lumped model described by a set of algebraic equations that utilizes heat and mass transfer coefficients to describe the interphase gradients. In the rest of this section we detail the model development for the lumped model as the other model has been discussed in the last chapter.

We denote the fluid phase cup-mixing mole fraction of the j-th species by y_j, solid-

fluid interfacial mole fraction by y_{js}, the fluid phase cup-mixing temperature by T_f , and the interfacial (or solid) temperature by T_s. Volumetric reaction rate for the homogeneous reaction is denoted by $r_h(\mathbf{y})$ and that for catalytic surface reaction by $r_c(\mathbf{y}_s)$. The parameter R_Ω denotes the channel hydraulic radius of the monolith, k_{cj} and h denote the interphase mass transfer coefficient of the j-th species and the interphase heat transfer coefficient, respectively. Mole and energy balances for an oxidation reaction of the type $A + \nu B \rightarrow P$ (in both the gas phase and catalyst) lead to the following model at the steady state:

$$\frac{(y_{A,in}(t) - y_A)}{\tau} - k_{cA}a_v(y_A - y_{As}) - \frac{\epsilon_f r_h(y_A, y_B, T_f)}{C_0} = 0, \tag{3.1}$$

$$\frac{(y_{B,in}(t) - y_B)}{\tau} - k_{cB}a_v(y_B - y_{Bs}) - \nu\frac{\epsilon_f r_h(y_A, y_B, T_f)}{C_0} = 0, \tag{3.2}$$

$$k_{cA}a_v(y_A - y_{As}) - \frac{\epsilon_s r_c(y_{As}, y_{Bs}, T_s)}{C_0} = 0, \tag{3.3}$$

$$k_{cB}a_v(y_B - y_{Bs}) - \nu\frac{\epsilon_s r_c(y_{As}, y_{Bs}, T_s)}{C_0} = 0, \tag{3.4}$$

$$\frac{(T_{f,in}(t) - T_f)}{\tau} + \frac{h}{\widetilde{c_{pf}}}a_v(T_s - T_f) + \frac{\epsilon_f(-\Delta H_R)r_h(y_A, y_B, T_f)}{\widetilde{c_{pf}}} = 0 \text{ and} \tag{3.5}$$

$$-\frac{h}{\widetilde{c_{pf}}}a_v(T_s - T_f) + \frac{\epsilon_s(-\Delta H_R)r_c(y_{As}, y_{Bs}, T_s)}{\widetilde{c_{pf}}} = 0. \tag{3.6}$$

We assume that the rate of the catalytic reaction (based on unit reactor volume or $\epsilon_s r_c$) depends only solid-fluid interfacial area and may be expressed in the form

$$\frac{\epsilon_s r_c(y_{As}, y_{Bs}, T_s)}{C_0} = \epsilon_f \times \frac{k_{0s}}{R_\Omega}\exp\left[-\frac{E_c/R}{T_s}\right] y_{As}^{n'} y_{Bs}^{m'}, \tag{3.7}$$

where k_{0s} (having units of velocity) is the rate constant for the surface reaction. [Remark: For non-porous catalysts, k_{0s} is determined experimentally by the surface site density. For the case of a thin washcoat in which no diffusional limitations exist and all the catalytic sites are accessible, k_{0s} may be related to the rate constant based on washcoat volume (k_{0v}) and thickness (δ_c) by $k_{0s} = \delta_c k_{0v}$].

[Remarks: (i) We have expressed the rates in terms of mole fractions rather than concentrations. This makes the calculations more convenient. (ii) An average value for $\widetilde{c_{pf}}$ is used in the calculation of (ΔT^*_{ad}) so that the adiabatic temperature rise predicted by the model is close to the true value with physical property variations].

Here, ϵ_f and ϵ_s ($= 1 - \epsilon_f$) are the fluid and solid volume fractions in the reactor and a_v is the solid-fluid interfacial area per unit reactor volume. It is related to the hydraulic radius of the flow channel by

$$a_v = \frac{\epsilon_f}{R_\Omega}. \tag{3.8}$$

[The hydraulic radius R_Ω is defined as the open cross-sectional area (volume) available for gas flow over the solid-fluid interfacial perimeter (area). For a circular (square) channel of diameter (side) $2a$, $R_\Omega = a/2$. For a channel of arbitrary shape, the hydraulic diameter d_h is defined as $d_h = 4R_\Omega$. For the case of parallel plates separated by a distance $2a$, $R_\Omega = a$]. The parameter σ is the ratio of solid to fluid volumetric heat capacities, ϵ_c is the void fraction within the solid (catalyst) phase (ϵ_c is zero for non-porous catalysts), $\widetilde{c_{pf}}$ is the average volumetric heat capacity of the gas mixture ($\widetilde{c_{pf}} = \widehat{c_{pf}}\ C_0$, $\widehat{c_{pf}}$ = average molar heat capacity of the gas mixture), C_0 is the total

molar concentration in the gas phase and

$$\Delta T_{ad}^{*} = \frac{(-\Delta H_R) C_0}{\widetilde{c_{pf}}} \tag{3.9}$$

is a reference adiabatic temperature rise [When A is the limiting reactant or A and B are in stoichiometric amounts in the feed, the actual adiabatic temperature rise is $(\Delta T_{ad}^{*}) y_{A,in}$. Here, D_{mj} and $\alpha_f = k_f / \widetilde{c_{pf}}$ are the mass diffusivity of species j and thermal diffusivity of the gas mixture, respectively.]. To complete the model, we need to specify how the heat and mass transfer coefficients depend on the inlet gas velocity and other system parameters. Based on the work of Gupta and Balakotaiah (2001), we use the following correlations for the transfer coefficients in monoliths that are applicable for circular channels when the velocity profile in the channels is uniform (or not developed):

$$k_{cj} = 2\frac{D_{mj}}{R_\Omega} + \left(\frac{D_{mj}}{\tau}\right)^{0.5}$$

and

$$\frac{h}{\widetilde{c_{pf}}} = 2\frac{\alpha_f}{R_\Omega} + \left(\frac{\alpha_f}{\tau}\right)^{0.5}. \tag{3.10}$$

Similar correlations for other flow conditions in monoliths such as simultaneously developing velocity, concentration and temperature profiles or fully developed laminar velocity profile but developing concentration and temperature profiles in most common geometries, as given in Gundlapally and Balakotaiah (2011) can be used without changing any of the qualitative features of the model. Further, the above form of the correlations is also applicable for other systems such as foam, fibermat,

gauze type and shallow packed-bed reactors. [Remarks: The numerical coefficient in the first term of the above correlations represents the asymptotic shape normalized Nusselt/Sherwood number and depends only on the geometry of the channel open to flow. The numerical coefficient and exponent in the second term depend on the flow conditions (e.g. fully developed or simultaneously developing boundary layers) but are independent of channel geometry. For the case of shallow packed-beds, the form of the second term is different, where the exponents are different on the velocity (or Reynolds number) and diffusivity (or Schmidt/Prandtl number), see for example, Agrawal et al. (2007). Again, this new form does not alter any of qualitative bifurcation features studied here]. Here, D_{mj} and $\alpha_f = k_f/\widetilde{c_{pf}}$ are the mass diffusivity of species j and thermal diffusivity of the gas mixture, respectively. The above lumped model is completed by specifying the initial conditions. Finally, it should be pointed out that for simplicity, we consider here only the adiabatic case and hence do not include any heat loss terms either in the fluid or solid phase energy balances.

As stated in the previous chapters, more detailed models that include spatial gradients in all directions and the coupling between the continuity, momentum, species and energy balances can be developed. However, the bifurcation analysis of such detailed models is rather difficult without a good understanding of the kinds of models considered here.

Adiabatic Invariants:

When the inlet conditions are independent of time, the steady-state lumped model is described by six algebraic equations for the state variables y_A, y_B, y_{As}, y_{Bs}, T_f, and T_s. However, in the adiabatic case considered here, we can reduce the number of variables by taking advantage of the invariants. In this specific case, we can express five of the state variables in terms of the fluid temperature as follows:

$$y_A = y_{A,in} - \frac{(T_f - T_{f,in})}{(\Delta T^*_{ad})}, \tag{3.11}$$

$$y_B = y_{B,in} - \frac{(T_f - T_{f,in})\nu}{(\Delta T^*_{ad})}, \tag{3.12}$$

$$y_{As} = y_A - \frac{1}{k_{cA} a_v \tau}\left[y_{A,in} - y_A - \tau \frac{\epsilon_f r_h(y_A, y_B, T_f)}{C_0}\right], \tag{3.13}$$

$$y_{Bs} = y_B - \nu \frac{k_{cA}}{k_{cB}}\left[y_A - y_{As}\right] \text{ and} \tag{3.14}$$

$$T_s = T_f + \frac{\widetilde{c_{pf}}}{h a_v}\left[\frac{(T_f - T_{f,in})}{\tau} - (\Delta T^*_{ad})\frac{\epsilon_f r_h(y_A, y_B, T_f)}{C_0}\right]. \tag{3.15}$$

Substitution of these relations into the solid phase energy balance leads to a single equation for the steady-state temperature of the fluid:

$$F(T_f, \mathbf{p}^*) \equiv \tau(\Delta T^*_{ad})\left[\frac{\epsilon_f r_h(y_A, y_B, T_f)}{C_0} + \frac{\epsilon_s r_c(y_{As}, y_{Bs}, T_s)}{C_0}\right] - (T_f - T_{f,in}) = 0. \tag{3.16}$$

Here, $\mathbf{p}^*$ is a vector of various parameters characterizing the steady-state behavior of the system. For example, these include the inlet mole fractions ($y_{A,in}$,$y_{B,in}$), the space time (τ), inlet fluid temperature ($T_{f,in}$), the channel dimensions (R_Ω), operating pressure (through the reaction rates), the catalyst properties and the kinetic

parameters.

It is interesting to note that in the absence of spatial gradients and heat losses, the coupled homogeneous-catalytic reaction system is completely characterized by the fluid exit temperature. Once T_f is known, the other five state variables are uniquely determined from the above relations. In the terminology of bifurcation (and singularity) theory, the lumped model studied here is a *one state variable bifurcation problem*. However, this may not be the case, when spatial gradients or heat losses are included.

3.3 Bifurcation Analysis

In this section, we present an analysis of propane oxidation using global kinetic models. We use global kinetics because our goal is to understand the thermal effects and coupling between the catalytic and homogeneous chemistry, and without understanding the thermal effects, one cannot hope to solve the more complicated problem where both thermal and chemical coupling (as a result of multiple reactions) are possible. The complete combustion of propane in air is given by

$$C_3H_8 + 5O_2 \rightarrow 3CO_2 + 4H_2O, \;\; \Delta H_R^0 = -2044 \; kJ/mol. \tag{3.17}$$

The homogeneous rate expression for this global reaction is adapted from Westbrook and Dryer (1981), while the catalytic rate expression is taken from Hiam et al. (1968). We use global kinetics and assume that the rate of the homogeneous reaction can be

expressed as

$$\frac{\epsilon_f r_h(y_A, y_B, T_f)}{C_0} = \epsilon_f \times k_{0h} \exp\left[-\frac{E_h/R}{T_f}\right] y_A^n y_B^m. \tag{3.18}$$

We also assume that the rate of the catalytic reaction (based on unit reactor volume or $\epsilon_s r_c$) depends only solid-fluid interfacial area and may be expressed in the form

$$\frac{\epsilon_s r_c(y_{As}, y_{Bs}, T_s)}{C_0} = \epsilon_f \times \frac{k_{0s}}{R_\Omega} \exp\left[-\frac{E_c/R}{T_s}\right] y_{As}^{n'} y_{Bs}^{m'}, \tag{3.19}$$

where k_{0s} (having units of velocity) is the rate constant for the surface reaction. [Remark: For non-porous catalysts, k_{0s} is determined experimentally by the surface site density. For the case of a thin washcoat in which no diffusional limitations exist and all the catalytic sites are accessible, k_{0s} may be related to the rate constant based on washcoat volume (k_{0v}) and thickness (δ_c) by $k_{0s} = \delta_c k_{0v}$].

The various parameters used for the case of propane oxidation are listed in table 1. [Remarks: (i) We have expressed the rates in terms of mole fractions rather than concentrations by using an average total concentration (21.3 moles/m^3) over which these expressions were validated (ii) average value for $\widetilde{c_{pf}}$ is used in the calculation of (ΔT_{ad}^*) so that the adiabatic temperature rise predicted by the model is close to the true value with specific heat variation with temperature].

Before we analyze the coupled system, we consider some limiting cases that are helpful in the understanding of the bifurcation features of the full system using the lumped model. The three limiting cases of interest are (a) homogeneous reaction only (b) catalytic reaction only and (c) negligible interphase gradients.

Table 3.1: List of kinetic, thermodynamic and transport parameters used in calculations for propane oxidation.

Parameter	Value
α_f	9.80 x $10^{-10}\frac{T^{1.75}}{P}$ m^2/s (T in K and P in bars)
c_{pc}	1000 J/kg.K
$\widetilde{c_{pf}}$	875 J/(m^3.K)
ϵ_f	0.9
$D_{propane}$	5.25 x $10^{-10}\frac{T^{1.75}}{P}$ m^2/s (T in K and P in bars)
D_{oxygen}	9.24 x $10^{-10}\frac{T^{1.75}}{P}$ m^2/s (T in K and P in bars)
k_{0h}	2.67×10^8 s^{-1}
k_{0s}	5.06×10^4 m/s
E_h/R	15097 K
E_c/R	8555 K
n	0.1
m	1.65
n'	1
m'	0.5
ΔT^*_{ad}	49757 K
ν	5

(a) Homogeneous reaction only:

The case of homogeneous reaction alone can be studied completely by analytical techniques. This case serves as a useful reference point when we compare it to the coupled system or the case in which only catalytic reaction operates. For simplicity, we consider here only the case in which the feed contains stoichiometric amounts of hydrocarbon (A) and oxygen (B). In this case, the steady-state equation simplifies to

$$F_1(T_f, T_{f,in}, \tau, y_{A,in}) \equiv \tau(\Delta T^*_{ad}) \left[\frac{\epsilon_f r_h(y_A, y_B, T_f)}{C_0}\right] - (T_f - T_{f,in}) = 0. \qquad (3.20)$$

This algebraic equation may be used to make a plot (bifurcation diagram) of exit fluid temperature (T_f) or conversion ($\chi = 1 - (y_A/y_{A,in})$) for any fixed residence time

(τ) and inlet mole fraction ($y_{A,in}$). Alternately, we can write this relationship in a parametric form by a rearrangement of the above equation (and using the adiabatic invariants). For example, we can express both $T_{f,in}$ and T_f in terms of conversion as

$$T_{f,in} = \frac{E_h/R}{\ln(\frac{Da(1-\chi)^N}{\chi})} - (\Delta T_{ad})\chi \quad ; \quad \Delta T_{ad} = \Delta T^*_{ad} y_{A,in}, \tag{3.21}$$

$$T_f = T_{f,in} + (\Delta T_{ad})\chi \text{ and} \tag{3.22}$$

$$Da = k_{0h}\tau\epsilon_f y^{N-1}_{A,in}\nu^m \quad ; \quad N = n + m. \tag{3.23}$$

Now, a bifurcation diagram of T_f versus $T_{f,in}$ can be constructed for any fixed $y_{A,in}$ and τ by varying the conversion χ in the range $(0, 1)$ and plotting equations (3.21) and (3.22). To obtain the bifurcation set (i.e. the locus of ignition and extinction points) in the ($T_{f,in}, y_{A,in}$) plane, we differentiate equation (3.21) w.r.t. χ and solve it along with eqns.(3.21-3.22). This leads to a parametric representation of the bifurcation set

$$\Delta T_{ad} = \frac{E_h/R(1 + (N-1)\chi)}{\chi(1-\chi)(\ln(\frac{Da(1-\chi)^N}{\chi}))^2} \text{ and} \tag{3.24}$$

$$T_{f,in} = \frac{E_h/R}{\ln(\frac{Da(1-\chi)^N}{\chi})} - \frac{E_h/R(1 + (N-1)\chi)}{(1-\chi)(\ln(\frac{Da(1-\chi)^N}{\chi}))^2}. \tag{3.25}$$

The hysteresis locus, i.e. the locus of points where the ignition and extinction points coalesce and disappear as the free parameter Da (or the residence time) is now varied, can be obtained by solving for simultaneous vanishing of the function and the first two derivatives of the equation (3.20) with respect to T_f. After some algebraic

manipulation, we can express this locus in parametric form as:

$$Da = \frac{\chi}{(1-\chi)^N} \exp\left(\frac{2(\frac{1}{\chi} + \frac{N}{1-\chi})^2}{(\frac{N}{(1-\chi)^2} - \frac{1}{\chi^2})}\right) \text{ and} \tag{3.26}$$

$$\Delta T_{ad} = \frac{E_h/R(1+(N-1)\chi)}{\chi(1-\chi)(\ln(\frac{Da(1-\chi)^N}{\chi}))^2}, \quad 0 < \chi < 1. \tag{3.27}$$

We can use equations (3.22) and (3.23) to revert to variables τ and $y_{A,in}$ instead of Da and ΔT_{ad} and plot the hysteresis locus in the (τ, $y_{A,in}$) plane. This is shown in figure3-1. This locus serves as the boundary between the regions of uniqueness and multiplicity of steady states. In the region above the curve we have S-shaped bifurcation diagrams of fluid exit temperature (T_f) or conversion versus the inlet temperature ($T_{f,in}$), but below the hysteresis locus, the bifurcation diagrams are single-valued. As the inlet mole fraction of the fuel at hysteresis increases, the temperature attained at the hysteresis point also increases due to increased adiabatic temperature rise. We also note that decreasing the residence time shifts the bifurcation diagrams to the right, i.e. the system has to reach higher temperatures before igniting because of the short residence time.

We note that for higher values of the residence time and mole fraction, the extinction point can move to quite low values of inlet temperatures. In physical terms, this implies that for high adiabatic temperature rise and residence time, the reaction cannot be quenched even by sufficiently reducing the inlet temperature (as it becomes autothermal or self sustaining). We call the locus of parameter values where the extinction point is at $T_{f,in} = 300\ K$ the *boundary limit set* (see Balakotaiah and Luss (1983)). This can also be determined in a parametric form. It is also shown

in figure3-1. Finally, using standard approximations (Zeldovich et al. (1985)), we note that the ignition locus (whenever it exists) can be expressed analytically by the expression

$$\left(\frac{\Delta T^*_{ad} y_{A,in}}{T_{f,in}} \frac{E_h}{RT_{f,in}}\right) \left[k_{0h} \tau \epsilon_f y^{N-1}_{A,in} \nu^m \exp(-\frac{E_h}{RT_{f,in}})\right] = 0.368. \tag{3.28}$$

[Remark: The factor in the first bracket of Eq.(3.28) is the Zeldovich number while the second term is the Damköhler number at inlet conditions]. Eq.(3.28) may be used to determine the inlet temperature ($T_{f,in}$) at which ignition of the homogeneous reaction occurs for any fixed values of inlet mole fraction ($y_{A,in}$) and residence time (τ). For example, keeping $y_{A,in}$ fixed at 0.02 and changing τ from 1 to $0.001s$ increases the ignition temperature from $639K$ to $948K$. Similarly, keeping τ fixed at $0.001s$ and decreasing the fuel mole fraction from 0.02 to 0.002 increases the ignition temperature further to $1350K$. Thus, as can be expected intuitively, homogeneous ignition is suppressed at low fuel mole fractions and short residence times. We return to this observation as it is important in the understanding of the thermally coupled system discussed later.

To summarize, the homogeneous reaction system has no ignition or extinction points for sufficiently low values of inlet fuel mole fraction and/or residence times, has one ignition and extinction point for intermediate values of τ and $y_{A,in}$, and only an ignition point for values of (τ, $y_{A,in}$) above the boundary limit set (BLS).

(b) Catalytic reaction only:

The equations determining the limiting case of catalytic reaction only can be

obtained from the general model by taking the homogeneous reaction rate to be zero. Thus, we have the steady state equation

$$F_2(T_f, T_{f,in}, \tau, y_{A,in}) \equiv \tau(\Delta T^*_{ad}) \left[\frac{\epsilon_s r_c(y_{As}, y_{Bs}, T_s)}{C_0} \right] - (T_f - T_{f,in}) = 0, \qquad (3.29)$$

where

$$y_{As} = y_{A,in} - \left(1 + \frac{1}{k_{cA} a_v \tau}\right) \left(\frac{T_{f,in} - T_f}{\Delta T^*_{ad}}\right), \qquad (3.30)$$

$$y_{Bs} = \nu \left[y_{A,in} - \left(1 + \frac{1}{k_{cB} a_v \tau}\right) \left(\frac{T_{f,in} - T_f}{\Delta T^*_{ad}}\right) \right], \text{ and} \qquad (3.31)$$

$$T_s = T_f + \frac{\widetilde{c_{pf}}}{h a_v} \left[\frac{(T_f - T_{f,in})}{\tau} \right]. \qquad (3.32)$$

The analysis of Eq.(3.29) is similar to that of the homogeneous case, except that simple analytical expressions are not possible (and the computations have to be carried out numerically) due to the nonlinear dependence of the heat and mass transfer coefficients on the residence time. As in the homogeneous case, for sufficiently low values of inlet mole fraction and/or residence times, the bifurcation diagram of T_f (or T_s, or χ) is single valued. It has one ignition and extinction point for intermediate values of τ and $y_{A,in}$, and only an ignition point for values of (τ, $y_{A,in}$) above the boundary limit set. figure3-1 shows the hysteresis and boundary limit (BL) loci corresponding to R_Ω of 1.32 mm. Since the catalytic reaction has a higher rate and lower activation energy compared to the homogeneous case, both the hysteresis and BL loci move to lower values of inlet mole fraction or residence time (as expected). Our calculations

also show that the solid temperatures attained at hysteresis point increase as the inlet mole fraction of propane increases, which can be explained by increased adiabatic temperature rise. The conversion at the hysteresis point, however, shows a small decrease. It is evident that the hysteresis locus for the catalytic reaction always lies below that for the homogeneous reaction. This implies that the catalytic chemistry is dominant and leads to ignition first even with the large value of the hydraulic radius ($R_\Omega = 1.32$ mm) selected. To make the homogeneous reaction dominant, we have to increase R_Ω further to unrealistically higher values. The fact that catalytic reaction dominates the homogeneous chemistry is a recurring feature in ensuing work when the thermally coupled system is analyzed. We return to this when we consider the lean oxidation of methane.

One fundamental difference between the homogeneous and catalytic reaction case is that, in the latter case, the conversion on the ignited branches can be small as it is determined by the mass transfer of the reactants from the fluid phase to the wall. In the limiting case in which the inlet temperature is very high, the catalytic reaction can enter the mass transfer controlled regime practically at the inlet to the channel. In this case, the concentration of the limiting reactant at the wall is zero. For the case of propane oxidation, propane has smaller diffusivity than oxygen and hence is the limiting reactant when the feed is stoichiometric. [However, for methane oxidation studied later, oxygen is the limiting reactant for stoichiometric feed as diffusivity of methane is higher than that of oxygen for any given temperature]. Setting $y_{As} = 0$ and replacing the catalytic reaction rate by the mass transfer rate gives a linear equation, from which the conversion of the fuel, the solid and fluid temperatures can

be determined to be

$$\chi = \frac{k_{cA} a_v \tau}{1 + k_{cA} a_v \tau}, \tag{3.33}$$

$$T_f - T_{f,in} = \chi \Delta T_{ad}, \tag{3.34}$$

$$T_s - T_{f,in} = \chi \Delta T_{ad} (1 + \frac{\widetilde{c_{pf}}}{h a_v \tau}), \text{ and} \tag{3.35}$$

$$k_{cA} a_v \tau = \frac{\epsilon_f}{P} \left[2 + \sqrt{P} \right]. \tag{3.36}$$

From the above relations, it is easily seen that for $\tau \rightarrow 0$, the solid temperature near the inlet (after ignition) approaches the limit $T_{f,in} + \frac{\Delta T_{ad}}{Le_{fA}^{0.5}}$. After ignition, both the solid and fluid temperatures increase monotonically with τ for $Le_{fA} > 1$ [Remark: For the case of $Le_{fA} < 1$, the solid temperature decreases while the fluid temperature increases as τ increases. Also, as stated in the model formulation section, the exponent on the Lewis number Le_{fA} depends on the nature of the flow conditions in the inlet]. It is clear from Eqs.(3.33) and (3.36), the important dimensionless parameter that determines the conversion on the ignited branches is the transverse Peclet number defined by Balakotaiah et al. (2000)

$$P = \frac{R_\Omega^2}{\tau \overline{D_{m,j}}}, \tag{3.37}$$

where $\overline{D_{m,j}}$ is the average value of diffusivity of the limiting reactant in the gas phase. It can be seen from Eq.(3.33) that for $P \gg 1$, the conversion on the ignited branch

is mass transfer limited and is given by

$$\chi \approx \frac{\epsilon_f}{\sqrt{P}} \quad \text{for } P \gg 1. \tag{3.38}$$

[see also Gupta et al, 2001 for more accurate expressions for χ]. Thus, in figure3-1, while the catalytic reaction is ignited in the region of low residence times and high mole fractions, the conversion is low (due to mass transfer limitations). In contrast, in the region of high residence times (P values of order 1 or smaller), the conversion is high on the ignited branches. This transition point (at P values of order unity) is very important in the understanding of the coupling between catalytic and homogeneous chemistry. For example, when the inlet temperature is high, catalytic reaction can ignite at extremely low values of τ(or very near the inlet when considering spatial profile) but the reactant conversion (and fluid temperature) continues to increase (in the mass transfer controlled regime) and reaches high values only for τ values of order $\frac{R_\Omega^2}{D_{m,j}}$ (which is the characteristic transverse diffusion or mass transfer time).

We note that the channel hydraulic radius, which is the channel volume to surface ratio, is a very important parameter that determines the conversion obtained in the mass transfer controlled limit and also the degree of coupling between the homogeneous and catalytic reaction. For example, decreasing the hydraulic radius (by a factor 5) from 1.32mm to 264 μm shifts the hysteresis curve only slightly but moves the transitional value of the residence time (at which $P = 1$) by a factor 25, from 0.035s (for R_Ω =1.32mm) to 0.0014s (for $R_\Omega = 264\mu m$). Decreasing R_Ω impacts the catalytic reaction in two ways: (a) it enhances the catalytic reaction rate

per unit reactor volume (b) it reduces the interphase heat and mass transport times (and the transverse gradients) and increases the conversion on the ignited branches. Thus, with other parameters fixed, decreasing the channel hydraulic diameter makes the catalytic reaction more dominant (assuming that the catalytic activity per unit surface area remains constant).

For low residence times, we observe that catalytic ignition may be favored by lower heat transfer rate from surface to gas phase. Thus, the dependence of catalytic hysteresis locus is not monotonic with respect to the channel hydraulic radius. This can be better seen by determining the catalytic ignition locus using the standard approximations as in the homogeneous case (Zeldovich et al., 1985). Such approximations were developed by Ramanathan et al. 2003. In the present case, the ignition locus may be expressed as

$$\left(\frac{\Delta T_{ad}^{*} y_{A,in}}{T_{f,in}} \frac{E_c}{RT_{f,in}}\right) \left[\frac{k_{0s}}{R_\Omega} \epsilon_f y_{A,in}^{N'-1} \nu^{m'} \exp(-\frac{E_c}{RT_{f,in}}) \left(\tau + \tau_h\right)\right] = 0.368, \tag{3.39}$$

where $N' = n' + m'$ and the interphase heat transfer time τ_h is defined by

$$\frac{1}{\tau_h} = \epsilon_f \left[2\frac{\overline{\alpha_f}}{R_\Omega^2} + \sqrt{\frac{\overline{\alpha_f}}{\tau R_\Omega^2}}\right]. \tag{3.40}$$

Here $\overline{\alpha_f}$ is a constant value for the thermal diffusivity used in the approximation (we took this value to be $7 \times 10^{-5} \mathrm{m}^2/s$), as the thermal diffusivity does not change much in the temperature range of interest. Eq.(3.39) may be used to determine the inlet temperature ($T_{f,in}$) at which the catalytic ignition occurs for any fixed values of the

inlet fuel mole fraction ($y_{A,in}$), residence time (τ) and channel hydraulic radius (R_Ω). We have plotted the ignition temperature as a function of the hydraulic radius at a fixed value of residence time and inlet mole fraction in figure 3-2. As can be expected, depending on the channel hydraulic diameter, for the same residence time and inlet fuel mole fraction, the catalytic ignition temperature is about 150 to 200$^\circ C$ lower than the corresponding homogeneous value. We have compared the ignition temperatures computed from the governing equation with the value determined by the analytical ignition criterion and found an excellent agreement. As stated earlier, $T_{f,in}$ at ignition is not a monotonic function of R_Ω. This is due to the fact while higher values of R_Ω lead to reduced reaction (or heat production) rate per unit reactor volume, they also reduce the heat removal rate from the catalytic surface to the bulk gas (and hence higher temperature difference between surface and bulk), thus pushing the ignition temperature to lower values. In contrast, lower R_Ω values increase the reaction rate but also the heat removal rate from catalyst surface (with very small values of R_Ω corresponding to the homogeneous limit). Thus, the highest ignition temperature may occur at intermediate values of R_Ω. This can be seen more explicitly when we rewrite the term $(\tau + \tau_h)/R_\Omega$ as

$$\frac{\tau + \tau_h}{R_\Omega} = \frac{\tau}{R_\Omega} + \frac{R_\Omega}{\epsilon_f \left[2\overline{\alpha_f} + R_\Omega \sqrt{\frac{\overline{\alpha_f}}{\tau}}\right]}. \tag{3.41}$$

When the first term in Eq.(3.41) dominates (at lower R_Ω), the ignition occurs at the reactor level with high conversion on the ignited branches. When the second term dominates, we have local (catalytic) ignition with high surface temperature but low

reactant conversion. The factor goes through a minimum (or the ignition temperature is highest) when

$$R_\Omega = \frac{2\sqrt{\tau\overline{\alpha_f}}}{(\sqrt{\frac{2}{\epsilon_f}-1})}. \tag{3.42}$$

This is confirmed in figure 3-2. It can be seen that the maximum in the ignition temperature becomes prominent at higher residence times (where the Nusselt number attains a constant asymptotic value) like the value used for figure 3-2. The ignition temperature reaches an asymptotic value at higher values of R_Ω [Remark: The non-monotonic dependence of the catalytic ignition temperature on the channel hydraulic diameter appears to be a new result predicted by the model but it needs to be validated experimentally].

(c) No interphase gradients:

If the system has negligibly small interphase gradients, the two-phase model effectively behaves as a one phase system. This can be seen easily by taking the transfer coefficients to be infinite in our full thermally coupled lumped model. Using the adiabatic invariants then yields:

$$y_{As} = y_A, \tag{3.43}$$

$$y_{Bs} = y_B, \text{ and} \tag{3.44}$$

$$T_s = T_f. \tag{3.45}$$

This system is the homogeneous limit of the two-phase model and we need only one temperature and concentration variable for each of the species. In this section, we

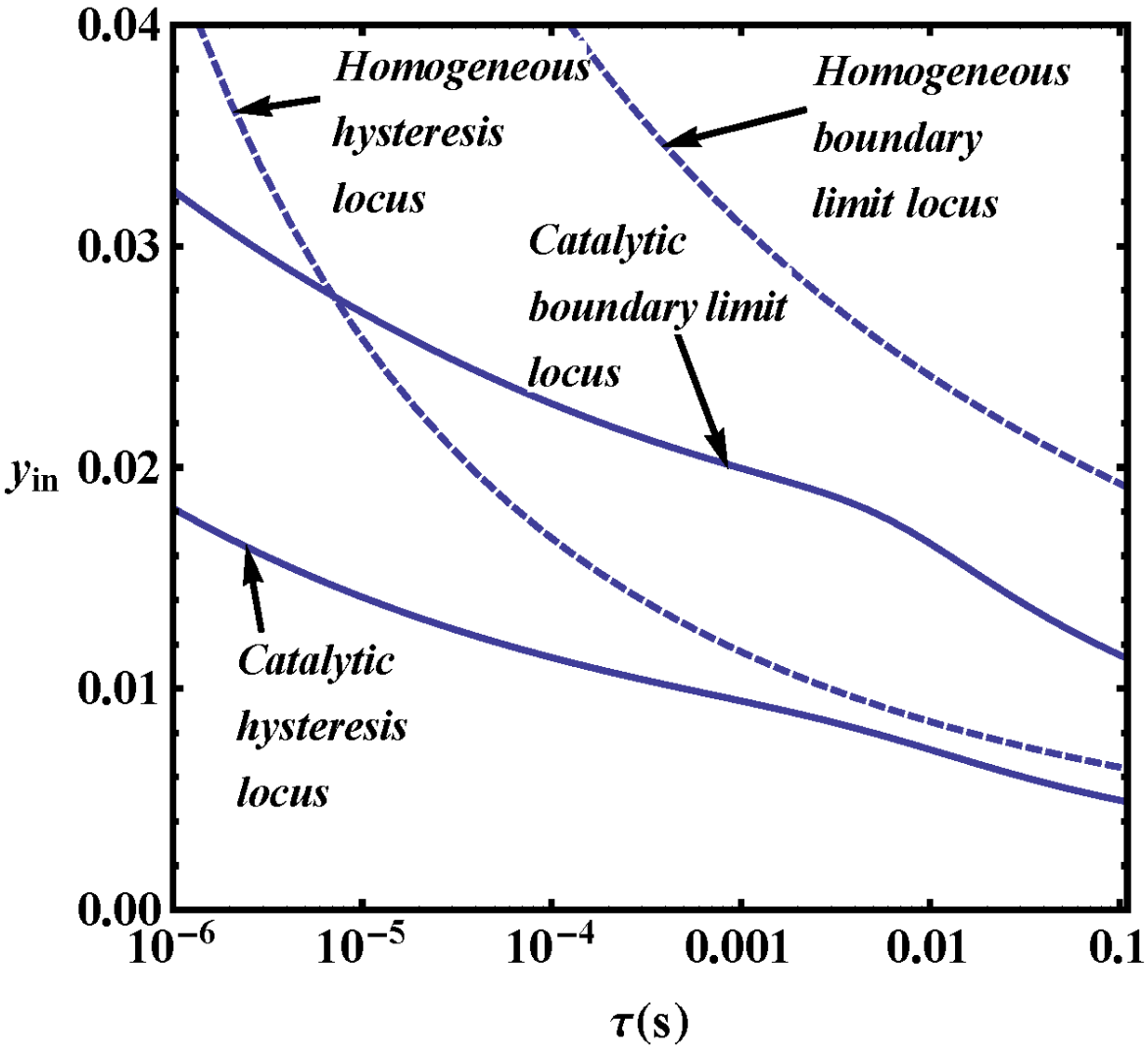

Figure 3-1: Hysteresis and boundary limit loci for propane oxidation when only the catalytic reaction operates for R_Ω of 1.32 mm and when only the homogeneous reaction operates and for kinetic parameters in table 1.

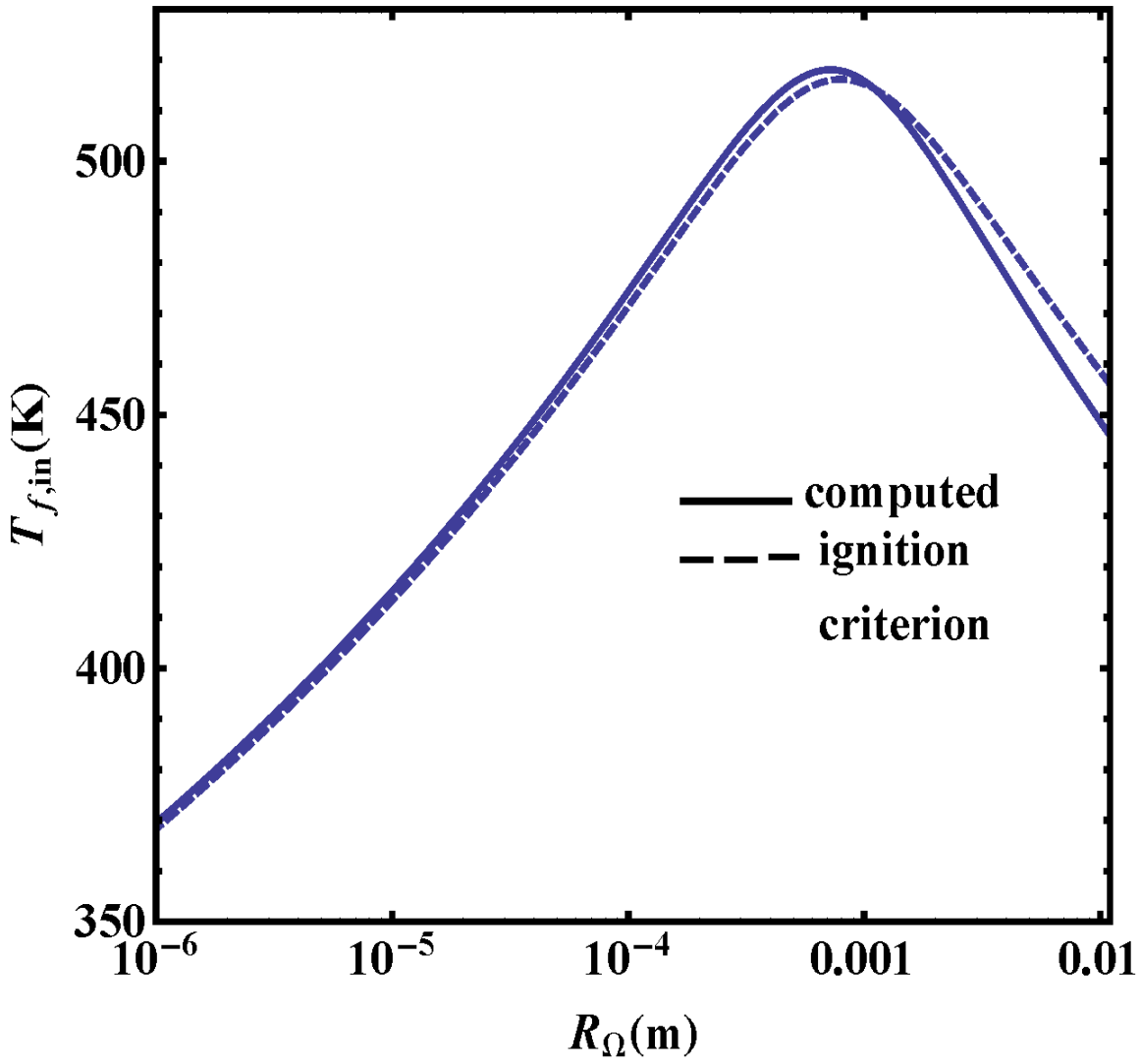

Figure 3-2: Dependence of the feed temperature required for ignition as a function of R_Ω for the case of catalytic propane oxidation for a residence time of 1 s and inlet propane mole fraction of 0.02.

denote the mole fractions of reactants A and B by the symbols y_A and y_B, respectively, and use the symbol T for the common temperature. We then obtain the following limiting model:

$$\tau(\Delta T^*_{ad})\left\{\epsilon_f \times k_{0h}\exp\left[-\frac{E_h/R}{T}\right] y_A^n y_B^m + \epsilon_f \times \frac{k_{0s}}{R_\Omega}\exp\left[-\frac{E_c/R}{T}\right] y_A^{n'} y_B^{m'}\right\} - (T - T_{f,in}) = 0, \tag{3.46}$$

$$y_A = y_{A,in} - \frac{(T - T_{f,in})}{(\Delta T^*_{ad})} \text{ and} \tag{3.47}$$

$$y_B = y_{B,in} - \frac{(T - T_{f,in})\nu}{(\Delta T^*_{ad})}. \tag{3.48}$$

Like the previous two limiting cases, here too we get only S-shaped bifurcation curves. This is because for the system to have no interphase gradients, the characteristic times of heat and mass diffusion have to be small compared to residence and characteristic reaction times, leading to very small transverse Peclet numbers. This is possible for micro-channels or low reactant concentrations or operations with large residence times. The hysteresis loci for this case turn out to be almost the same as those for catalytic reaction acting alone discussed above (this is expected because we only have S-shaped diagrams and the hysteresis locus essentially accounts only for strong catalytic reaction rates). We have not shown hysteresis plots here so as to avoid redundancy. Instead, we show two other plots that provide some insight on the impact of channel hydraulic radius and catalyst loading on the relative importance of the catalytic and homogeneous reactions. In figure 3-3, we show two plots comparing

the characteristic times of the catalytic and homogeneous reactions as a function of temperature for two values of R_Ω, namely (the unrealistic value) 3 cm in (a) and 1320 μm in (b). These characteristic reaction times at feed composition and temperature are defined as

$$t_{R,\mathrm{hom}\,o} = \frac{C_0}{r_h(y_{A,in}, \nu y_{A,in}, T)} \text{ and} \tag{3.49}$$

$$t_{R,cat} = \frac{R_\Omega C_0}{r_c(y_{A,in}, \nu y_{A,in}, T)}, \tag{3.50}$$

where the value of y_{in} has been fixed at 0.02, respectively. We note that the catalytic reaction time is larger than the homogeneous reaction time i.e. the homogeneous reaction becomes important only at high values of T for very large value of R_Ω (this can also be achieved for much lower values of catalyst activity). This is intuitively expected as the only way to make the homogeneous and catalytic rates comparable (for fixed activation energies) is to reduce the catalytic activity either directly or through reduced surface area.

Figure 3-4 shows a typical bifurcation set in the plane of R_Ω and τ, calculated by fixing values of $T_{f,in}$ and $y_{A,in}$ and using stoichiometric feed of propane and oxygen. This bifurcation set is composed of two curves, both of which start out as straight lines with nonzero slopes and eventually become horizontal. The upper curve represents the ignition locus and the lower curve represents the extinction locus. From the governing equation (3.46), it can be seen that when the term containing the homogeneous reaction rate is small, only the ratio $\frac{\tau}{R_\Omega}$ matters for the bifurcation diagram and the bifurcation set. However, if the term due to homogeneous reaction term dominates

that due to the catalytic reaction, R_Ω becomes inconsequential. This explains why the ignition and extinction loci first behave as non-horizontal straight lines (catalytic dominance) and then turn into horizontal asymptotes for sufficiently large values of R_Ω (homogeneous dominance). Another salient feature is that the horizontal asymptote is not reached at the same value of R_Ω for the ignition and extinction loci. This can be accounted for by the fact that during ignition (on the quenched branches), only the catalytic reaction contributes but on the ignited branches both reactions contribute to the fuel conversion if the residence time is greater than that corresponding to the horizontal asymptote of the homogeneous ignition point ($\approx 0.01s$ in figure 3-4). We also note that the turnover from catalytic dominance to homogeneous dominance occurs at different R_Ω values on the quenched and ignited branches (and depends on the inlet temperature). In the next section, we observe that we can get double S shaped diagrams in a certain range of parameters where the diffusion time is finite and the residence time is small (much larger values of the transverse Peclet number) and we show that larger transverse Peclet numbers (or shorter contact times) are responsible for additional steady states when finite interphase gradients are present.

(d) Thermally coupled system:

In this subsection, a comprehensive analysis of both the one dimensional short monolith model and its lumped two-mode version is presented. Our calculations reveal that for both these models, aside from the standard S-shaped bifurcation diagrams that were shown in the previous section, we can also obtain double S-shaped bifurcation diagrams with two ignition and two extinction points. As stated earlier, the locations of these ignition and extinction points is of interest in the design and

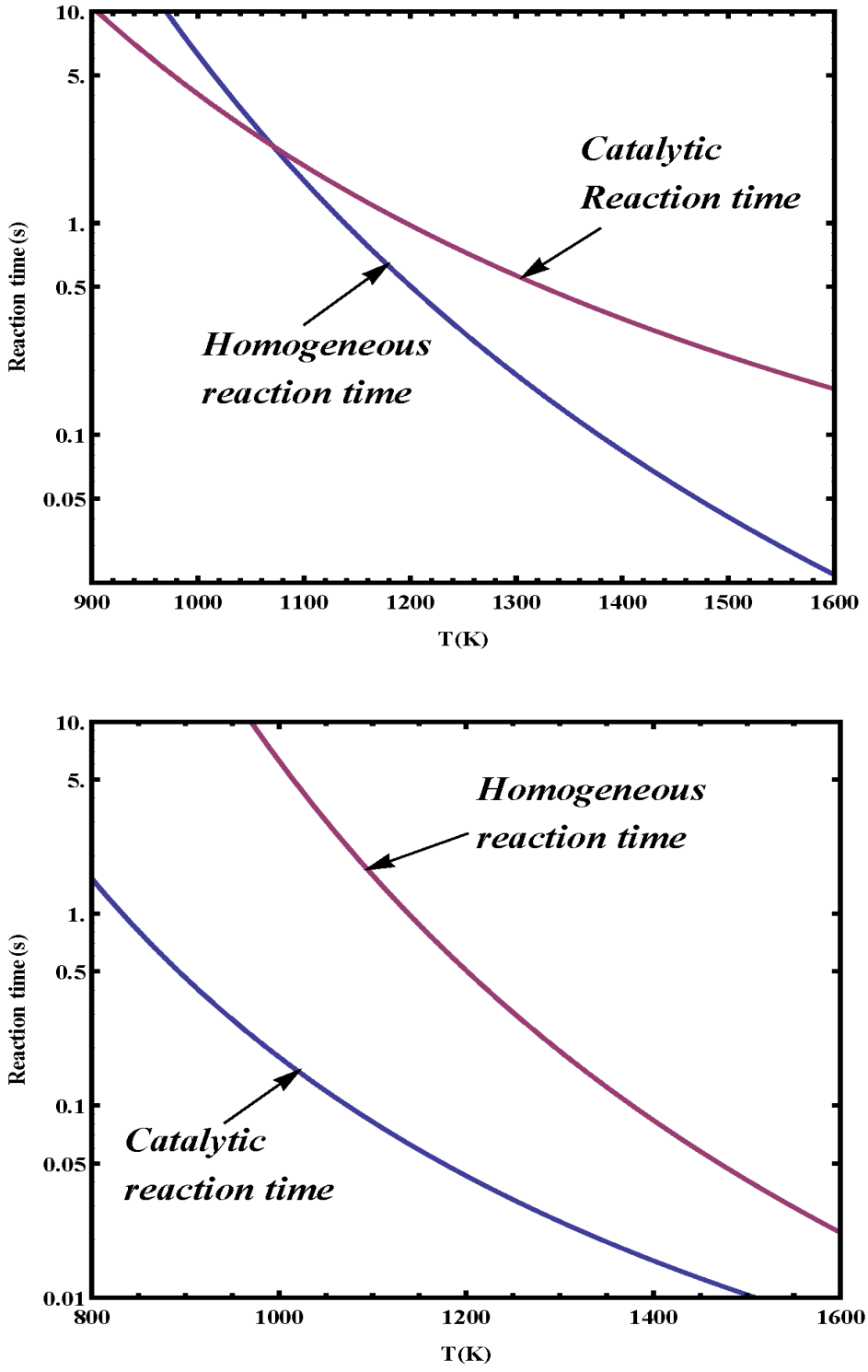

Figure 3-3: The characteristic reaction times of the catalytic and homogeneous reactions as functions of the temperature corresponding to $y_{A,in}$ =0.02 for (a)R_Ω =3 cm and (b) R_Ω = 1.32 mm.

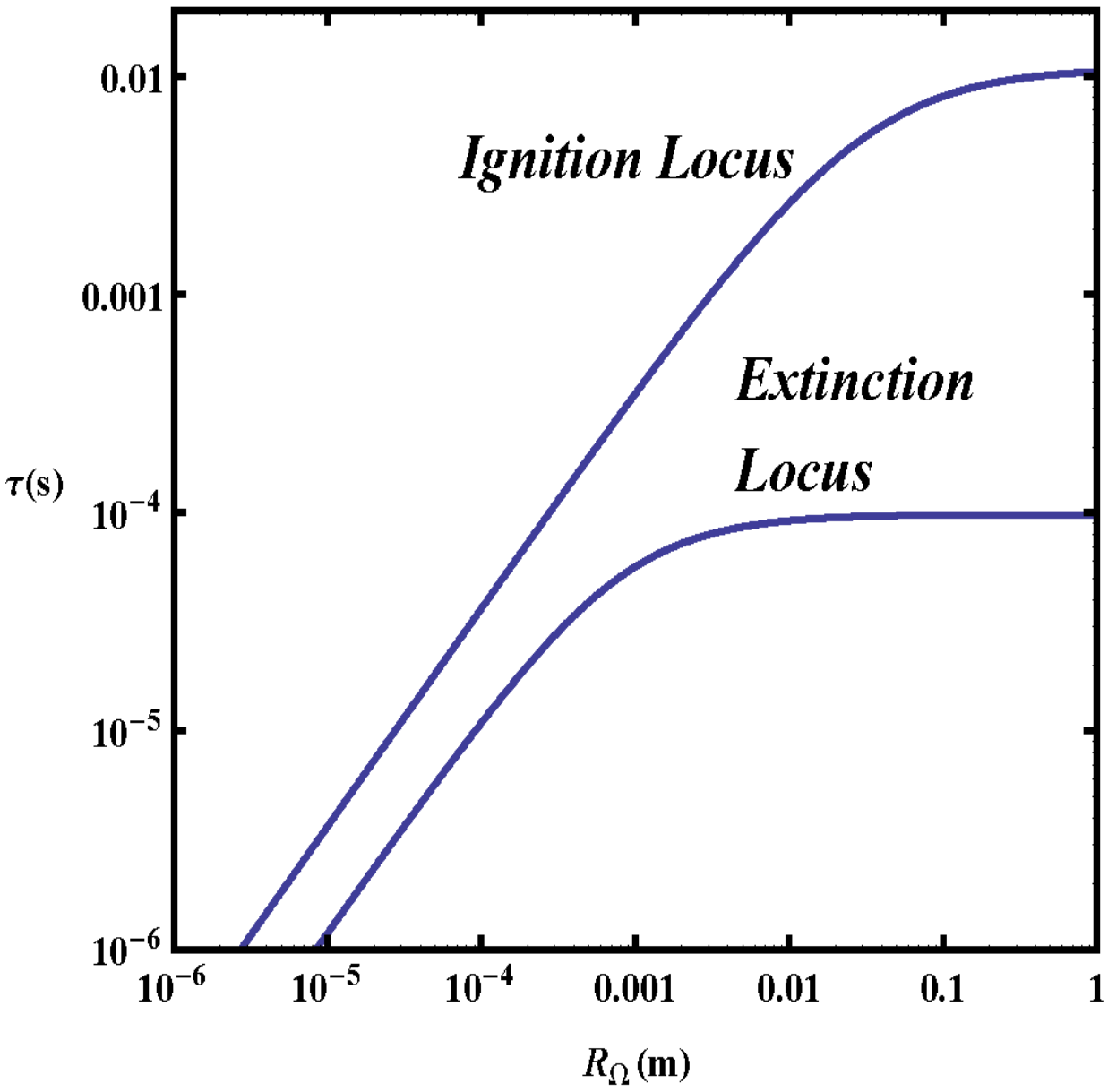

Figure 3-4: Bifurcation set for propane oxidation for inlet mole fraction of 0.02 and inlet temperature of 700 K in the residence time- hydraulic radius plane, when interphase gradients are neglected.

scale-up of reactors in which both catalytic and homogeneous reactions occur. The relevance of the diagram type where the second ignition is to the right of the first stems from the fact that we can then access an intermediate stable branch at which temperatures are comparatively low and the homogeneous reaction is not ignited (This behavior may also be of interest in partial oxidations with appropriate modifications in the reaction steps and kinetics). Another important bifurcation diagram is a double-S where the second ignition is to the left of the first. This means that the system jumps to the high temperature ignited branch upon the first ignition. This situation is of interest in the design of catalytically assisted burners.

We note that S and double-S bifurcation diagrams are persistent bifurcation diagrams in the unfolding of the singularity $g(x, \lambda) := x^5 - \lambda$ (Balakotaiah and Luss (1983), Golubitsky and Schaeffer (1985)). This makes us suspect the presence of this singularity in the phase space described by our model. According to the singularity theory with one distinguished variable (the bifurcation variable) the singularity $g(x, \lambda) := x^5 - \lambda$ has the universal unfolding given by

$$G(x, \lambda, \alpha, \beta, \gamma) := x^5 - \alpha x^3 - \beta x^2 - \gamma x - \lambda. \tag{3.51}$$

Here, x is the state variable and α, β and γ are the unfolding parameters that are necessary to describe all the persistent bifurcation diagrams of the system near the singular point. We show in figure 3-5 schematic diagrams of the seven types of bifurcation diagrams of x versus λ that exist next to the singular point.

To understand our combustion system in terms of the schematic diagrams of

figure 3-5, we need to find analogs of the variable x and the parameters α, β and γ. Let us first focus on the lumped version of the model. This model is described in terms of the state variable T_f and several control parameters. In this section, we take $T_{f,in}$ as the bifurcation variable [Bifurcation diagrams with residence time or the operating pressure as distinguished bifurcation variable are shown in later sections]. The auxiliary control parameters in the model, namely, the residence time, the inlet mole fraction of reactants, and the hydraulic radius of the channel can serve as the unfolding parameters [Remark: The pre-exponential factor and activation energy for the catalytic reaction, which can be varied by changing the catalyst properties can also be used as unfolding parameters but in this specific case, we take them as fixed.]. Solutions of equation (3.16) for fixed values of the auxiliary parameters leads to the bifurcation diagrams. Following the ignition and extinction points in the bifurcation diagram as one of the extra parameters is allowed to vary generates a bifurcation set. We have shown one such bifurcation set projected into the plane of inlet mole fraction-inlet temperature for $R_\Omega = 1.32$ mm and a residence time of 3 ms for standard kinetic parameters in propane oxidation (figure 3-6). Furthermore, we show a projection of the same bifurcation set in the plane of inlet mole fraction-solid temperature (figure 3-7, top) and a projection showing the difference between the solid phase and fluid phase temperatures as the inlet mole fraction of propane is changed (figure 3-7, bottom). Beyond a certain value of $y_{A,in}$, the catalytic extinction moves outside feasible region and leads to physically meaningless catalytic extinction points. This is why the curve corresponding to the catalytic extinction has not been continued for high $y_{A,in}$ values. The fact that the difference $T_S - T_f$ always stays

positive shows that along the entire locus, the solid phase is hotter than the gas phase as a result of the catalytic reaction being dominant for the parameters selected. The temperature difference between the two phases is especially large on the ignited branches. We have marked seven special points in the bifurcation set (figure 3-6): A and B representing hysteresis points, C and D, the double limit points and the three boundary limit points: E, F and G. As the variables in our model pass through the hysteresis point, the bifurcation diagrams undergo a transition from the situation where locally a single-valued solution curve as a function of the bifurcation variable (here $T_{f,in}$) is present to the case in which multiple solutions corresponding to some range of $T_{f,in}$ exist. We can now allow one more parameter to be freed and trace the locus of the hysteresis points as this parameter changes. Tracing the curve of points of intersection C and D from the bifurcation set generates a double limit locus. A double limit locus describes the occurrence of more than one limit point at a single value of the bifurcation variable (inlet temperature). As in the previous section, for sufficiently large residence times and inlet mole fractions, a bifurcation diagram may become impractical as a part of the diagram crosses 300 K. As before, we call the locus of points where the ignition or extinction points touch 300 K temperatures the boundary limit locus. Together the hysteresis, the boundary limit and the double limit loci constitute a complete phase diagram for the system and divide the phase space into various regions within which bifurcation diagrams are qualitatively similar. We have shown a complete phase diagram for the system at R_Ω of 1.32 mm in figure 3-8. Of the seven local bifurcation diagrams corresponding to the singularity above, five are possible in this phase diagram. We

have marked the regions corresponding to these by the letter denoting the diagram type from figure 3-5. The boundary limit locus classifies these five diagram types further, and regions where diagram (c) is observed, for instance, gets divided into three subregions denoted by (c1) through (c3). In theory, we obtain eleven qualitatively different regions. We note that the hysteresis region to the right to the boundary limit loci has no practical significance as the thermally coupled hysteresis moves to very low temperatures. Thus, for regions marked as (c1) and (b1) in figure 3-9, only a single ignition followed by a high temperature ignited branch are seen, and there is practically no difference between the bifurcation diagrams corresponding to the two regions. In figure 3-9, we show the bifurcation diagrams corresponding to the regions where double S-shaped bifurcation diagrams are observed. In figure 3-9, we have named the bifurcation diagrams with letters that match the archetypal bifurcation diagram shown in figure 3-5 in order to clarify the analogy between our model and the unfolding of the singularity. Case (c) corresponds to $y_{A,in}$ of 0.022 and τ of 5 ms, case (e) corresponds to $y_{A,in}$ of 0.026 and τ of 1 ms and case (g) corresponds to $y_{A,in}$ of 0.024 and τ of 0.2 ms. We note that for inlet mole fractions greater than 0.025, say, the adiabatic temperature rise is quite large, and therefore, on the ignited branches the temperatures reached are very high. Thus, although we have shown the full phase diagram for the sake of theoretical understanding and completeness, only the part of the diagram corresponding to inlet mole fractions below 0.025 may be physically relevant [We also note that bifurcation diagrams denoted as (d) and (f) in figure 3-5 can be observed only when a large enough value is selected for R_Ω so that the homogeneous reaction dominates or when the catalytic reaction rate is reduced

by a factor hundred or more, but we have not pursued this calculation].

We now show the phase diagram for the one-dimensional short monolith model in figure 3-10. It is obvious that this phase diagram is very similar to figure 3-8. There is a slight increase in the regions of multiplicity which can be attributed to the fact that approximations to transverse gradients using heat and mass transfer coefficients were used in the lumped model. All the calculations till now use flat velocity profiles. In figure 3-11, we show the computed phase diagram for the case of a fully developed velocity profile. The first catalytic portion of the hysteresis locus is almost unchanged, while the parabola-shaped thermally coupled portion of hysteresis has slightly moved up compared to the previous phase diagrams. This can be attributed to the fact that the Sherwood number (or the mass transfer coefficient) for a parabolic velocity profile is less than that for a flat velocity (see Gupta and Balakotaiah, 2001). Less concentration flux to the wall where the catalytic reaction takes place leads to less temperature rise in the fluid phase and hence, a later ignition due to the homogeneous reaction. Thus, our calculations for the one-dimensional short monolith model reveal very similar bifurcation features to the lumped model both qualitatively and quantitatively. This vindicates our extensive use of the lumped model and shows that the heat and mass transfer coefficients are indeed very useful to simplify models and study bifurcation phenomena. In the rest of this chapter and the next, we confine ourselves to lumped models as our main goal to understand qualitatively the bifurcation phenomena.

Before we close this subsection, let us make a comment about the 1D model with axial gradients only. That model is valid in the limit of $P \rightarrow 0$ and does not

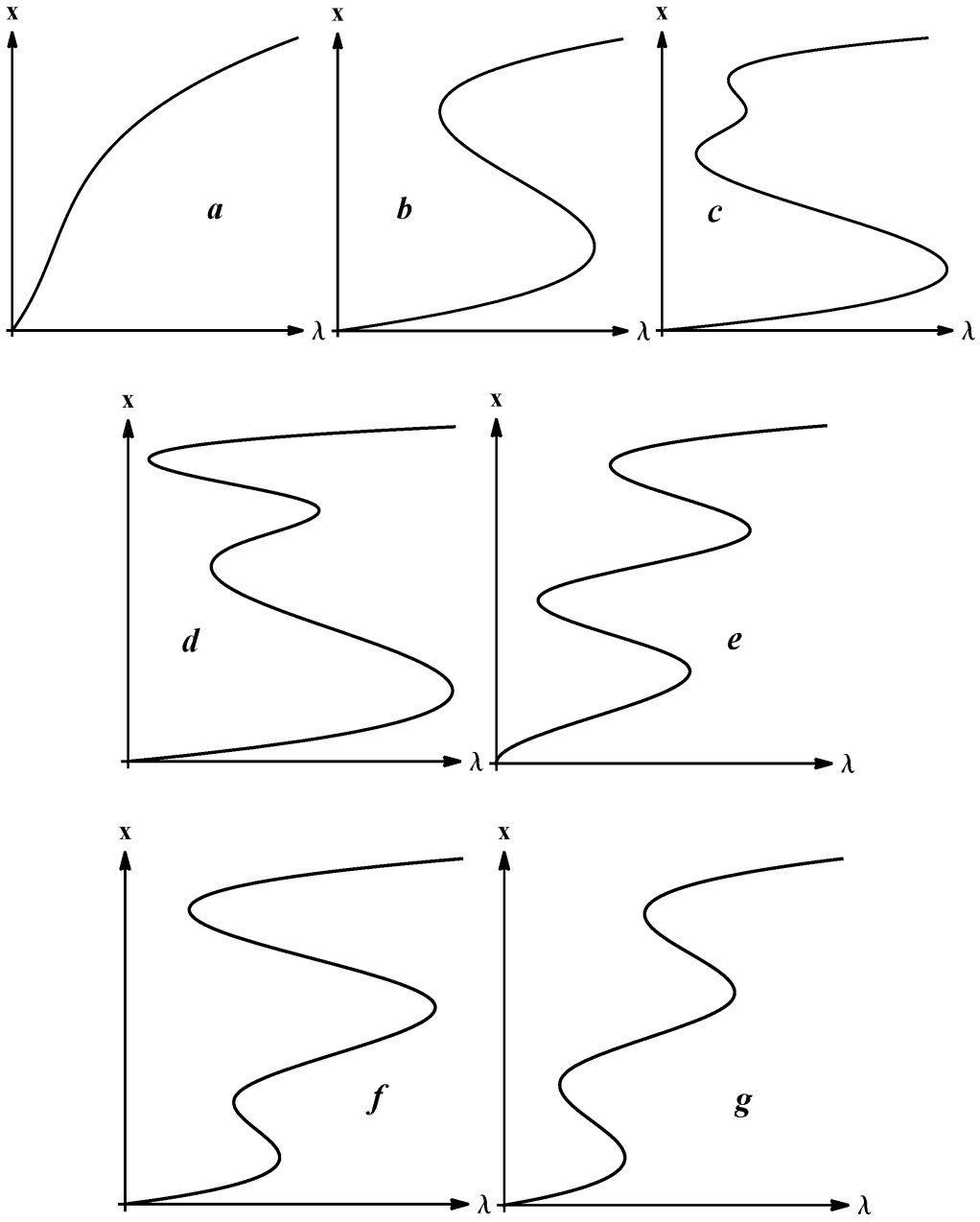

Figure 3-5: Schematic Bifurcation diagrams that exist in the unfolding of the singularity $x^5 - \lambda = 0$.

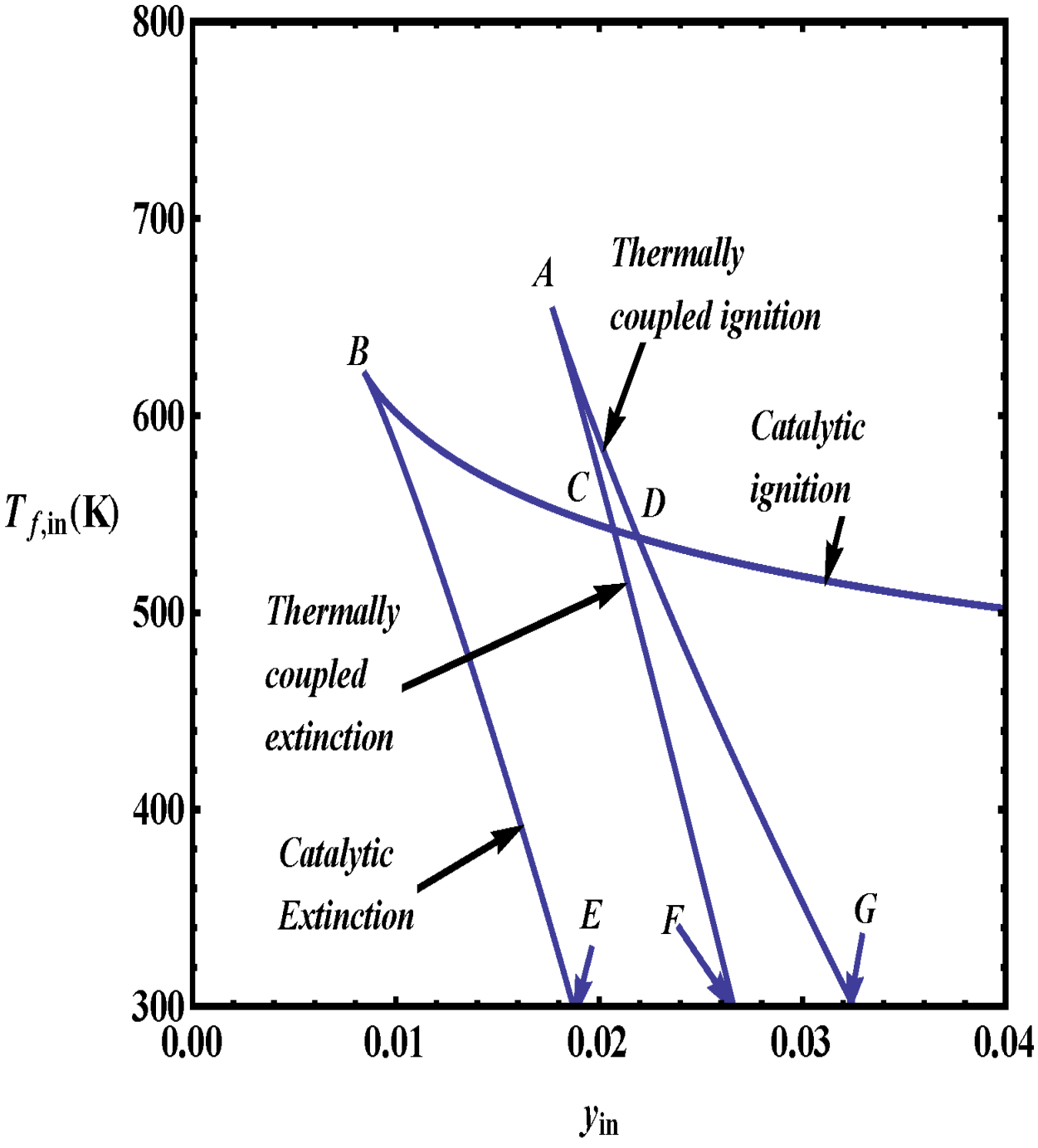

Figure 3-6: Projection of the bifurcation set (ignition/ extinction locus) for propane oxidation for residence time of 3 ms and hydraulic radius of 1.32 mm in the inlet temperature- mole fraction plane.

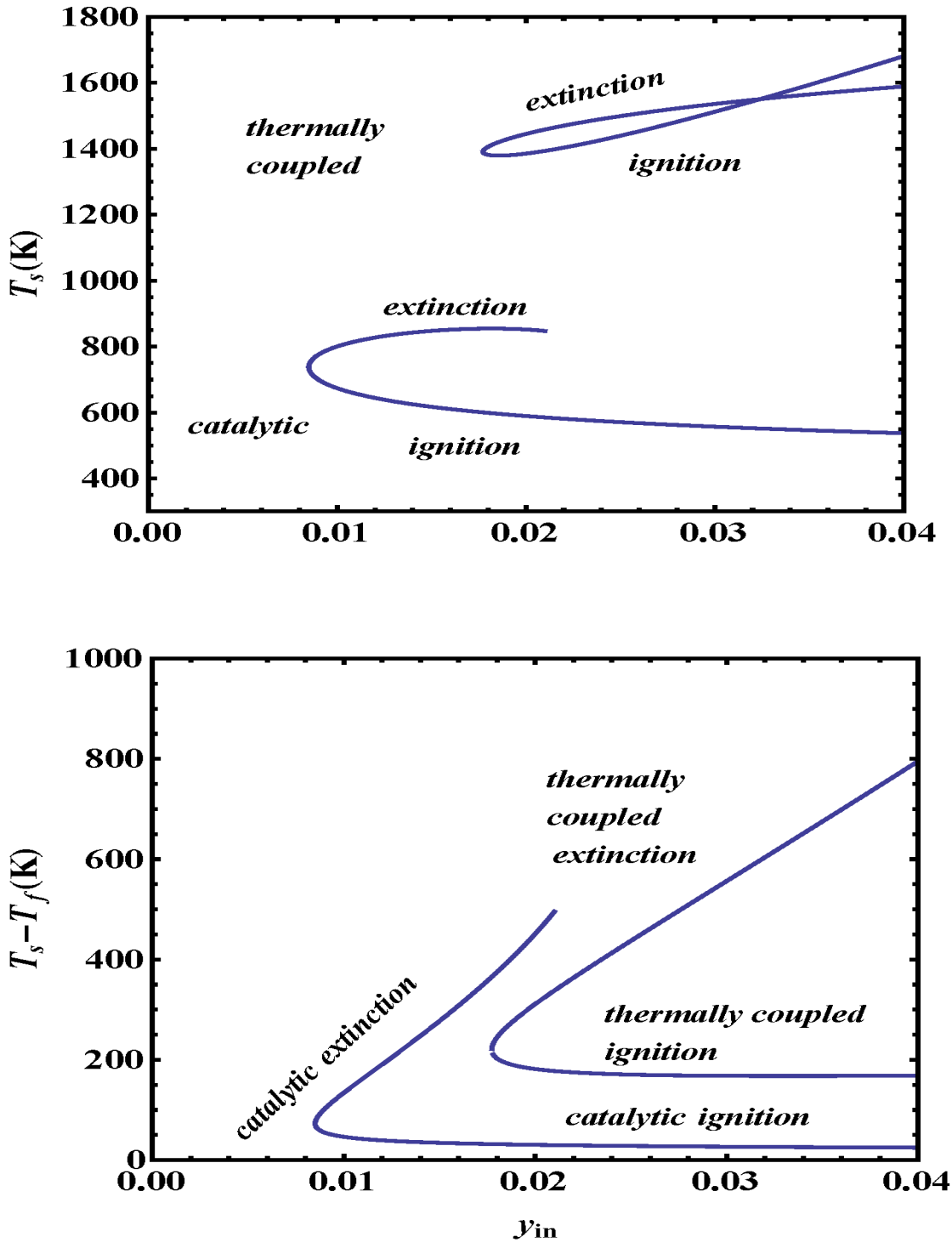

Figure 3-7: Projections of the bifurcation set for propane oxidation for residence time of 3 ms and hydraulic radius of 1.32 mm in the solid temperature- mole fraction plane (top) and difference of solid and gas temperatures- mole fraction plane (bottom).

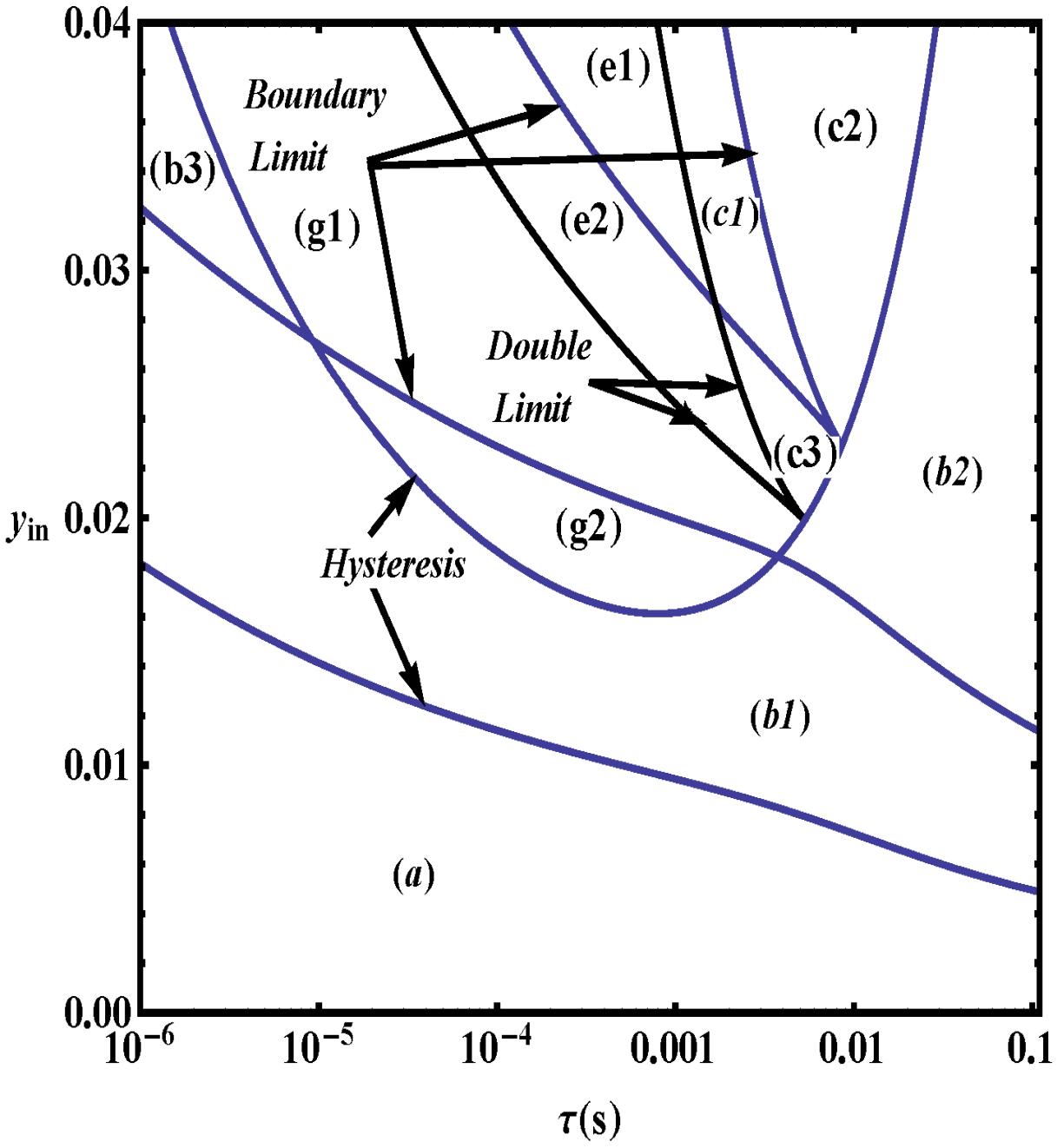

Figure 3-8: Phase diagram for classification of different possible bifurcation diagrams of state variables (conversion, fluid/solid temperature) versus inlet temperature forpropane oxidation for hydraulic radius of 1.32 mm.

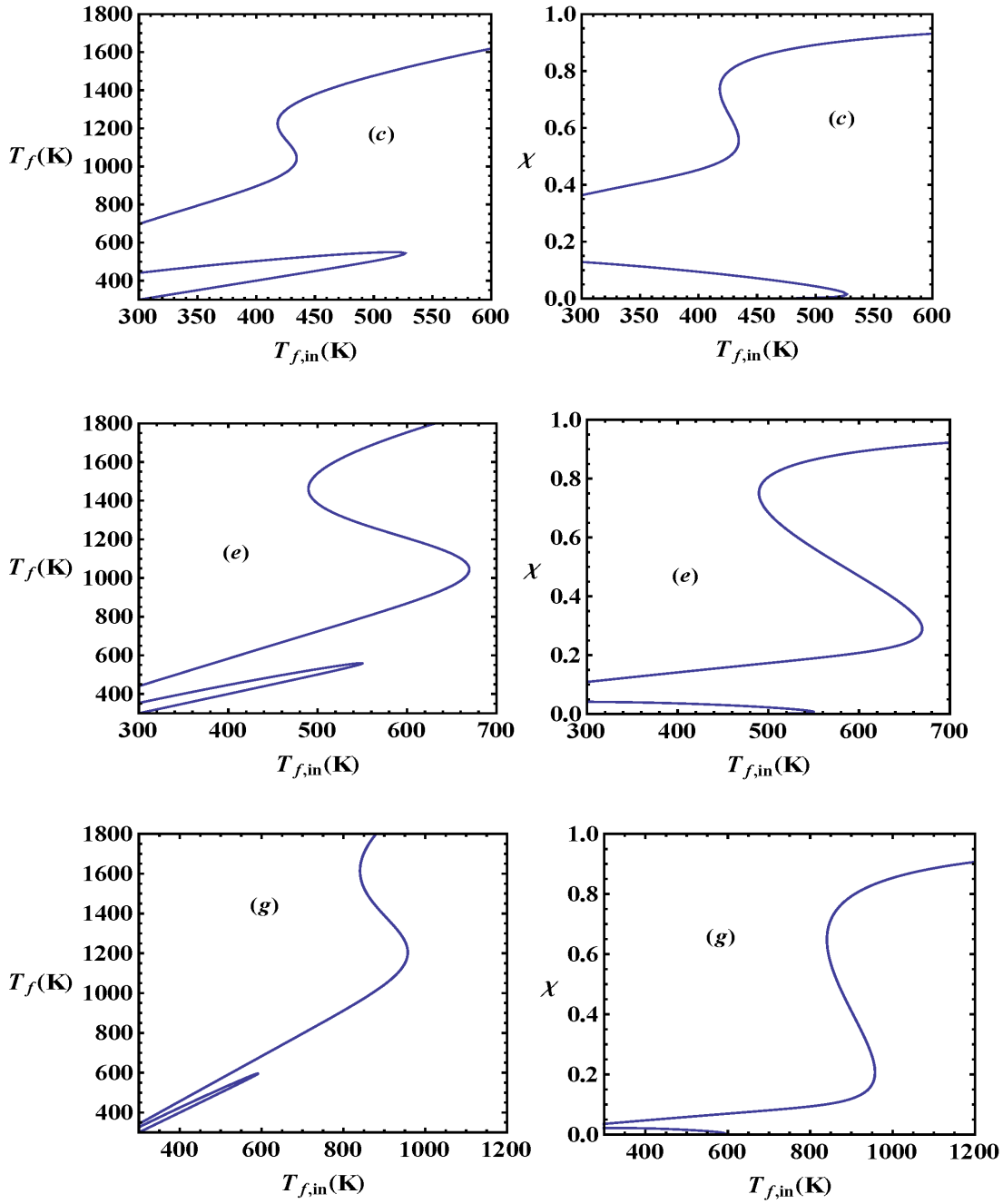

Figure 3-9: Bifurcation diagrams of the exit fluid temperature (T_f) and conversion versus the feed temperature ($T_{f,in}$) for propane oxidation for (c) $y_{A,in}$= 0.022 and τ= 5 ms, (e) $y_{A,in}$= 0.026 and τ= 1 ms and (g) $y_{A,in}$= 0.024 and τ= 0.2 ms.

consider any interphase gradients. We find that only S-shaped bifurcation diagrams are possible (the bifurcation behavior is very similar to that shown in section 3.3 (c)). This is because when the channel spacing is small, the catalytic reaction completely dominates the homogenous reaction and the catalytic reaction is never mass transfer controlled. Thus the thermal coupling effects that lead to double S shaped bifurcation diagrams never come into the picture. A single catalytic hysteresis locus is observed. As such the behavior of this model is not so interesting and we choose not to show calculations for bifurcation diagrams or higher order singularities.

(e) Effect of channel hydraulic radius on thermal coupling:

We repeat the calculation of the hysteresis loci for different values of the hydraulic radius, R_Ω and note that the parabolic shape obtained keeps shrinking as the channel hydraulic diameter decreases. Upon consistently decreasing the hydraulic radius, we find that the hysteresis locus is always composed of two disconnected smooth curves, one resembling a straight line in log-linear scale and the other resembling a parabola (as in figure 3-8). For brevity, we will refer to them as the lower and the upper branch, respectively. It is notable that the catalytic contributions to the hysteresis locus can be observed to be almost unchanged from the hysteresis with only catalytic reaction taking place. This means that (for the values of the kinetic parameters used) the homogeneous reaction does not influence the onset of multiplicity (or ignition/ extinction) due to catalytic reaction. This can be interpreted as meaning that at low inlet fuel mole fractions and temperatures, the two reactions start off behaving like sequential and uncoupled processes due to much higher activation energy of homoge-

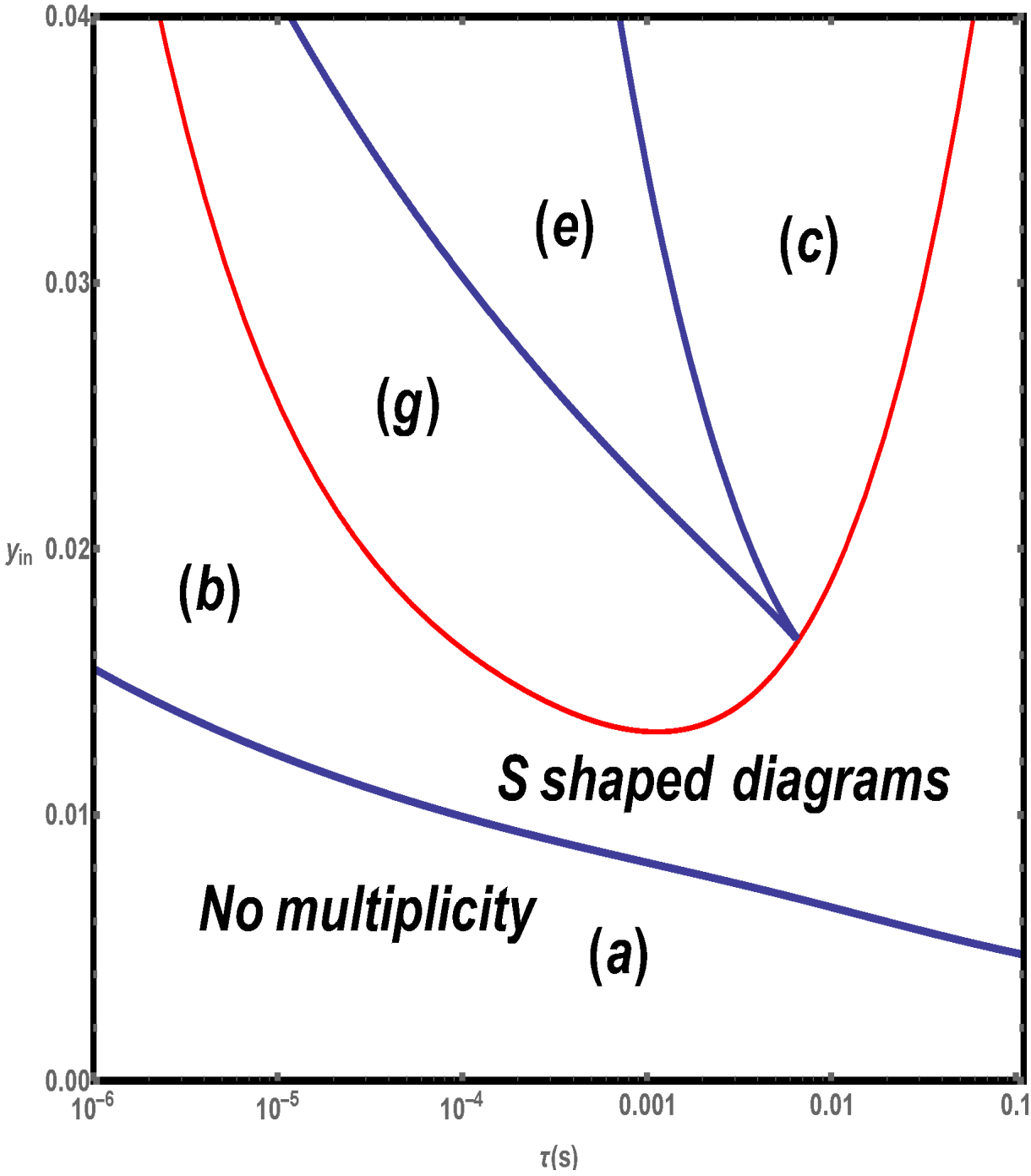

Figure 3-10: Phase diagram for the 1-D short monolith model with transverse gradients (for flat velocity) for propane oxidation with R_Ω of 1.32 mm in the plane of residence time and inlet mole fractions of propane.

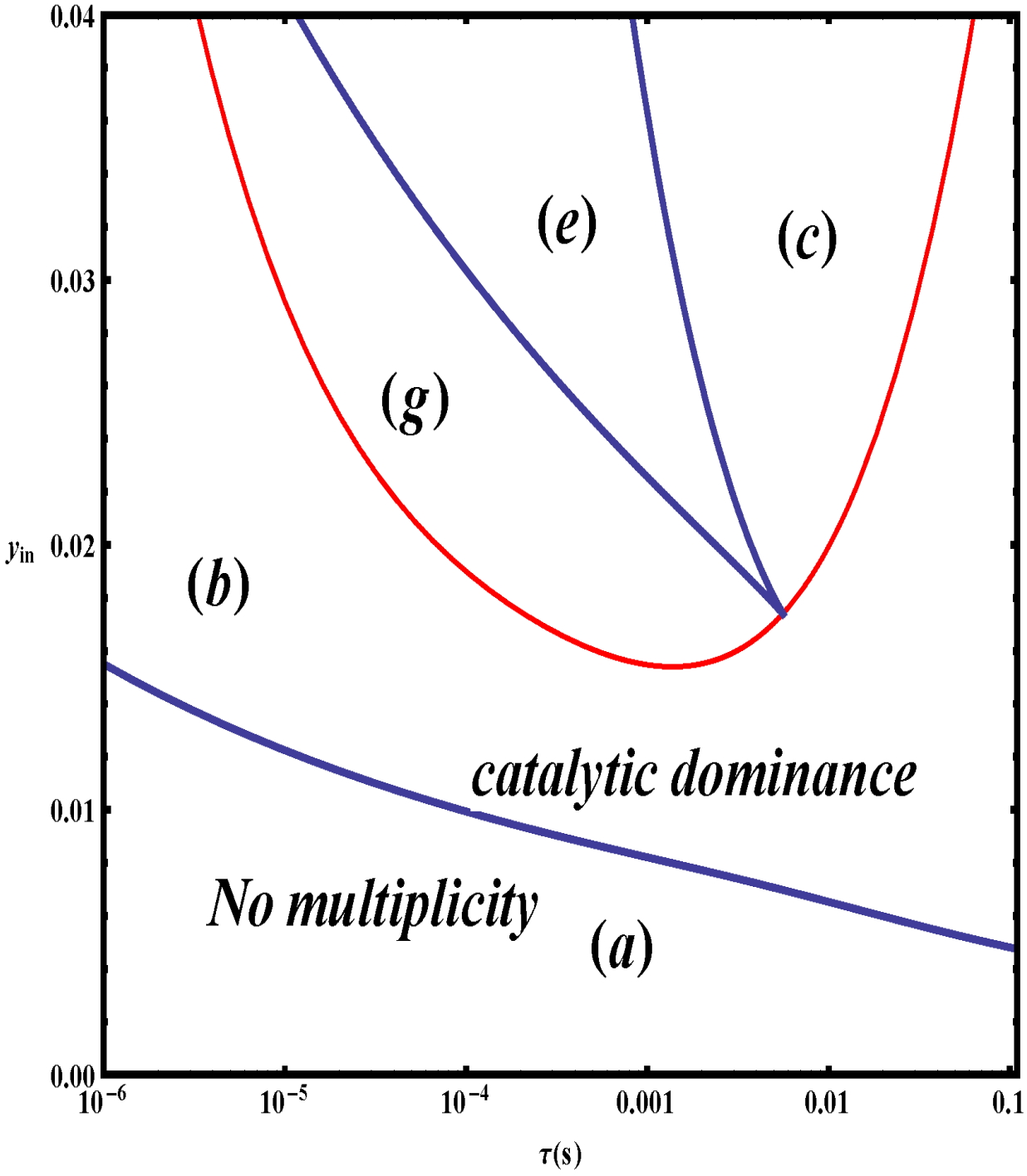

Figure 3-11: Phase diagram for the 1D short monolith model with parabolic velocity profile for propane oxidation with R_Ω of 1.32 mm in the plane of residence time and inlet mole fractions of propane.

neous reaction, but at higher inlet mole fractions (or ΔT_{ad}), both reactions operate side by side and influence each other.

In section 3(a), we showed that the homogeneous hysteresis (figure 3-1) by itself shows a monotonic behavior, namely the residence time at hysteresis decreases as the inlet mole fraction of propane is increased. However catalytically assisted combustion shows a parabola-like hysteresis locus. We contend that this change is due to coupling between the catalytic and homogeneous chemistry. In figure 3-12, we show a comparison of the thermally coupled portion of the hysteresis loci for the cases of just homogeneous chemistry and for the catalytically assisted combustion for R_Ω values of 1320 μm and 264 μm. As the value of R_Ω decreases, the thermally coupled portion of hysteresis shrinks and moves up. At sufficiently small values of R_Ω like 50 μm, we do not observe the upper branch at all. This means that as the channel diameter decreases, the gradients between the two phases become smaller, until eventually we reach the limit of the homogeneous model analyzed in the previous section. Further, in this region, the bifurcation features are completely dominated by the catalytic reaction [Remark: From the discussion in the previous section, it can be seen that the coupled hysteresis locus can only exist in the region corresponding to $P > 1$, i.e. when the catalytic reaction is mass transfer controlled. Thus, the right branch of the parabola (in figure 3-12) may be termed "catalytically limited homogeneous hysteresis" while the left branch is much closer to the hysteresis for homogeneous reaction only]. One important observation from figure 3-12 is that for practical cases where fuel mole fraction is below 0.03, the thermally coupled hysteresis does not exist for R_Ω values below 264 μm (curve a). A second important observation from figures 3-8

and 3-12 is that most numerical simulations of propane oxidation in the literature using more detailed model with spatial gradients or micro-kinetics were for smaller values of R_Ω (below 264 μm) and higher residence times (0.1 to 1s) corresponding to regions (b1) and (b2) of figure 3-8 (see for example,Karagiannidis et al., 2011). In this region of parameter space, ignition (as well as extinction) is mainly dictated by catalytic chemistry alone and (as explained further in the next section) depending on the inlet temperature and fuel mole fraction, both reactions may contribute to the fuel conversion on the ignited branches.

(f) Residence time as bifurcation variable :

We have analyzed the system behavior with feed temperature as the bifurcation variable as it can be changed easily both in laboratory experiments as well as in large scale system. In this analysis, the inlet fuel mole fraction, channel hydraulic diameter and residence time (or flow rate/space velocity) are taken as fixed (unfolding) parameters. While there are advantages to this analysis (e.g. the bifurcation diagrams are qualitatively the same when the system is close to adiabatic or when heat losses are small and $T_{f,in}$ can be varied more easily and in a wider range than other operating variables), the independence of the variables from axial variation is a limitation of the models of this chapter. However, we can obtain insight on the axial variation of the state variables and the correct qualitative picture of the appropriate profiles by taking the residence time as the bifurcation variable. As residence time is directly proportional to the length of the reactor for a fixed velocity, changes in residence times are analogous to varying axial positions in more detailed models with axial gradients. While this does not mean exact prediction of features of more

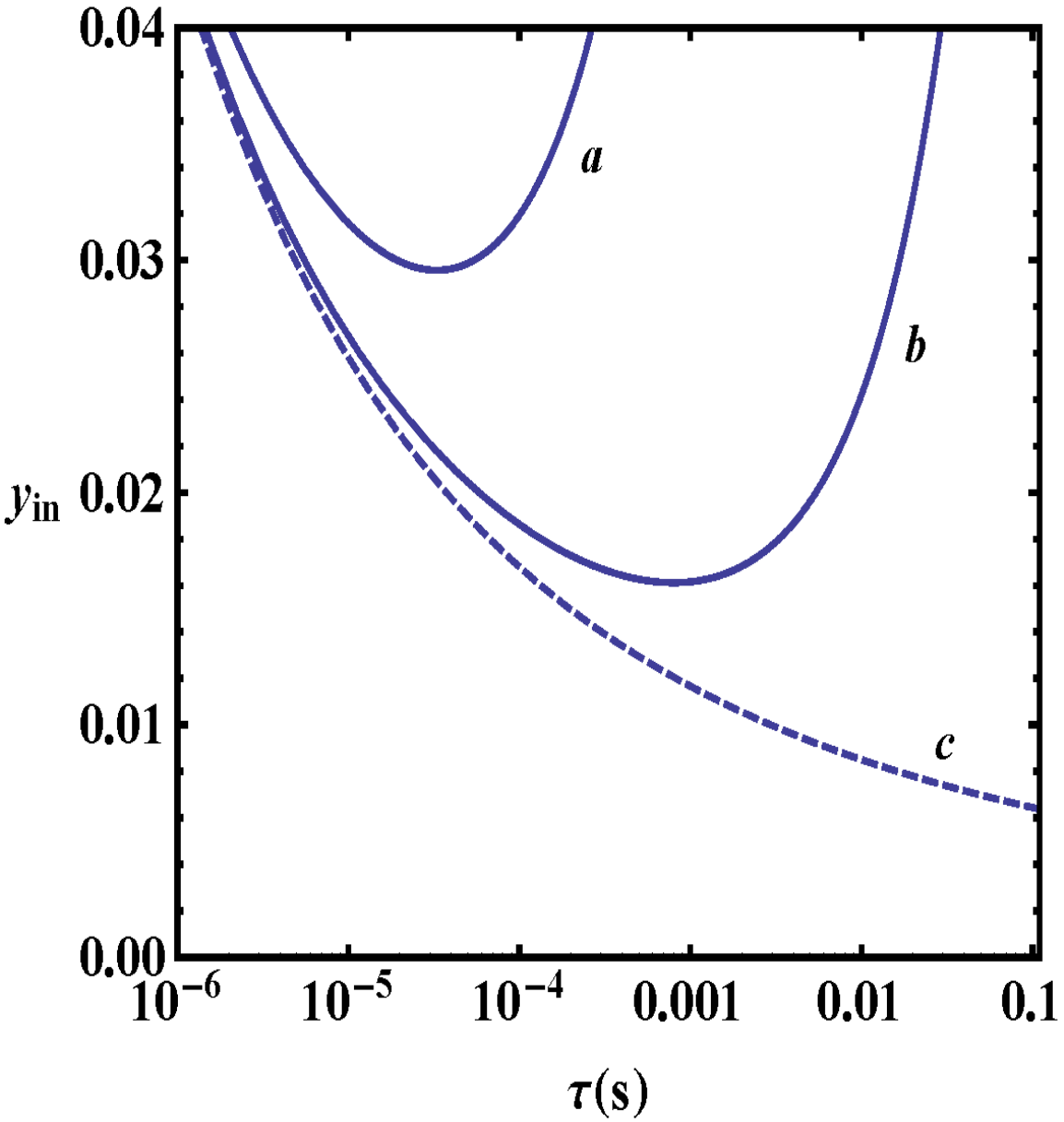

Figure 3-12: Comparison of the coupled catalytic-homogeneous portion of the hysteresis loci for propane oxidation for (a) R_Ω = 264 μm and (b) R_Ω = 1.32 mm with (c) the hysteresis locus for the homogeneous reaction alone.

complex models with spatial gradients (in the flow direction) can be done using a lumped model, some important qualitative features can still be studied by interpreting residence time as taking on the role of length/location along the flow direction. This is certainly meaningful for the adiabatic case considered here. For example, for the case of a single step homogeneous or catalytic reaction only, the lumped model always predicts the profiles qualitatively and even the quantitative differences are small (e.g. for homogeneous singe step reaction, the difference between the ignition points predicted by the two extreme cases of axial Peclet numbers of zero (CSTR) and infinity (PFR) models is only a factor 2.718 in residence time or about 10 to 15K in temperature. The same analogy applies for the catalytic reaction only case in both the kinetic and mass transfer controlled regimes, see for example Gupta et al., 2001). Further, when residence time is the bifurcation variable, as shown in by Balakotaiah et al. 1995, the spatial profiles of the distributed model can be inferred from that of the lumped model. Thus, in this section, we analyze the bifurcation behavior briefly using the residence time as a bifurcation variable. [Remark: As stated in the model formulation section, when the interphase gradients are negligible, the temperature profile ($T_f = T_s = T$) is obtained by integration of the initial value problem (that follows from equation 3.46):

$$\begin{aligned} \frac{dT}{d\tau} &= (\Delta T^*_{ad}) \left\{ \begin{array}{c} \epsilon_f \times k_{0h} \exp\left[-\frac{E_h/R}{T}\right] y_A^n y_B^m \\ +\epsilon_f \times \frac{k_{0s}}{R_\Omega} \exp\left[-\frac{E_c/R}{T}\right] y_A^{n'} y_B^{m'} \end{array} \right\}, \\ T &= T_{f,in} \quad \text{at } \tau = 0. \end{aligned} \tag{3.52}$$

While this model always has a unique solution (and is structurally unstable, as mentioned earlier), the two-mode version of this model (or the addition of transverse) gradients, as in boundary layer models, leads to an index infinity differential-algebraic system that has an infinite number of solutions (see Gupta et al., 2001, Gupta and Balakotaiah, 2001). When either axial or axial and transverse diffusion (conduction) are included (and Danckwerts' boundary conditions are used in the flow direction), and the axial Peclet numbers are not high, the bifurcation features of the 1-D/2-D (elliptic) model are again similar to the lumped model discussed here (see Gupta et al., 2001, Balakotaiah et al. 1995).]

We show in figure 3-13 three bifurcation diagrams (of solid, fluid temperatures and conversion versus residence time) for different inlet temperatures. In case (a), the inlet temperature is low ($T_{f,in} = 400K$) and hence the catalytic reaction requires longer residence times to ignite (with ignition at $\tau = 1.2s$). However, after ignition, the conversion is nearly unity as the inter-phase gradients are small in this region of high residence times (or length along the flow direction) and the minimum residence time needed to get complete conversion in the mass transfer controlled regime $\frac{R_\Omega^2}{D_{m,j}} = 0.035s$ is much smaller than the actual residence time. Interphase temperature gradients still exist at residence times (or distances) much smaller than $0.035s$. Also, the profiles of fluid temperature and conversion are similar to the upper branch of the bifurcation diagram (when local residence time is scaled by the total residence time to obtain dimensionless distance along the reactor). We also note that the logarithmic scale used in these figures resolves the profiles much better than linear scales used in most literature studies. For example, with a residence time of 1s, the solid temper-

ature profile on the ignited branch will appear nearly flat on a linear scale and solid and fluid temperatures differ only in the front 1% of the length and fuel conversion is nearly complete in the front 10% of the length. Further, the homogeneous reaction shows no ignition by itself but contributes to the reactant conversion for fluid temperatures exceeding about 1100K. However, by the time the fluid temperature reaches $1100K$, 70% of the reactant is already converted by the catalytic reaction (with the solid temperature still higher than fluid temperature) and both reactions contribute to the conversion of the remaining fuel. We also note that the extinction point is at extremely short residence times (four orders of magnitude in length or velocity) and is determined by the catalytic chemistry alone. As the inlet temperature is increased to $500K$ (case (b)) the bifurcation diagram contains four limit points with the homogeneous reaction also having ignition and extinction. However, these homogeneous limit points occur for residence times lower than that at the (first) catalytic ignition (at $\tau = 1.83 \times 10^{-2}s$). Thus, the system goes to high conversion state upon first ignition with both homogeneous and catalytic reactions contributing to the reactant conversion. [Remark: The two extinctions, first the homogeneous and then catalytic, can be observed only when the residence time (velocity) is decreased (increased)]. As the inlet temperature is increased further to $600K$, the catalytic reaction ignites at very short residence time (or length) of $\tau = 2.1 \times 10^{-4}s$ (and enters the mass transfer controlled regime) but the conversion and temperature in the fluid phase increase only slowly until the homogeneous reaction also ignites at $\tau = 4.3 \times 10^{-3}s$ and $T_f \approx 1000K$, $T_s \approx 1470K$ and about 40% conversion of the reactant.

At sufficiently high inlet temperatures, the residence time at the ignition point

of the catalytic reaction becomes exponentially small and the catalytic reaction is in the mass transfer controlled regime from practically $\tau = 0$. Further, the separation between the catalytic and homogeneous ignition becomes larger (or the the hysteresis loops are clearly separated with the catalytic ignition/extinction at extremely short residence times compared to homogeneous case). This is shown in figure 3-14 (a) for $T_{f,in} = 700K$. In the same figure, we have also shown the rates of the homogeneous and catalytic reactions along the bifurcation diagrams. It is obvious from figures 3-14 (b) and (c) that the catalytic reaction ignites at much lower residence times (or shorter distances) than the homogeneous reaction. Also the catalytic reaction rate upon ignition is about four times larger than that of homogeneous reaction upon ignition. The two rates become comparable only around $1100K$ and then the homogeneous reaction dominates (but with only a small amount of fuel left). Upon repeating this calculation for different values of $T_{f,in}$ (though we have not shown it here for brevity), we found (as expected) that this temperature at which the two reaction rates become comparable is always achieved at around 1100 K, and changes only with R_Ω (moving to higher values with increasing R_Ω).

In order to illustrate further how the homogeneous and catalytic chemistry separately contribute to the fuel conversion, we show in figure 3-15, bifurcation diagrams for $T_{f,in} = 700K$ in the thermally coupled system (top), the system with catalytic reaction alone (middle), and the system with homogeneous reaction alone (bottom). These calculations were done with stoichiometric feed, $y_{A,in} = 0.02$, R_Ω of 500 μm and ϵ_f of 0.83 so as to make some qualitative comparisons between our calculations with the stability maps presented in Karagiannidis et al. (2011). Their calculations

with channel flow microreactors take heat losses into account. However, the adiabatic system appears as a special case when the external heat transfer coefficient is zero. The stability maps presented in Karagiannidis et al. (2011) always show one ignition-extinction pair for the systems they consider. We are unable to match their calculated residence times for ignition or extinction with our calculations of thermally coupled or catalytic reaction system. In fact, in our model, catalytic chemistry ignites and attains a mass transfer controlled regime at much lower residence times than the limit points shown in Karagiannidis et al. (2011). We believe that this disparity is due to different catalytic kinetics considered in Karagiannidis et al. (2011) than the global kinetic model used in our calculations [Remark: Another possible reason for the disagreement may be the mesh resolution used in the calculations. Our calculations in figure 3-15 indicate that in order to observe catalytic ignition and extinction in a 1-D or 2-D model with Danckwerts' boundary condition at the inlet and a residence time of about $1s$, one need to use about 10^6 or more mesh points in the axial direction alone. We also note our model becomes more accurate at short residence times]. However, we note that the ignition and extinction points calculated by our model where only the homogeneous chemistry is acting shows good agreement with the limit points in the stability map presented in Karagiannidis et al. (2011). We present more detailed comparisons in the next chapter on methane oxidation where we consider lean feed as well as combustion at higher pressures.

(g) Infinitely fast catalytic reaction:

The final limiting case we consider is that of infinitely fast wall reaction. First, as we have already illustrated above, this limiting case is not realistic at lower feed

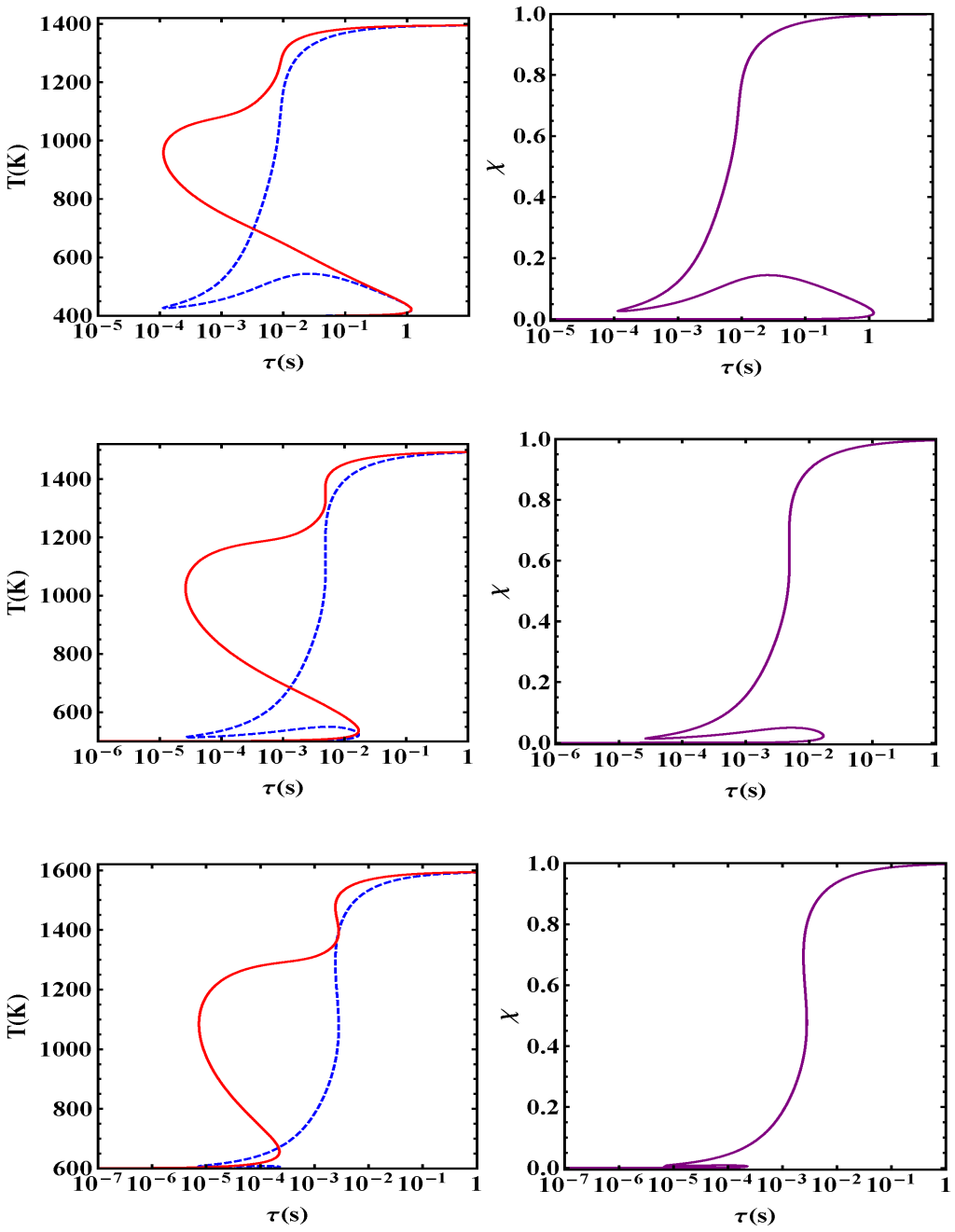

Figure 3-13: Bifurcation diagrams of fluid temperature (dashed lines), solid temperature (solid lines) and conversion (χ) versus the residence time (τ) for $y_{A,in}$ =0.02, R_Ω= 1.32 mm and $T_{f,in}$ = 400 K (top), 500 K (middle) and 600 K (bottom).

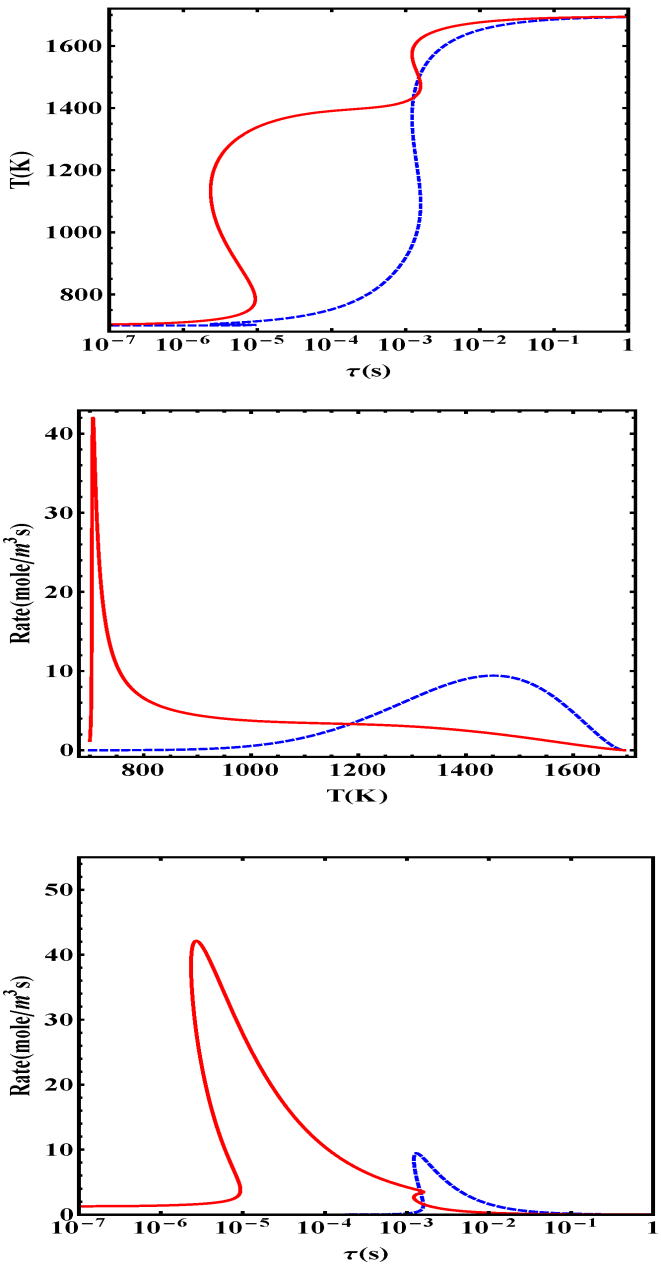

Figure 3-14: Bifurcation diagrams ((a)) of the exit fluid temperature (dashed lines) and solid temperature (solid lines) versus the residence time (τ) and reaction rates along them ((b) and (c)) for $y_{A,in}$= 0.02, $T_{f,in}$= 700 K and R_{Ω}=1.32 mm.

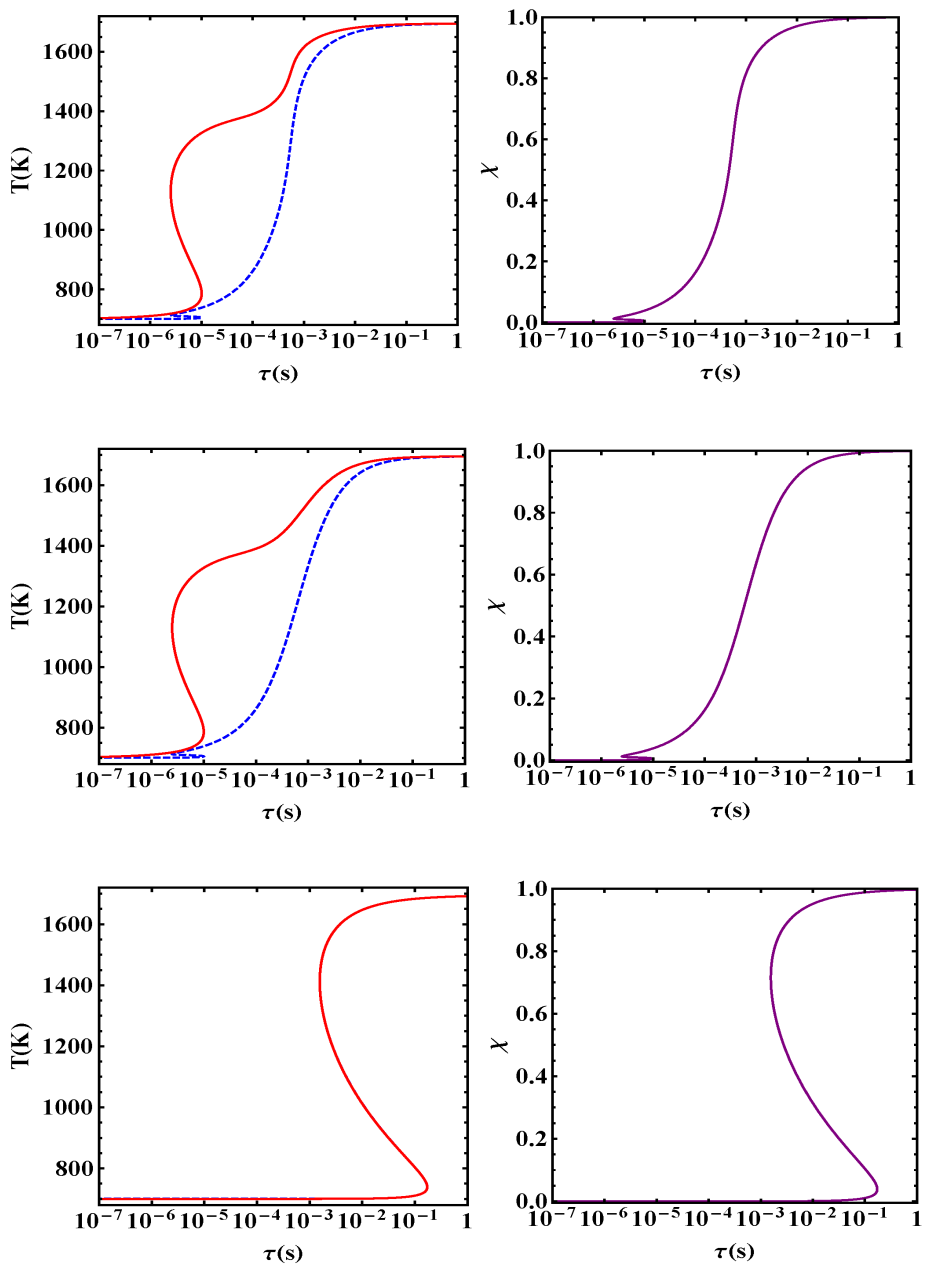

Figure 3-15: Bifurcation diagrams of the exit fluid temperature (dashed lines), solid temperature (solid lines) and conversion (χ) versus the residence time (τ) for propane oxidation for $y_{A,in} = 0.02$. R_Ω= 500 μm and $T_{f,in}$= 700 K. The top figure corresponds to thermally coupled system, the middle figure to the case when only catalytic reaction operates, and the bottom picture to the case when only homogeneous reaction operates.

temperatures where the catalytic reaction may not ignite for short residence times. For longer residence times and lower inlet temperatures, the catalytic reaction ignites but the conversion is nearly unity on the ignited branch. However, for higher inlet temperatures, as illustrated in figures 3-13 and 3-15, the catalytic reaction ignites very near the inlet and is practically in the mass transfer controlled regime over the entire length of the monolith. Thus, while the bifurcations due to catalytic reaction may be eliminated with the assumption of infinitely fast wall reaction, there is an advantage in analyzing this limiting case as it avoids the numerical difficulties associated with calculation of the catalytic ignition and extinction points. A second reason we consider this case is that it can reveal the utility as well as any limitations of our 0-D 2-mode model by comparing the predictions with the asymptotic analysis and CFD computations presented in the literature, see for example the work of Zheng and Mantzaras (2014). Again, for simplicity, we consider here only propane oxidation with stoichiometric feed. In this case, as already noted above, the assumption of infinitely fast reaction corresponds to setting $y_{As} = 0$ and simplifies the steady-state equation to

$$F_\infty(T_f, \mathbf{p}^*) \equiv \tau(\Delta T_{ad}^*) \left[\frac{\epsilon_f r_h(y_A, y_B, T_f)}{C_0} + k_{cA} a_v y_A \right] - (T_f - T_{f,in}) = 0 \qquad (3.53)$$

with y_A and $y_B (= \nu y_A)$ defined by Eq.(3.11).

Since the bifurcation analysis of Eq.(3.53) is similar to that of the homogeneous reaction only (the main difference being the extra mass transfer term), we present

only some sample results for comparison with literature values. We show in figure 3-16 (A) (top left diagram) the hysteresis curves for three values of R_Ω ($1320\mu m$, $900\mu m$ and $600\mu m$) and note that these are practically the same as those shown in figure 3-12 with finite rate of wall reaction. This confirms our earlier explanation, i.e. the upper branch of hysteresis locus corresponds to the ignition of the homogeneous reaction with catalytic reaction already in the mass transfer controlled regime. Figure 3-16 (parts B, C and D) compares the bifurcation diagrams of solid and fluid temperatures as well as fuel conversion as a function of residence time with and without the assumptions of infinitely fast catalytic reaction for parameter values corresponding to $R_\Omega = 600\mu m$, $T_{f,in} = 600$ K and $y_{A,in} = 0.02$ (typical to the case considered in Zheng and Mantzaras (2014), except for the pressure]. As expected, even at this high inlet temperature, the difference between the two cases is large at short residence times (near the inlet to the channel).

Zheng and Mantzaras (2014) present asymptotic analysis as well as numerical calculations for the case of propane (as well as other fuels) oxidation using detailed models that account for flow development effects as well as physical property variations and homogeneous chemistry but with the assumption of infinitely fast catalytic reaction. These authors discuss the possibility that when the Lewis number for the limiting reactant is larger than unity, the temperature of the fluid (e.g. at the center of the channel) can exceed that of the wall leading to super-adiabatic temperatures in the gas phase. The model analyzed here, which uses only two temperatures to measure transverse gradients, does not predict such solutions (if they exist). As stated in the model formulation section, this limitation of the two-mode model can

be removed by using the three-mode model. However, it should also be pointed out that super-adiabatic conditions may occur only either in a very narrow range of parameters or not at all. We observe that in predicting the superadiabatic conditions, Zheng and Mantzaras make several unrealistic assumptions such as infinitely fast wall reaction (not valid at low temperatures) and negligible axial diffusion/conduction (or no upstream diffusion effects) which are known to lead to physically (or thermodynamically) inconsistent results. We discuss these issues further in Chapter 5 after discussing methane oxidation in the next chapter.

3.4 Summary and discussion

To sum up, the following important observations follow from the bifurcation analysis of propane oxidation:

(i) For the rate expressions we have used and for the values of R_Ω below 1.32 mm, the catalytic reaction dominates, and the first ignition is due to catalytic reaction alone. The lower branch of hysteresis locus is nearly the same as that obtained by considering only the catalytic reaction.

(ii) For the kinetics used in this work, thermal coupling between the homogeneous and catalytic oxidation can occur either for higher values of R_Ω and/or at short contact times and/or higher inlet mole fractions.

(iii) When the catalytic reaction dominates, the solid phase temperature at ignition or extinction is always larger than the gas phase temperature. [Since the Lewis number for propane oxidation is greater than unity, the surface/solid temperature after ignition is lower than the adiabatic value, as can be seen in figures 3-13, 3-14 and

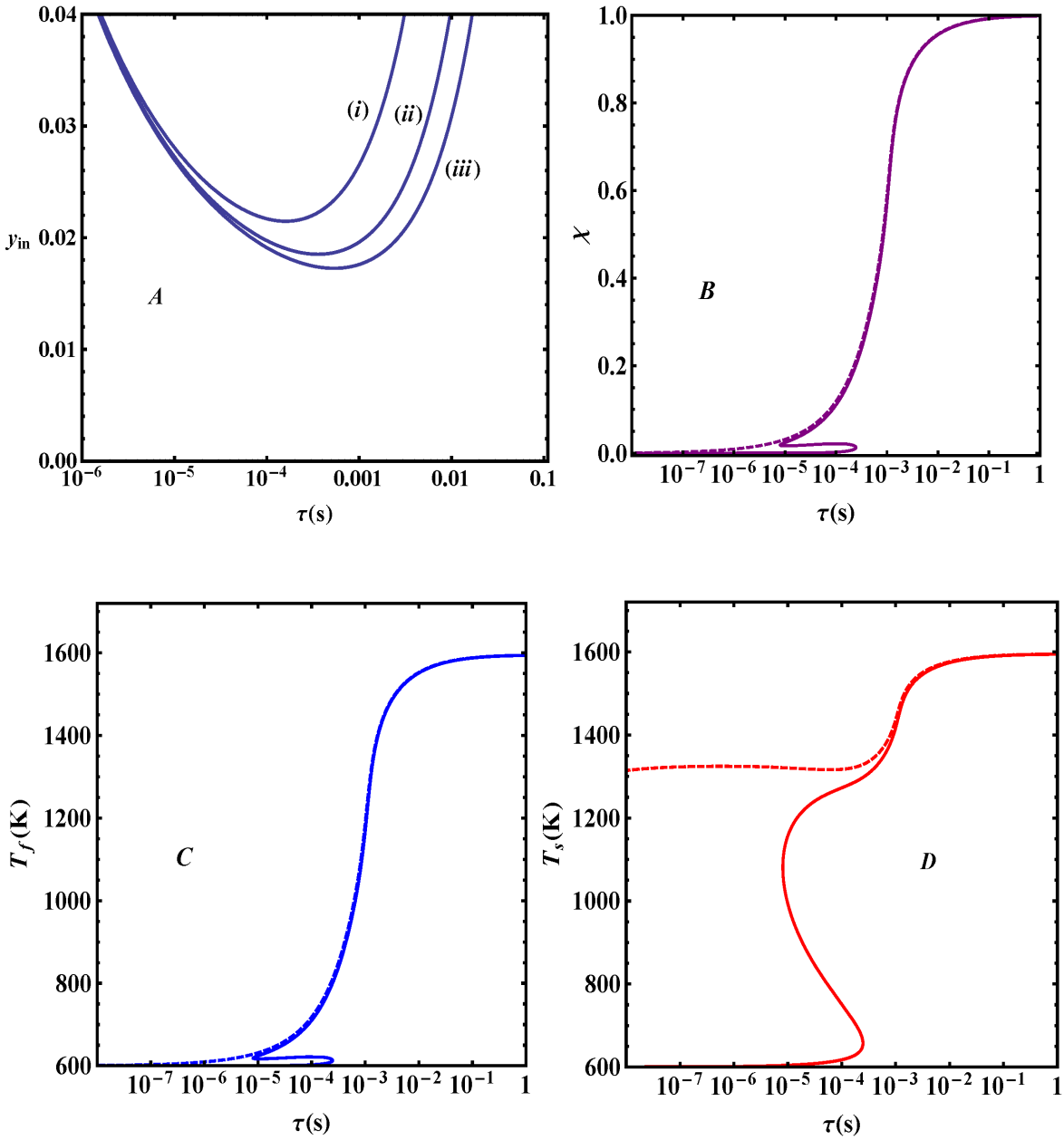

Figure 3-16: For the case of infinitely fast wall reactions, hysteresis loci for R_Ω of (i) 600μm, (ii) 900 μm and (iii) 1.32 mm, and bifurcation diagrams (solid lines for finite catalytic rates) with R_Ω=600 μm, $y_{A,in} = 0.02$ and $T_{f,in} = 600$ K.

3-15. Further, when residence time is taken as the bifurcation variable, no isolated branches can exist in the adiabatic case. However, this is not the case when the Lewis number is less than unity (especially if it is less than 0.5 as in the case of hydrogen oxidation). Also, the case of fluid temperature being higher than solid temperature can occur when the homogeneous reaction dominates. This case as well as the conditions for existence of super-adiabatic temperatures is left for future investigations].

(iv) For certain values of parameters (inlet temperatures, residence time and inlet mole fractions), we can obtain a stable intermediate temperature branch where only the catalytic reaction is ignited and the conversion of the reactant is much lower than unity. The rest of the thermally coupled region of hysteresis leads directly to a high conversion, high temperature branch.

Chapter 4

Bifurcation Analysis for Oxidation of Methane

4.1 Analysis of bifurcation features of methane oxidation with a Pt based catalyst

In this chapter, the important practical case of methane oxidation is examined for the case of both lean and rich feeds with the operating pressure as the bifurcation variable and the predicted results are compared with available experimental results and calculations based on CFD models in the literature.

Having analyzed the phase space of propane oxidation system in the last chapter, we can now follow the same procedure for methane oxidation. Calculation of bifurcation diagrams, bifurcation sets and hysteresis loci for methane oxidation requires no methodological changes and yields results that are qualitatively very similar to the case of propane oxidation when we use kinetic parameters values from Westbrook and Dryer, 1981 and Hiam et al. 1968 (henceforth referred to as the base case). [Remark: In addition to changes in the activation energies, the maximum fuel mole fraction in a stoichiometric feed is now 0.095]. However in industrial settings, methane ox-

idation is often carried out using catalysts based on transition metal oxides rather than precious metals. These transition metal oxides tend to have lower activity when compared to precious metals based on which the rate expressions in Westbrook and Dryer, 1981 and Hiam et al. 1968 have been calculated. Therefore in this section, we also show bifurcation features of systems where the catalytic reaction rate is hundred and thousand times smaller than those estimated in Hiam et al. 1968. For brevity, we only present some sample calculations and some comparisons with literature for the base case where the results are similar to those presented above for propane oxidation because the catalytic reaction dominates over the homogeneous. We then discuss bifurcation features when the catalyst loading is decreased from the base case and note the qualitative differences that appear. In the next section we show bifurcation calculations using the more commonly used transition metal catalysts.

We start by showing a computed phase diagram for the base case for $R_\Omega = 1.32$ mm in figure 4-1. The hysteresis diagram in figure 4-1 again consists of two disconnected curves: one that looks linear and another that looks parabolic. A narrow double limit locus of the same shape as that in figure 3-9 also exists, but we have not shown it here. We also plot a comparison of the thermally coupled portion of the hysteresis diagrams for methane oxidation as the channel hydraulic radius is decreased (figure 4-2). This diagram is analogous to figure 3-11, except for the fact that it takes lower values of R_Ω to make the hysteresis diagram move out of the plane of feasible mole fractions and residence times.

If we lower the catalyst loading to make the reaction rate hundred times less than that in the base case, we still encounter a hysteresis locus of the same shape as those

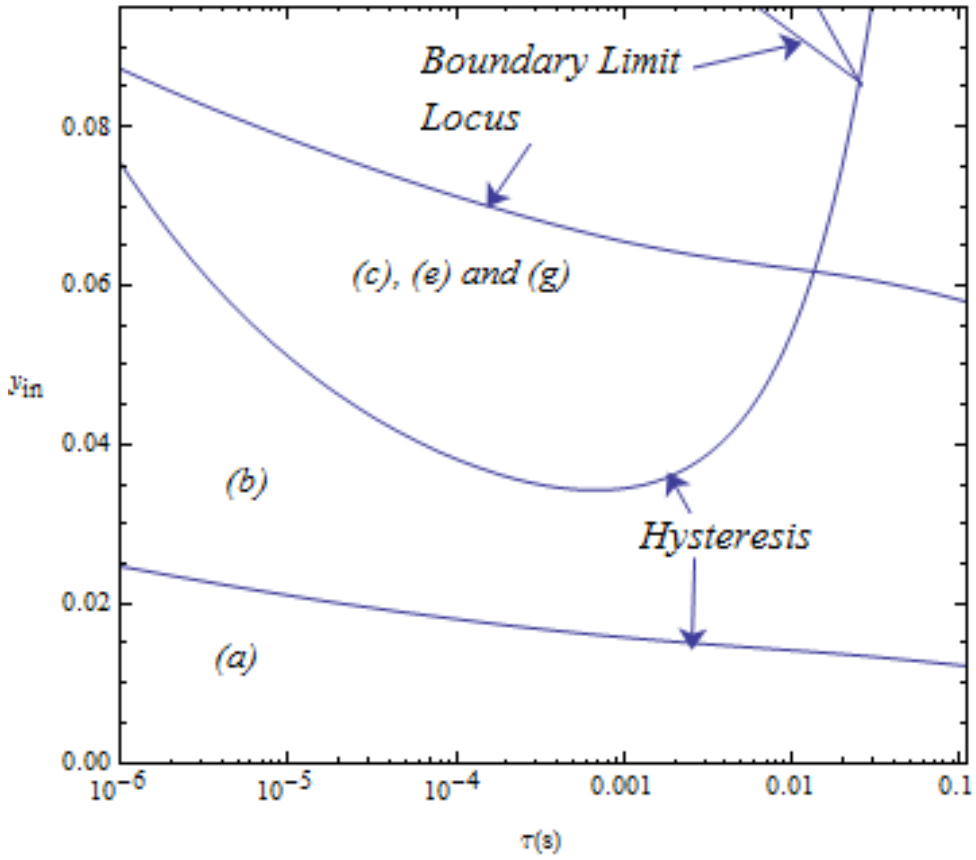

Figure 4-1: Hysteresis and boundary limit locus for methane oxidation for R_Ω of 1.32 mm with $k_{0h} = 1.15 \times 10^{10}\ s^{-1}$ and $E_h/R = 25356\ K$ and $k_{0s} = 6 \times 10^6\ m/s$ and $E_c/R = 16204\ K$.

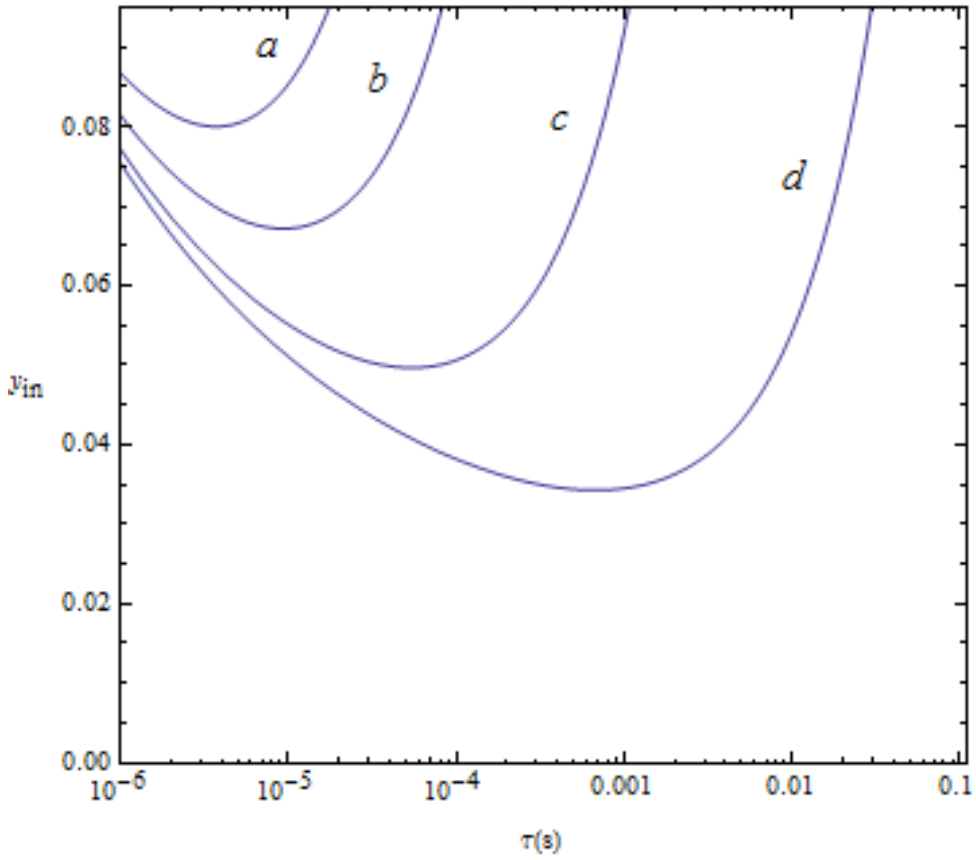

Figure 4-2: Comparison of the coupled catalytic-homogeneous portion of the hysteresis loci for methane oxidation for R_Ω of (a) 60 μm, (b) 100 μm, (c) 264 μm and (d) 1.32 mm, respectively.

presented above. To avoid redundancy, we instead show a bifurcation set for the system with $k_{0s} = 6 \times 10^4 m/s$ with R_Ω of 400 μm in the plane of inlet temperature and residence time when the inlet mole fraction of methane is fixed at 5 % (figure 4-3). We have marked three special points in the diagram: points A, B and C which are hysteresis points. As the residence time is varied, there is only one hysteresis point for a single value of inlet mole fraction of methane. However the thermally coupled portion of the bifurcation set admits two hysteresis points, meaning that for the same value of y_{in}, as τ is varied two hysteresis points are possible. This is an obvious consequence of the parabolic shape of the typical hysteresis loci shown above. Also the thermally coupled portion of the bifurcation set is shaped like a crescent. Its narrow width indicates that the region of thermally coupled hysteresis is very small.

If we decrease the catalyst loading further and reduce the k_{0s} to be $6 \times 10^3 m/s$, a change in the shape of the phase diagram is observed (figure 4-4. There are still two disconnected portions of the hysteresis locus, but the lower of these is now due to homogeneous reaction. This is verified by comparing the hysteresis diagrams when only the homogeneous reaction operates to the thermally coupled case. No appreciable changes in the hyperbola-shaped lower branch of the hysteresis curve is observed when catalytic reaction is turned off. The upper branch of the hysteresis locus no longer looks parabolic and instead has two smooth components joining each other sharply at a point. In figure 4-4, this sharp point is marked as point A. It is a higher order singularity at which the hysteresis point is the result of three limit points merging together (The analogous point in Catastrophe Theory is called a Swallowtail. Singularity Theory with a distinguished variable, however, refrains from using any

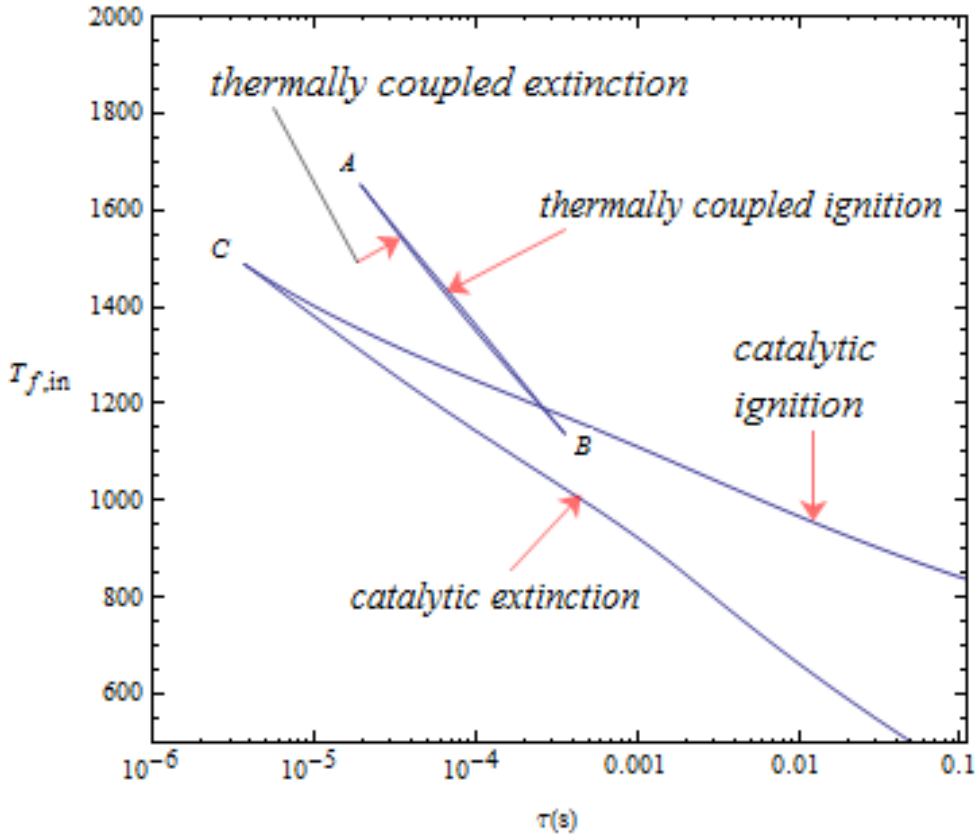

Figure 4-3: Bifurcation set for methane oxidation in the plane of inlet temperature and residence times when the catalyst activity is lowered to make $k_{0s} = 6 \times 10^4 m/s$ and $y_{A,in} = 0.05$ and $R_\Omega = 400\mu m$.

names for this singularity). The double limit locus is also of a different type in this case- it starts at point A and consists of just a single curve, demarcating two different regions of five steady states. Calculation of bifurcation diagrams in these two regions yields the archetypal diagrams (d) and (f) shown in figure 3-5, which could not be obtained in the calculations for propane oxidation. In contrast to propane oxidation, we now have a "homogeneously-assisted catalytic combustion". We have shown two typical bifurcation diagrams corresponding to the thermally coupled region in figure 4-5 - case (i) corresponds to the archetypal diagram (d) and case (ii) corresponds to the archetypal diagram (f). Note that both these bifurcation diagrams have been shown here only to illustrate the configurations of various ignitions and extinctions; from a practical standpoint, both diagrams in figure 4-5 are useless.

To explain why the dramatic change from the usual phase diagram occurs in this case, we compare the hysteresis loci due to homogeneous reaction acting alone with those for catalytic reaction acting alone for three different values of k_{0s} : 6×10^6 m/s, $6 \times 10^4 m/s$ and 6×10^3 m/s when the hydraulic radius is fixed at 400 μm (figure 4-6). We notice that for the case of $k_{0s} = 6 \times 10^6$ m/s, the catalytic hysteresis is much below the homogeneous hysteresis curve, meaning that the system is dominated by the catalytic reaction. In the case of $k_{0s} = 6 \times 10^4$ m/s, the location of hysteresis curve is somewhat comparable to homogeneous hysteresis and our calculations show that the thermally coupled hysteresis diagram obtained in this case has a lower (almost linear) branch that is very close to the hysteresis due to catalytic reaction alone. However when k_{0s} is taken to be 6×10^3 m/s, the homogeneous hysteresis is strictly below the catalytic hysteresis and the system is dominated by homogeneous reaction

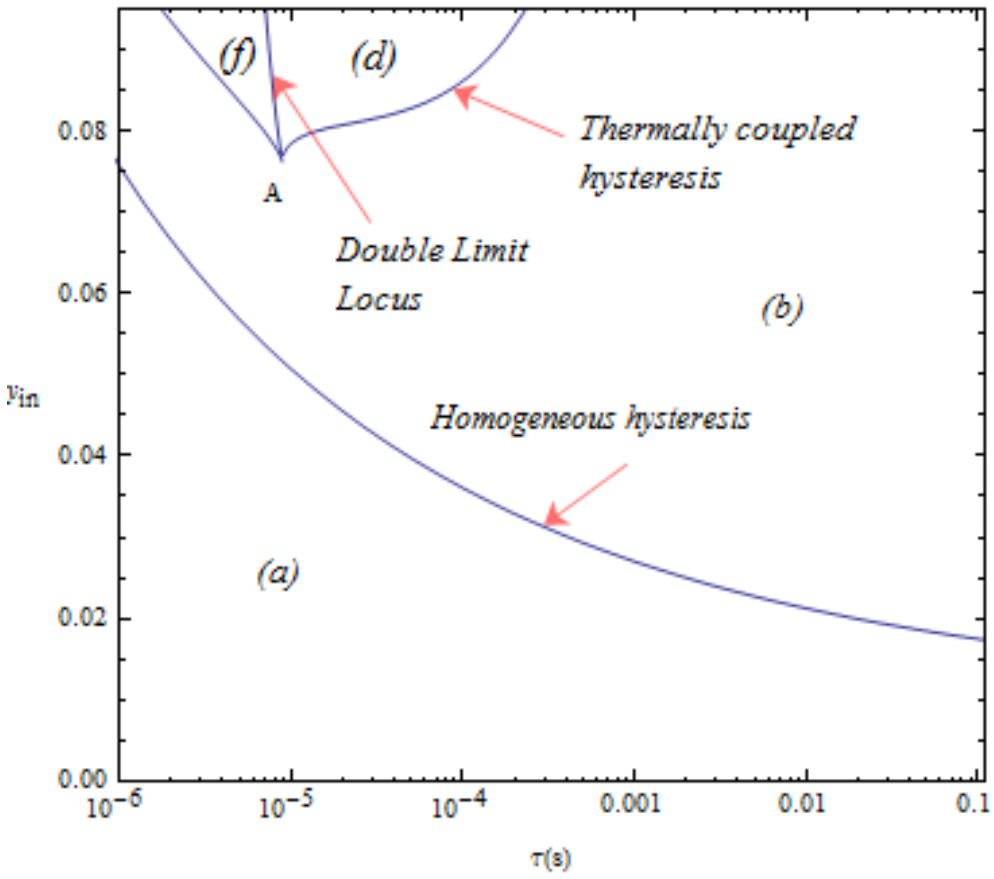

Figure 4-4: Hysteresis and double limit locus for methane oxidation for R_Ω of 400 μm with $k_{0h} = 1.15 \times 10^{10}\ s^{-1}$ and $E_h/R = 25356\ K$ and $k_{0s} = 6 \times 10^3\ m/s$ and $E_c/R = 16204\ K$.

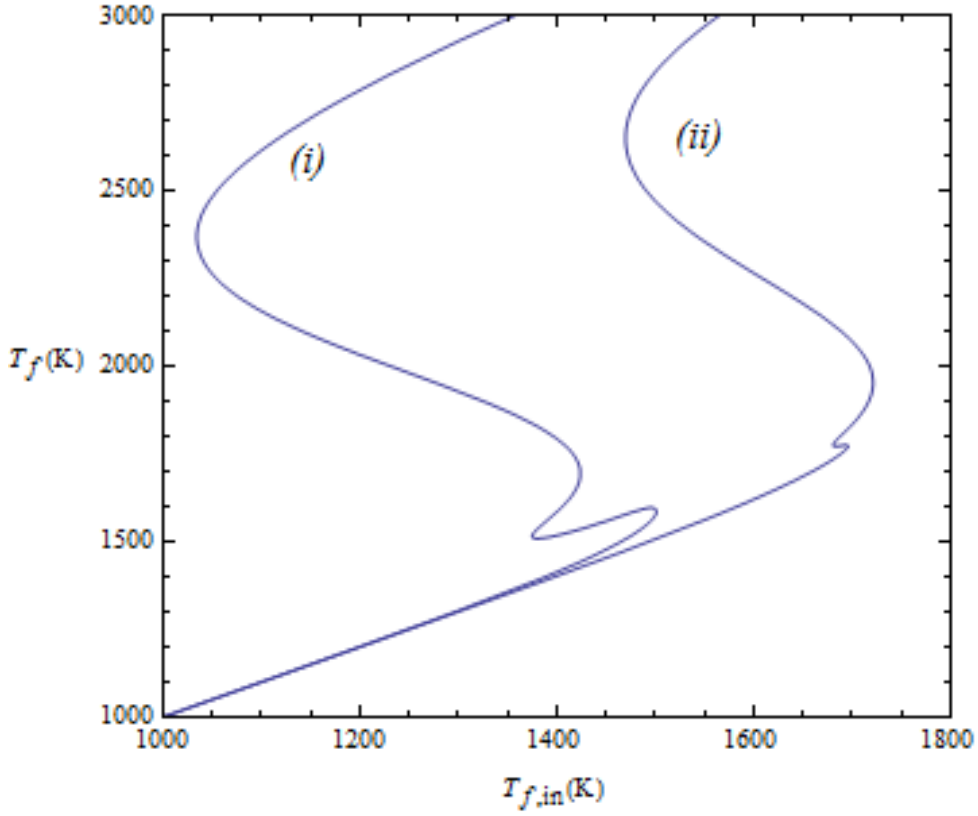

Figure 4-5: Bifurcation diagrams for methane for R_Ω of 400 mm with $k_{0h} = 1.15 \times 10^{10}$ s^{-1} and $E_h/R = 25356$ K and $k_{0s} = 6 \times 10^3$ m/s and $E_c/R = 16204$ K. We have chosen $y_{A,in} = 0.09$ and (i) $\tau = 2.4 \times 10^{-5}$s and (ii) $\tau = 4.5 \times 10^{-6}$s.

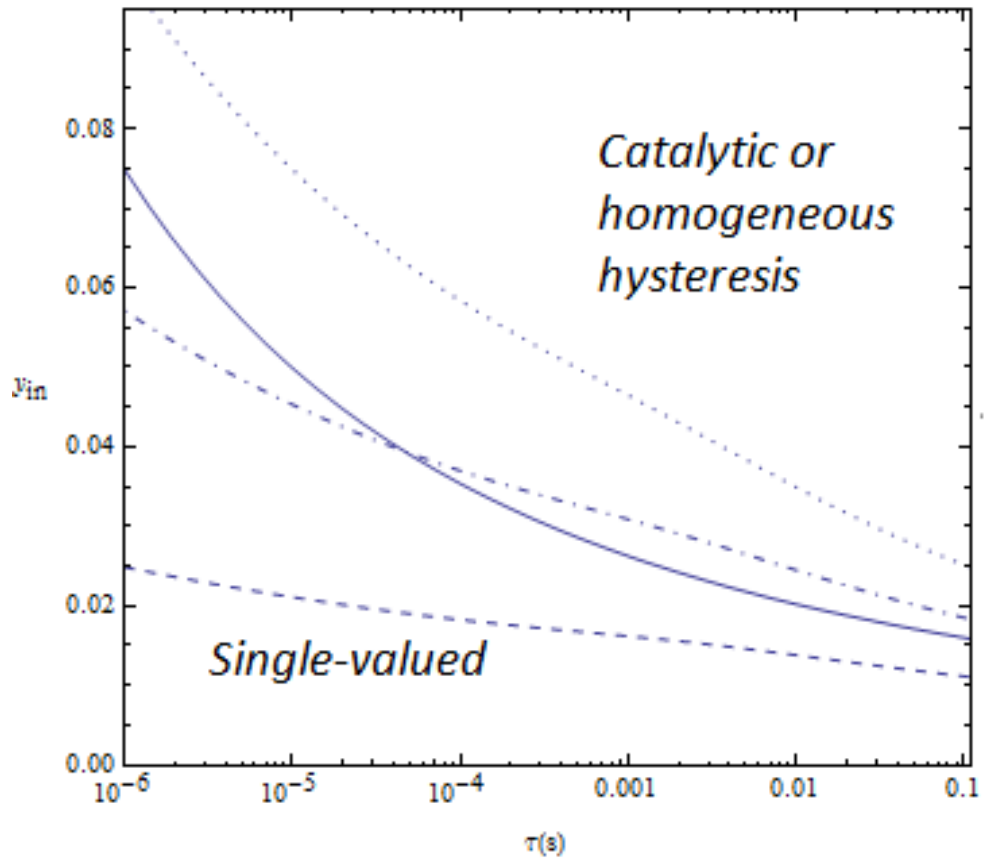

Figure 4-6: Hysteresis locus for methane oxidation for the case of homogeneous reaction acting alone (solid curve) and catalytic reaction acting alone ($- - -$ $k_{0s} = 6 \times 10^6 m/s$, $- \cdot - \cdot -\cdot$ $k_{0s} = 6 \times 10^4 m/s$ and $\cdots$ $k_{0s} = 6 \times 10^3 m/s$) for $R_\Omega = 400 \mu m$).

rather than the catalytic. Recall that all our calculations for propane oxidation were for systems where the catalytic reaction dominated. This explains why we are now able to obtain the other two bifurcation diagrams (d) and (f): they show up when the system is dominated by homogeneous reaction, which turns out to be the case when the catalyst activity is lowered. Thus, either the catalytic or the homogeneous chemistry can be made to dominate by appropriately varying the catalyst loading/ activity or the hydraulic radius.

Finally, we consider what happens when one of the few parameters whose variation

we have not considered yet, namely C_0 (or the variable expressing the effect of operating pressure) is changed. The work of Di Benedetto et al. (2012) and Barbarato et al. (2012) considers computations and experiments where the operating pressure is used as the bifurcation variable. The following computation serves as a point of qualitative comparison with their work (in the next section we use the same kinetics as used in these works and make more comparisons). A plot of the projection of bifurcation set for methane oxidation in the plane of total concentration (C_0) and the residence time (τ) is shown in figure 4-7. We observe that the operating concentration (pressure) at ignition increases as the residence time is decreased and that the extinction curve always lies below the ignition curve. Both of these observations are quite expected. The width of the hysteresis decreases as the residence time is increased. This happens because we fix the inlet temperature at the particular value of $600K$ and at higher residence times, both ignition and extinction are driven to lower temperatures for most values of operating pressure.

To summarize the conclusions of this section, we note that if the catalytic rate is higher (as in the case of precious metal based catalysts), the bifurcation features of methane oxidation are similar to that for propane oxidation. However, with much lower catalytic rates (as in the case of transition metal oxides), the phase diagram describing different possible bifurcations undergoes a drastic change and either the catalytic or the homogeneous chemistry can be made to dominate by appropriately varying the catalyst activity, fuel mole fraction or channel hydraulic radius.

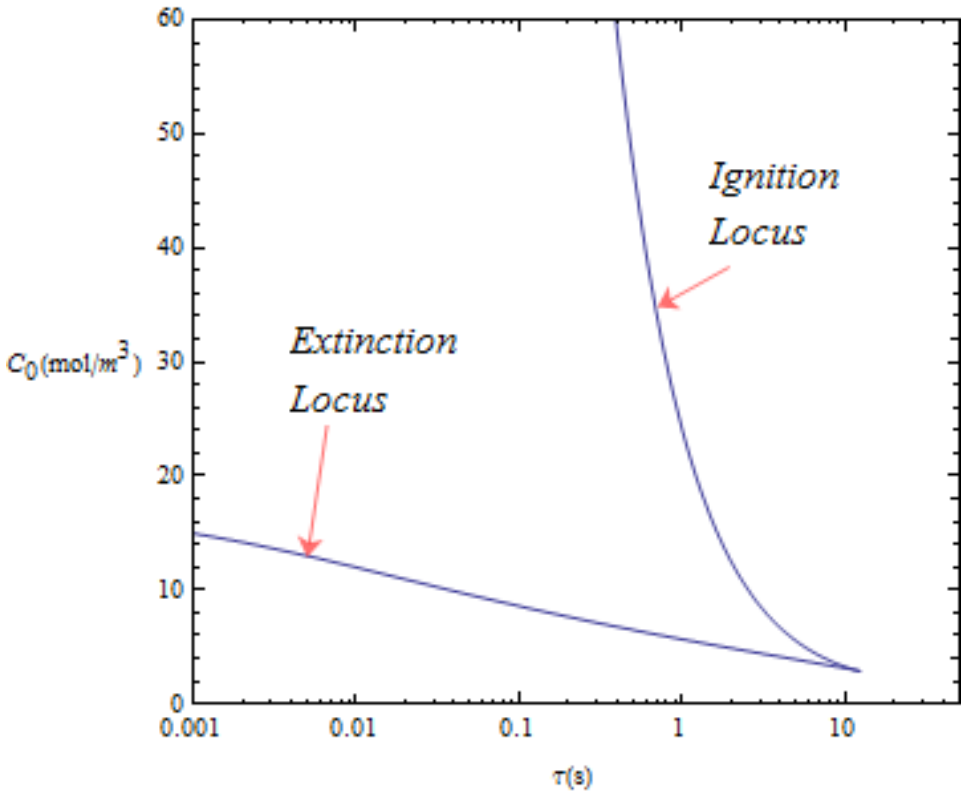

Figure 4-7: Projection of the bifurcation set for methane oxidation in the plane of total concentration (C_0) and the residence time (τ) when R_Ω is 400 μm with $T_{f,in}$ fixed at 600 K and $y_{A,in}$ at 0.05.

4.2 Bifurcation Analysis of methane oxidation with Transition Metal Oxide catalysts

Since we have already illustrated the bifurcation features with inlet temperature and residence time as bifurcation variables in the previous section, here we consider the operating pressure as the bifurcation variable. In practice, methane oxidation is often carried out using catalysts based on transition metal oxides rather than precious metals (as the former are more stable at high temperatures) and also under pressures that are higher than 1 bar, see for example [Di Benedetto et al. (2012), Barbato et al.(2012)]. The kinetics for the oxidation of methane on transition metal oxides is different than that on precious metals (e.g. Pt or Pd) and is generally slower by about one order of magnitude (at the same temperature). Further, in applications such as power generation, only lean combustion is of interest. (However in catalytic partial oxidations, bifurcation behavior with rich feed is of interest). Therefore, we examine here the bifurcation features of thermally coupled lean oxidation of methane using the recently established catalytic rate expressions used by Di Benedetto et al. In these calculations, we take mean specific heats (so that the adiabatic temperature rise is accurate) but include the dependence of the transport properties on the state variables.

The complete combustion of methane in air is given by

$$CH_4 + 2O_2 \rightarrow CO_2 + 2H_2O, \;\; \Delta H_R^0 = -802.6 \; kJ/mol. \tag{4.1}$$

The homogeneous rate expression which is adapted from Westbrook and Dryer, 1981 (valid for equivalence ratio between 0.5 and 1.5 and pressure up to 25 bars) may be expressed as

$$r_h(y_A, y_B, T_f) = k_{0h} \exp\left[-\frac{E_h/R}{T_f}\right] y_A^{0.2} y_B^{1.3} \left(\frac{P}{RT_f}\right)^{1.5}. \tag{4.2}$$

(with units of $moles.m^{-3}.s^{-1}$). The catalytic reaction rate for $LaMnO_3/La\text{-}\gamma\text{-}Al_2O_3$ catalyst is taken from Di Benedetto et al. [42] and may be expressed as

$$\epsilon_s r_c(y_{As}, y_{Bs}, T_s) = \frac{\epsilon_f \times 3.8 \times 10^3}{R_\Omega} \left(\frac{k_1 \exp\left[-\frac{E_{c1}/R}{T_s}\right] k_2 \exp\left[-\frac{E_{c2}/R}{T_s}\right] y_{CH_4,s} y_{O_2,s} P}{k_1 \exp\left[-\frac{E_{c1}/R}{T_s}\right] y_{O_2,s} + 2k_2 \exp\left[-\frac{E_{c2}/R}{T_s}\right] y_{CH_4,s}} \right). \tag{4.3}$$

(Here, $\epsilon_s r_c$ is the rate based on unit reactor volume and has units of $moles.m^{-3}.s^{-1}$). Besides the dependence of the transport properties on the state variables, the residence time (in the experiments that our model is applicable to) also changes with the pressure and flow rate. If Q is the gas flow rate (in liters/hour) at STP conditions, the velocity through the channels of a monolith is given by

$$\langle u \rangle = 3.75 \times 10^{-3} \frac{Q}{P} \frac{T_{f,in}}{273.15}, \tag{4.4}$$

where $\langle u \rangle$ is in m/s, $T_{f,in}$ is in Kelvins, Q is in slph and P is in bars. For channel of length 50 mm, the residence time (in seconds) then takes the functional form

$$\tau = 13.33 \left(\frac{P}{Q}\right) \left(\frac{273.15}{T_{f,in}}\right). \tag{4.5}$$

Table 4.1: List of kinetic, thermodynamic and transport parameters used in calculations for methane oxidation.

Parameter	Value
k_{0h}	2.119×10^{14} $(\text{moles/m}^3)^{-0.5}.s$
E_h/R	24356 K
k_1	3.52×10^5 $\text{moles/m}^2 bar.s$
E_{c1}/R	12632 K
k_2	2.83×10^{10} $\text{moles/m}^2 bar.s$
E_{c2}/R	26321 K
α_f	9.80 x $10^{-10}\frac{T^{1.75}}{P}$ m^2/s (T in K and P in bars)
$\widehat{c_{pf}}$	35 J/(mole-K)
ϵ_f	0.78
$D_{methane}$	9.88x 10^{-10} $\frac{T^{1.75}}{P} m^2/s$ (T in K and P in bars)
D_{oxygen}	9.24 x 10^{-10} $\frac{T^{1.75}}{P} m^2/s$ (T in K and P in bars)

The various parameters used in the model calculations are listed in table 2.

We start by showing a few bifurcation diagrams computed for the same operating conditions as the experimental results presented in Di Benedetto et al. (2012) and Barbato et al. (2012), namely $R_\Omega = 183\mu m$, $T_{f,in} = 733K$, $y_{A,in} = 3.7$ % and $y_{B,in} =$ 10 %. These authors also present computational results using the same global kinetics but with more detailed models that include spatial gradients. The calculations, shown in figure 4-8, reveal that our model predicts the ignition points quite close to the experimental data of Di Benedetto et al. (2012) and Barbato et al. (2012). However, the calculated extinction points do not match the experimental results. This discrepancy could be attributed to the fact that our model is adiabatic and laboratory scale experiments including those of Di Benedetto et al. (2012) involve heat losses, leading to different extinction points [Remark: The calculations of Barbato et al. for the adiabatic case with a different rate expression do not show extinction up to a pressure of 1 bar but these authors have not extended their calculations for operating

pressures below 1 bar]. Next, an ignition-extinction locus is calculated and plotted in the plane of operating pressure and the flow rate (figure 4-9). We find that the extinction locus is confined to very low operating pressures while ignition locus is quantitatively close to the results of Di Benedetto et al. (2012) and Barbato et al. (2012). For example, for $Q = 88$ slph, the experimentally observed ignition is at 8 bars, while our model predicts it at about 6 bars. Barbato et al. (2012) used a different rate expression (which is independent of oxygen concentration and does not agree with that given in Di Benedetto et al. (2012)) to simulate the same using CFD and found ignition at 8 bars and no extinction when P is reduced to low pressures. We believe that this small discrepancy of our result is within the accuracy of our model. As explained earlier, our model (which ignores spatial gradients) predicts ignition at a slightly higher temperature (by about 10 to $15K$) and when we reduce the inlet temperature by about $10K$, it predicts the same ignition pressure as that observed experimentally.

As can be expected intuitively, the experiments of Di Benedetto et al. (2012) predict that the ignition pressure is reduced when Q is reduced. This is also predicted by our model (figures 4-8 and 4-9). We observe that unless we consider very low inlet mole fractions of methane, for the practical range of pressure and flow rates, there is always a hysteresis (for this inlet temperature). Thus, calculation of the hysteresis locus does not add much new information and has not been pursued. Instead, we choose to show ignition locus in the plane of operating pressure and inlet fluid temperature, fixing Q at 88 slph for three different values of inlet mole fractions of methane to illustrate the impact of the inlet fluid temperature on the ignition point (fig 4-10). We

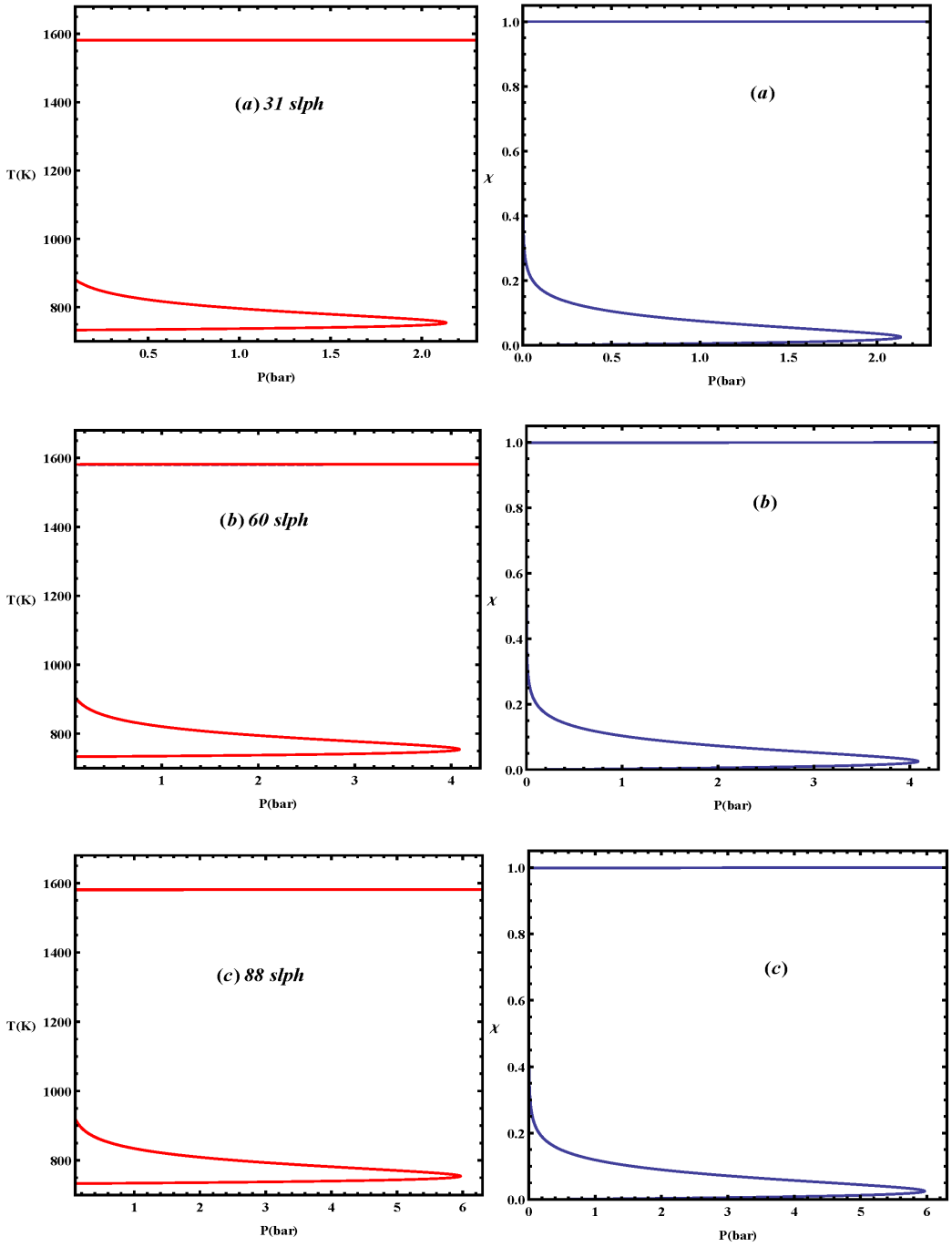

Figure 4-8: Bifurcation diagrams of fluid temperature (T) and conversion (χ) versus pressure (P) for methane oxidation with inlet mole fraction of methane at 0.037 and inlet temperature of 733 K for hydraulic radius 183 μm.

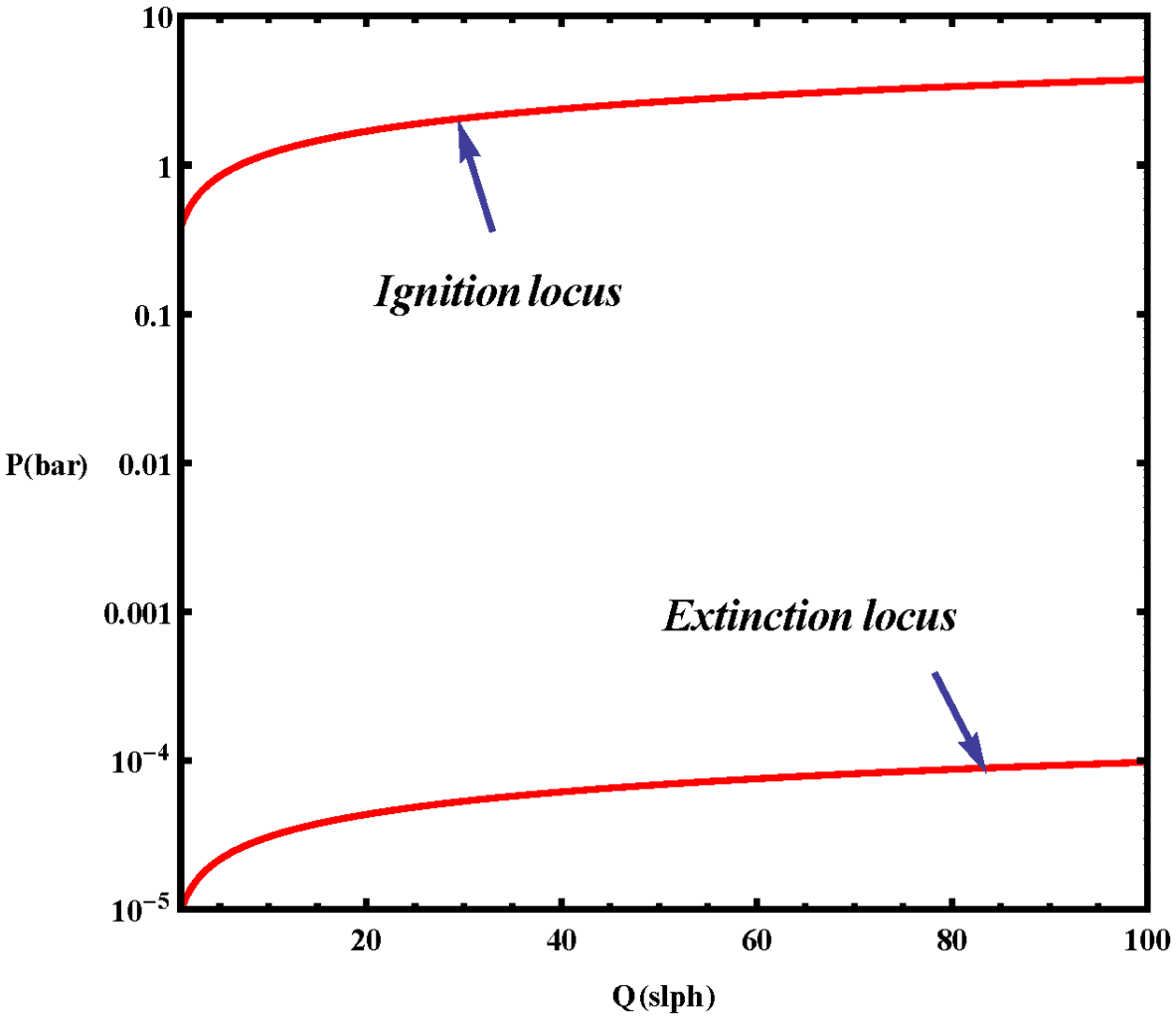

Figure 4-9: Projection of the bifurcation set for methane oxidation when pressure is the bifurcation variable. ($y_{A,in} = 0.037, T_{f,in} = 733K$, R_Ω =183 μm).

find that (as expected) increasing inlet temperature leads to a monotonic decrease in the operating pressure at ignition. Also, as the inlet mole fraction of methane ($y_{A,in}$) is decreased, the ignition locus moves to higher operating pressure or inlet temperatures (as expected). [Remark: The residence time along the ignition locus shown in figure 4-10 varies from about 0.05 to 1 second].

Our calculations in this section so far have yielded bifurcation diagrams with single ignition and extinction. In fact, even if we turn off the homogeneous reaction in these calculations, we observe no difference in our results, showing that the catalytic chemistry strongly dominates the homogeneous reaction in calculations shown above. As discussed in the previous section, one of the ways to increase the influence of the homogeneous reaction is by increasing the hydraulic radius, which has the effect of decreasing the catalytic reaction rate (per unit reactor volume) and also requiring longer residence times for conversion of the fuel. Figure 4-11 shows bifurcation diagrams for two different inlet mole fractions of methane when the hydraulic radius is increased by a factor 30 to 5.49 mm, Q is fixed at 88 slph and $T_{f,in}$ is taken to be 800 K. We now clearly observe double-S shaped bifurcation diagrams. Next, we take $T_{f,in}$ as the bifurcation variable and show bifurcation diagrams for two different inlet mole fractions of methane for $R_\Omega = 5.49\ mm, Q = 88$ slph and P fixed at 4 bars (which is a common operating pressure for methane catalytic combustion) in figure 4-12. Again we see two pairs of ignitions and extinctions [We also note that, in case (b), the catalytic reaction cannot be quenched unless feed temperature is reduced below the ambient value]. These calculations also confirm that the qualitative picture of the phase diagram for methane oxidation (with lean or stoichiometric feed) is

similar to that of propane discussed in the previous section, the main difference being in the transport properties (Lewis number for methane being slightly less than unity) and kinetic constants. The calculations shown in figure 19 and similar calculations at different values of R_Ω show that it is possible to increase R_Ω by about a factor of 5 or 10 (hence reducing the pressure drop) without changing the ignition temperature significantly.

It is of interest to examine bifurcation diagrams when the residence time is the bifurcation variable, where as in the previous section, we can interpret the residence time as a space coordinate, and compare the profiles with those computed by Di Benedetto et al. (2012) and Barbato et al. (2012). We fix P at 9 bars, $T_{f,in}$ at $733K$ and take $R_\Omega = 183\mu m$, $y_{A,in} = 3.7$ % and $y_{B,in} = 10$ %. Again, this yields a bifurcation diagram that is qualitatively very similar to the ones shown for propane oxidation. For the conditions chosen for the calculation, the experimental residence time is $0.5s$. Our model predicts the catalytic ignition (extinction) occurs at a residence time of $0.4s$ (about 10^{-8} s). Figure 4-13 shows the dependence of the solid and gas temperatures and the conversion on the residence time. As stated earlier, due to the logarithmic scale in τ, the distance over which T_s exceeds T_f is very small and may not be observed in experiments or calculations that use a linear scale. For example it is not observed in the calculations of Barbato et al (2012).] The fluid temperature increases monotonically to the adiabatic value. While ignition occurs only for residence times exceeding about $0.4s$, the ignited branch can persist for extremely small residence times or distances (which in this case is about seven orders of magnitude lower). We note that the profiles shown in figure 20 are in qualitative as well as quantitative

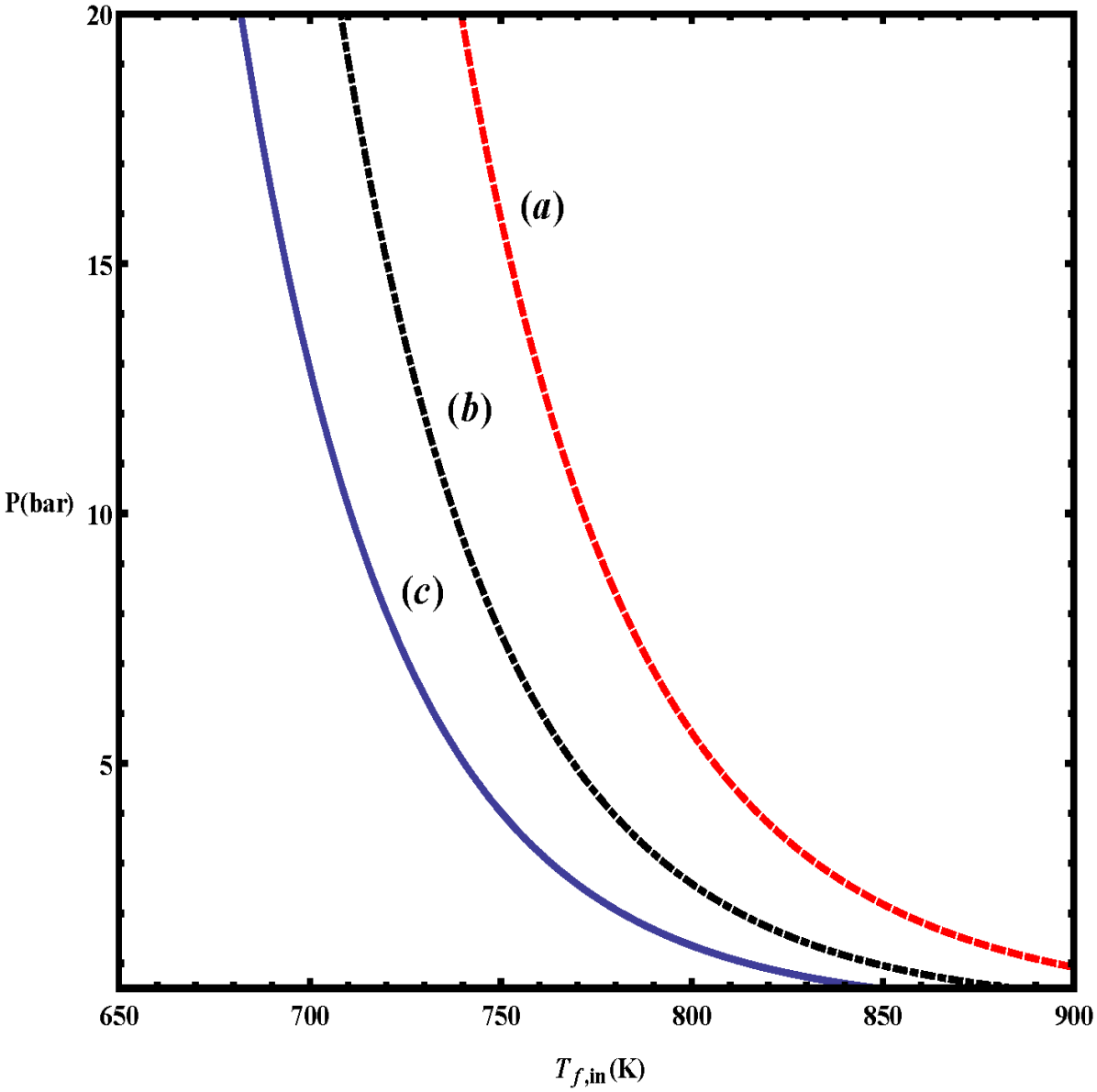

Figure 4-10: Dependence of the pressure at ignition on inlet temperature and mole fraction for lean oxidation of methane. ($Q_0 = 88$ $slph$, R_Ω =183 μm). The value of $y_{A,in}$ is (a) 0.01, (b) 0.02 and (c) 0.037.

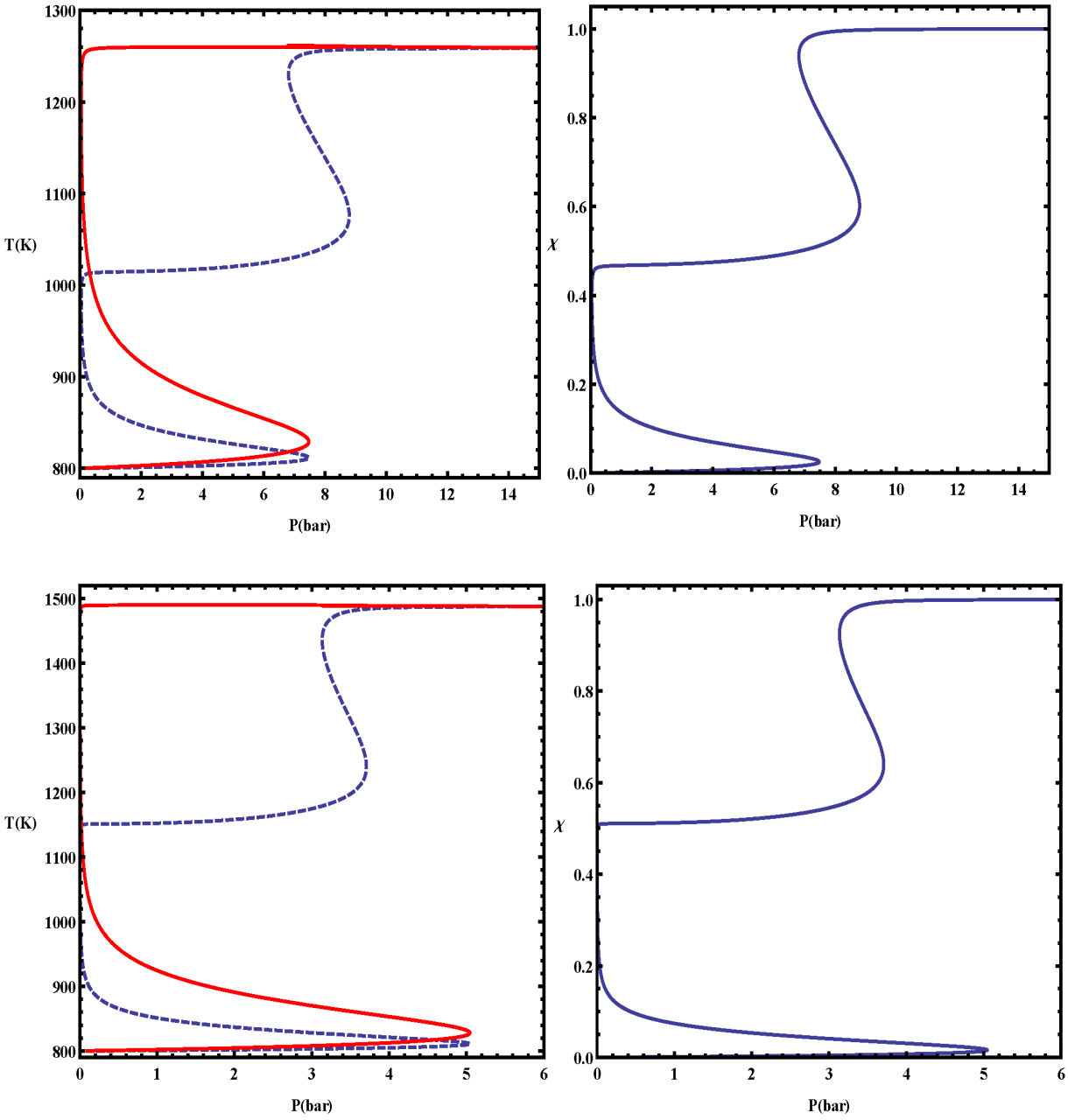

Figure 4-11: Bifurcation diagrams of fluid temperature (dashed), solid temperature (solid) and conversion (χ) versus pressure with $T_{f,in}$= 800 K, R_Ω= 5.49 mm and Q_0= 88 slph for $y_{A,in}$=0.02 (top) and $y_{A,in}$ = 0.03 (bottom).

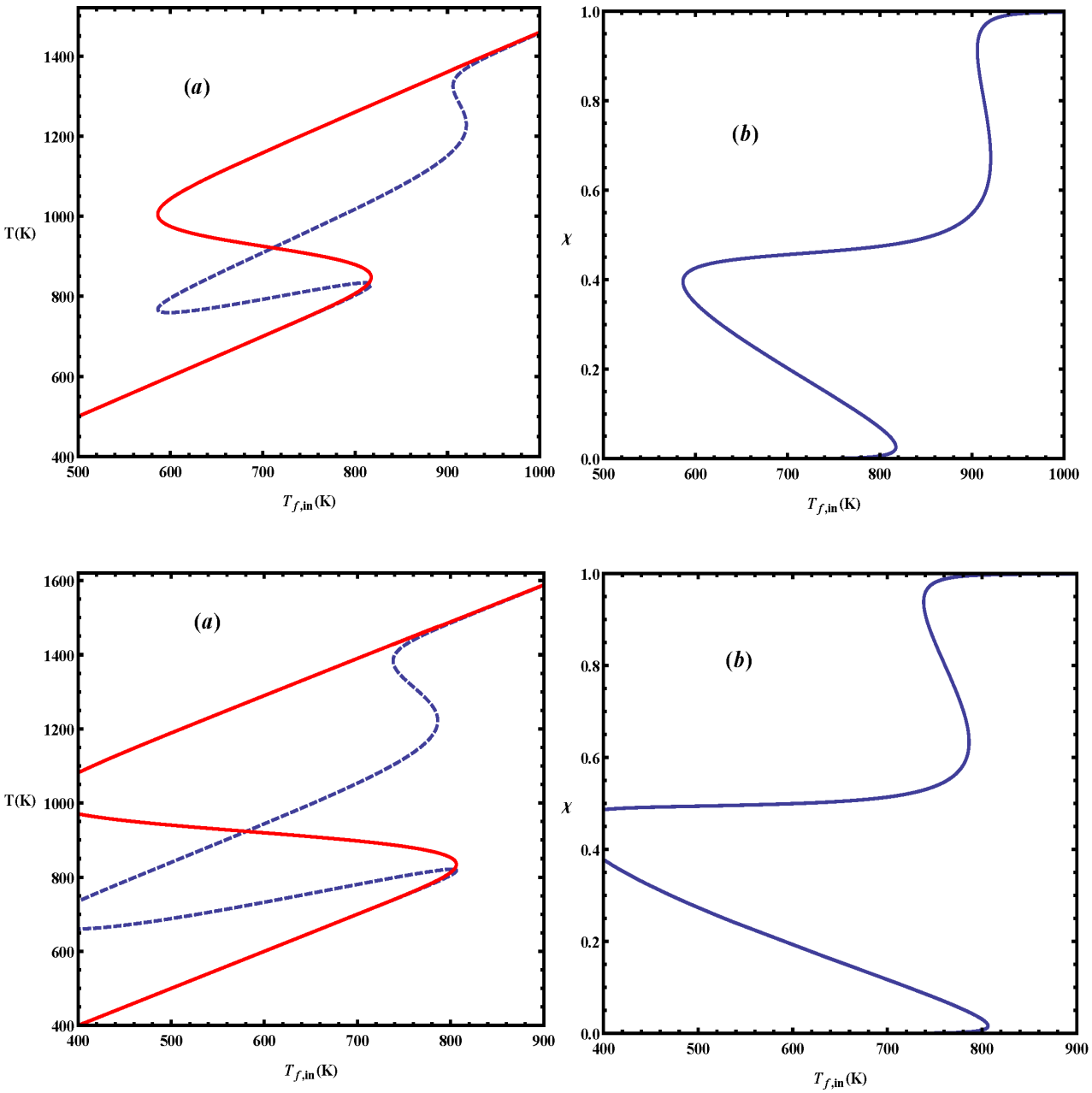

Figure 4-12: Bifurcation diagrams of fluid temperature (dashed lines), solid temperature (solid lines) and conversion (χ) versus inlet temperature for R_Ω= 5.49 mm, Q_0 = 88 slph and P= 4 bars for $y_{A,in}$=0.02 (top) and $y_{A,in}$ = 0.03 (bottom).

agreement with those based on more detailed models considered in Di Benedetto et al. (2012) and Barbato et al. (2012). Once again, *it should be pointed out that detailed models (and CFD codes even with global kinetics) may not have the mesh resolution needed to compute the ignited branches, especially the extinction point.*

As a final calculation, we show the computed bifurcation diagrams with rich feeds of methane (inlet mole fraction of methane taken to be 0.10 and that of oxygen taken to be 0.05) with P as the bifurcation variable when $T_{f,in}$ is taken to be 733 K (figure 4-14). Two diagrams corresponding to two hydraulic radii (7.32 mm and 5.49mm or 40 and 30 times the base value of $R_\Omega = 183\mu m$) have been shown. Increasing the hydraulic radius makes the second ignition to occur at lower operating pressures. Since the limiting reactant now is oxygen, the methane conversions obtained are always under 25 %, while oxygen conversions approach 100% on the high temperature branches. The existence of the intermediate branch (as in the top diagram of figure 19) where the catalytic reaction is ignited but homogeneous reaction rate is negligible is of interest in catalytic partial oxidations and in the interpretation of experimental data on oxidative coupling of methane.

4.3 Summary and discussion

To conclude, we have presented bifurcation diagrams for lean oxidation of methane with pressure as the bifurcation parameter. The predicted ignition locus compares favorably with experimental data and computational results based on more detailed models. Our analysis also shows that lean oxidation of methane is also catalytically dominant and the channel hydraulic diameter can be increased by a factor of ten

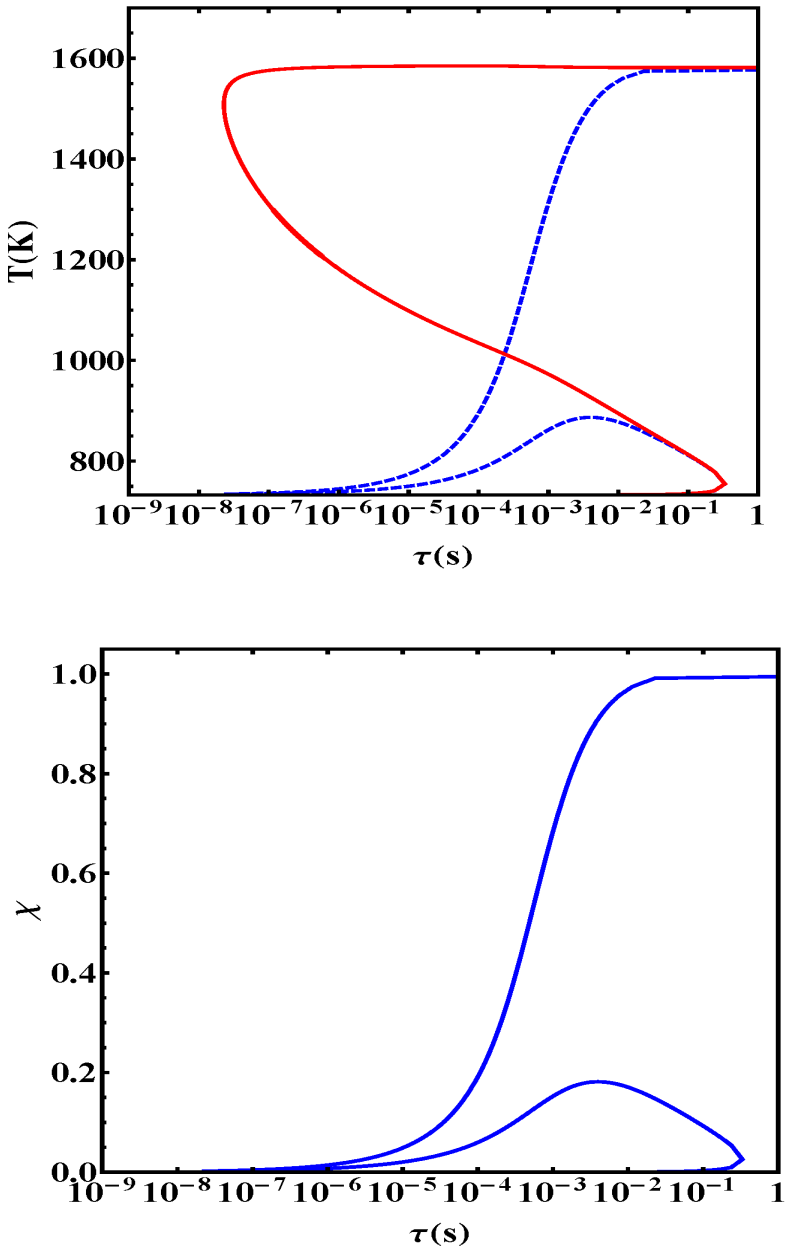

Figure 4-13: Bifurcation diagrams of fluid temperature (dashed), solid temperature (solid) and conversion (χ) versus τ with P=9 bars, $T_{f,in}$=733 K, R_Ω = 183μm, $y_{A,in}$ = 0.037 and $y_{B,in}$ = 0.01.

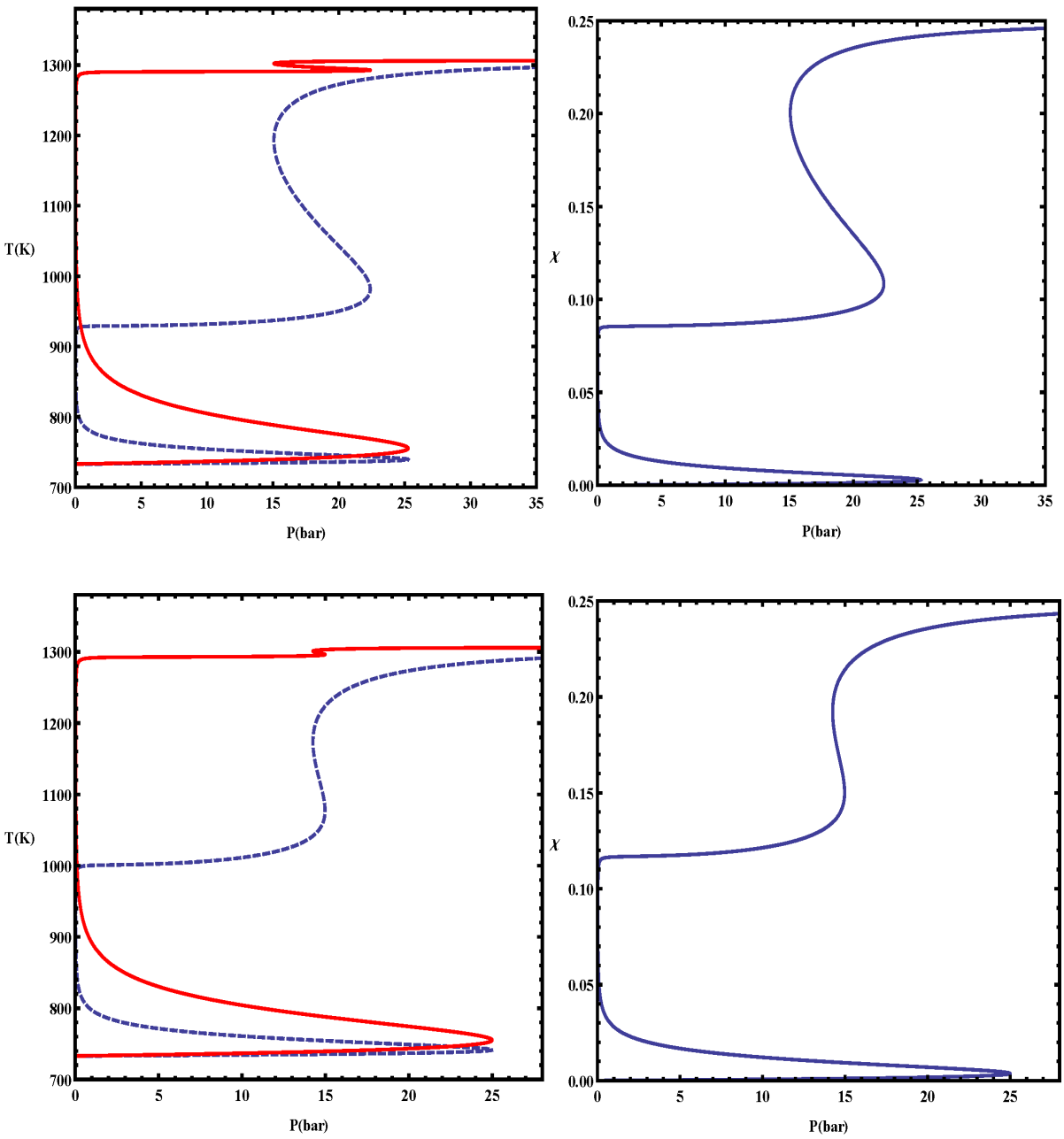

Figure 4-14: Bifurcation diagrams of fluid temperature (dashed), solid temperature (solid) and conversion (χ) versus pressure with rich feed ($y_{A,in}$ =0.1 and $y_{B,in}$ =0.05), $T_{f,in}$=733 K, Q_0= 88 slph, R_Ω=7.3 mm (top) and 5.49 mm (bottom).

or more without any significant change in the ignition (or operating pressure) or inlet temperature or methane conversion. In this chapter we saw a few bifurcation diagrams where the temperature on the ignited branch exceeds the adiabatic value. This can be attributed to transport effects (specifically, the fact that methane has a Lewis number that is less than one). In the next chapter, we proceed to discuss more on the transport effects focusing on the important issue of location of hot spot in combustion systems.

Chapter 5

Effects of Transport Phenomena on Maximum Temperatures

5.1 Introduction and Literature Review

The bifurcation analysis discussed in the last two chapters showed that in typical hydrocarbon oxidations, the first ignition-extinction pair is due to the catalytic reaction alone, while the thermally coupled ignition and extinction only come on the scene when the catalytic reaction is in the mass transfer controlled regime. Further, when the inlet temperature is sufficiently high, the onset of a second ignition and extinction for a thermally coupled system (with a finite wall reaction rate) and a system with infinitely fast catalytic reaction is practically indistinguishable. The case of homogeneous reaction in the fluid phase with an infinitely fast wall reaction has not been analyzed in detail in literature and is ripe for a theoretical analysis. The present chapter focuses on this limiting case (as well as other limiting cases) with an emphasis on the location of the hot spot, which is crucial for determining the reactor thermal stability. The Lewis number of the limiting reactant is an important parameter that dictates the trends in the maximum temperature. Other parameters

such as the Thiele moduli and Peclet numbers (axial, transverse and radial) also play a significant role. The effect of Lewis number (Le_f) on the surface temperature has been studied by various investigators (e.g. Satterfield et. al. (1954), Hegedus (1975), Pfefferle and Pfefferle, (1986, 1987) when only catalytic reaction is present and in the combustion literature when only the homogeneous reaction is present. When Lewis number is less than unity, the catalyst surface receives the limiting reactant faster than it can expel the heat produced due to the reaction. This situation leads to superadiabatic surface temperatures, the existence of which has been reported and verified in the literature (Satterfield et. al. (1954), Hegedus (1975)). Even though numerical simulations have been done demonstrating the effects of Lewis numbers greater than and less than unity on the maximum temperature in the solid phase (Satterfield et. al. (1954), Hegedus (1975), Pfefferle and Pfefferle (1986), Bui et al. (1996)), there have not been many studies which also study the effects on the gas phase temperatures. The recent work of Zheng and Mantzaras (2014) reports that in systems with fast catalytic and potential homogeneous reaction, the temperature within the reactor may exceed adiabatic values for Lewis numbers greater than 1. This has been presented as a novel and significant result. However, the analysis presented in this chapter demonstrates that these claims are questionable. We study a hierarchy of models asking the question: what is the maximum temperature attainable for the model and when is it achieved? We find that physically consistent 1-D and 2-D models do not lead to gas phase temperatures exceeding the adiabatic for $Le_f > 1$.

In the next section, we formulate a 3-D mathematical model that describes the

thermally coupled homogeneous-heterogeneous combustion in a parallel plate channel. We also formulate various limiting cases of this model that are amenable to analysis. In the following sections, the limiting models are analyzed to provide insight on the impact of various transport parameters representing the heat and mass transfer phenomena on coupled homogeneous-heterogeneous combustion. We provide the theory and analytical expressions for concentration and temperature fields in two-dimensional domains, and in limiting one dimensional models.

5.2 Mathematical Models

We consider a system consisting of flow between parallel plate reactors in which homogeneous reaction occurs in the fluid phase and catalytic reaction on the wall. For simplicity, the following assumption are made: (i) the velocity profile is invariant with axial position and the pressure drop is negligible so that the flow field can be decoupled from the species and energy balances (ii) one reactant (either fuel or oxygen) is in excess and the reaction rate is linear in the limiting reactant (iii) the physical properties can be assumed constant or taken to be average values without impacting the qualitative features (iv) The system is adiabatic. With these assumptions, the mathematical model for parallel plates with plate spacing $2a$ is given by

$$\begin{aligned} \overline{u} f(y') \frac{\partial C}{\partial x'} &= D_m \frac{\partial^2 C}{\partial x'^2} + D_m \left(\frac{\partial^2 C}{\partial y'^2} + \frac{\partial^2 C}{\partial z'^2} \right) - k_h(T) C, \\ \rho_f C_{pf} \overline{u} f(y') \frac{\partial T}{\partial x'} &= k_f \frac{\partial^2 T}{\partial x^2} + k_f \left(\frac{\partial^2 T}{\partial y'^2} + \frac{\partial^2 T}{\partial z'^2} \right) + (-\Delta H) k_h(T) C \quad ; \\ 0 &< x' < L, -a < y' < a, -b < z' < b \end{aligned} \tag{5.1}$$

with the inlet and boundary conditions given by

$$D_m \frac{\partial C}{\partial x'} = \overline{u} f(y')(C - C_{in}) \text{ and} \tag{5.2}$$

$$k_f \frac{\partial T}{\partial x'} = \rho_f C_{pf} \overline{u} f(y')(T - T_{in}) \text{ at } x' = 0, \tag{5.3}$$

$$\frac{\partial C}{\partial x'} = 0 \text{ and } \frac{\partial T}{\partial x'} = 0 \text{ at } x' = L \tag{5.4}$$

$$\mp D_m \frac{\partial C}{\partial y'} = k_s(T) C \text{ and} \tag{5.5}$$

$$\pm k_f \frac{\partial T}{\partial y'} = (-\Delta H_R) k_s(T) C \text{ at } y' = \pm a, \tag{5.6}$$

$$C(x', y', -b) = C(x', y', b) \text{ and } T(x', y', -b) = T(x', y', b). \tag{5.7}$$

Here $f(y')$ is the velocity profile(e.g. for a fully developed laminar flow the parabolic profile given by $f(y') = \frac{3}{2}(1 - \left(\frac{y'}{a}\right)^2)$ while for simultaneously developing flow with low Schmidt/Prandtl number, we can take the velocity profile to be flat, i.e. $f(y') = 1$). The above model describes both symmetric (or 2-D) solutions and non-symmetric (or 3-D) solutions (whenever they exist). The length scale b determines the periodicity of the solutions in the second transverse(azimuthal) direction. [Remark: When 3D solutions exist, the term "parallel plate" is not appropriate. In such cases, the above model describes flow in a circular channel with a large radius and 3D solutions correspond to those lacking azimuthal symmetry].

We assume Arrhenius type temperature dependence for both the homogenous and catalytic rate constants, introduce the following non-dimensional variables and

parameters,

$$\begin{aligned} c &= \frac{C}{C_{in}},\ \theta = \frac{T - T_{in}}{T_{in}\beta}, \\ x &= \frac{D_m x'}{a^2 \overline{u}}; y = \frac{y'}{a},\ z = \frac{z'}{b}, \\ \beta &= \frac{(-\Delta H_R) C_{in}}{\rho_f C_{pf} T_{in}}, \gamma_h = \frac{E_a}{RT_{in}},\ \gamma_c = \frac{E'_a}{RT_{in}},\ \phi^2 = \frac{k_v a^2}{D_m},\ \phi_s^2 = \frac{k_s a}{D_m}, \\ Le_f &= \frac{k_f}{\rho_f C_{pf} D_m},\ Pe_r = \frac{\overline{u} a}{D_m},\quad P = \frac{a^2 \overline{u}}{D_m L},\quad \alpha = \frac{b}{a} \end{aligned} \tag{5.8}$$

and express the model in the following dimensionless form:

$$f(y)\frac{\partial c}{\partial x} = \frac{1}{Pe_r^2}\frac{\partial^2 c}{\partial x^2} + \frac{\partial^2 c}{\partial y^2} + \frac{1}{\alpha^2}\frac{\partial^2 c}{\partial z^2} - \phi^2 c \exp\left[\frac{\gamma_h \beta \theta}{1+\beta\theta}\right] \tag{5.9}$$

$$f(y)\frac{\partial \theta}{\partial x} = \frac{Le_f}{Pe_r^2}\frac{\partial^2 \theta}{\partial x^2} + Le_f\left(\frac{\partial^2 \theta}{\partial y^2} + \frac{1}{\alpha^2}\frac{\partial^2 \theta}{\partial z^2}\right) + \phi^2 c \exp\left[\frac{\gamma_h \beta \theta}{1+\beta\theta}\right]; \tag{5.10}$$

$$0 < x < \frac{1}{P}, -1 < y < 1, -1 < z < 1$$

$$\begin{aligned} \frac{1}{Pe_r^2}\frac{\partial c}{\partial x} &= f(y)(c-1) \\ \frac{Le_f}{Pe_r^2}\frac{\partial \theta}{\partial x} &= f(y)\theta \quad \text{at } x = 0 \end{aligned} \tag{5.11}$$

$$\frac{\partial c}{\partial x} = 0 = \frac{\partial \theta}{\partial x} \quad \text{at } x = \frac{1}{P} \tag{5.12}$$

$$\begin{aligned} \frac{\partial c}{\partial y} &= \mp \phi_s^2 c \exp\left[\frac{\gamma_c \beta \theta}{1+\beta\theta}\right] \\ \frac{\partial \theta}{\partial y} &= \pm \frac{1}{Le_f}\phi_s^2 c \exp\left[\frac{\gamma_c \beta \theta}{1+\beta\theta}\right] \text{ at } y = \pm 1 \end{aligned} \tag{5.13}$$

$$c(x, y, -1) = c(x, y, 1); \theta(x, y, -1) = \theta(x, y, 1). \tag{5.14}$$

We note that the model contains 9 dimensionless groups: the dimensionless adiabatic temperature rise (β), the activation energies for the homogeneous and catalytic reactions (γ_h, γ_c), the (square of the) Thiele moduli for homogeneous and catalytic reactions (or ratio of characteristic diffusion time to reaction time at the inlet temperature, ϕ^2, ϕ_s^2), the radial Peclet number (Pe_r), the transverse Peclet number (ratio of transverse diffusion time to convection time, P), the Lewis number (ratio of fluid thermal diffusivity to mass diffusivity of limiting reactant, Le_f) and the aspect ratio α. Other dimensionless groups that may be used (but are not independent) are the axial Peclet number, Pe ($= Pe_r^2/P$), aspect ratio based on channel length and spacing ($P/Pe_r = \frac{a}{L}$), and the Damköhler numbers ($Da = \phi^2/P$, $Da_s = \phi_s^2/P$).

When the Lewis number is unity, the above model admits an invariant. Defining $\widehat{\theta} = c + \theta$, we observe that $\widehat{\theta}$ satisfies the following PDE:

$$\begin{aligned} f(y)\frac{\partial \widehat{\theta}}{\partial x} &= \frac{1}{Pe_r^2}\frac{\partial^2 \widehat{\theta}}{\partial x^2} + \left(\frac{\partial^2 \widehat{\theta}}{\partial y^2} + \frac{1}{\alpha^2}\frac{\partial^2 \widehat{\theta}}{\partial z^2}\right) \\ 0 &< x < \frac{1}{P}, -1 < y < 1, -1 < z < 1 \end{aligned} \tag{5.15}$$

$$\frac{1}{Pe_r^2}\frac{\partial \widehat{\theta}}{\partial x} = f(y)(\widehat{\theta} - 1) \quad \text{at } x = 0$$

$$\frac{\partial \widehat{\theta}}{\partial x} = 0 \quad \text{at } x = \frac{1}{P}$$

$$\frac{\partial \widehat{\theta}}{\partial y} = 0 \text{ at } \quad y = \pm 1$$

$$\widehat{\theta}(x, y, -1) = \widehat{\theta}(x, y, 1).$$

It may be shown (using the Finite Fourier Transform) that the only solution to this

model is $\widehat{\theta} = 1$, or $c = 1 - \theta$. This invariant lets us to simplify the model to a single differential equation for which the analysis is simplified. This special case has been studied by many investigators in the past, and therefore in the sequel, we focus on the more general model with an arbitrary Lewis number.

5.2.1 Limiting Models

We formulate below various limiting cases of the above general model containing fewer parameters. These limiting models are valid in the limit of some characteristic time (or parameter) being very small or large and provide insight on the behavior of the general model.

Dilute reactant model

When the concentration of the limiting reactant at the inlet to the channel is very small (or equivalently, the adiabatic temperature rise $\beta \rightarrow 0$), we can ignore the variation of the reaction rates with temperature and simplify the above model. It may be shown that in this limiting case, there are no 3-D solutions. Further, the species balance decouples from the energy balance and there are no ignitions or extinctions or multiple solutions. As shown in the next section, this limiting case retains the spatial variation of the temperature and concentration fields of the 2-D solutions (even for finite values of β) and provides insight on the impact of transport properties on the maximum temperature. This limiting model is of interest as it is linear (so that analytic solutions can be obtained) and contains only 5 parameters.

It is given by

$$
\begin{aligned}
f(y)\frac{\partial c}{\partial x} &= \frac{1}{Pe_r^2}\frac{\partial^2 c}{\partial x^2} + \frac{\partial^2 c}{\partial y^2} - \phi^2 c \text{ and} && (5.16)\\
f(y)\frac{\partial \theta}{\partial x} &= \frac{Le_f}{Pe_r^2}\frac{\partial^2 \theta}{\partial x^2} + Le_f\frac{\partial^2 \theta}{\partial y^2} + \phi^2 c; \quad 0 < x < \frac{1}{P}, 0 < y < 1, && (5.17)
\end{aligned}
$$

with same boundary conditions in the axial direction as the full model and

$$
\begin{aligned}
\frac{\partial c}{\partial y} &= -\phi_s^2 c; \quad \frac{\partial \theta}{\partial y} = \frac{1}{Le_f}\phi_s^2 c \quad \text{at} \;\; y = 1 \text{ and}\\
\frac{\partial c}{\partial y} &= 0 = \frac{\partial \theta}{\partial y} \;\; \text{at} \;\; y = 0. && (5.18)
\end{aligned}
$$

There is further simplification and limiting cases of this model but these will be considered in the next section, where an analysis of this model is presented.

Long channel 2-D Model:

In the limit of very long residence times ($P \to 0$), the exit boundary condition in the flow direction may be ignored and the channel may be considered infinitely long. In addition, if we consider only 2-D symmetric solutions, the number of parameters is reduced by two (eliminating α and P). We refer to this limiting case as the long channel model and do not list the model equations as they can be written down easily from the general case. A further limiting case of this model that is considered in most literature studies is obtained when the axial diffusion/conduction is neglected and inlet (Danckwerts) boundary conditions are simplified to the Dirichlet boundary conditions. Again, we consider this limiting model in the next section.

1-D Model with axial gradients:

The 1-D model becomes appropriate when the transverse gradients are negligibly small and any small variation in transverse direction can be averaged out (in the limit of $a \to 0$). When Pe_r^2 , ϕ^2 and $\phi_s^2 \to 0$, we can average the general model over the transverse directions (this can be done rigorously using the Liapunov-Schmidt averaging procedure) to obtain the 1-D model in the following form:

$$\frac{d\langle c\rangle}{dx} = \frac{1}{Pe_r^2}\frac{d^2\langle c\rangle}{dx^2} - \phi^2\langle c\rangle \exp\left[\frac{\gamma_h\beta\langle\theta\rangle}{1+\beta\langle\theta\rangle}\right] - \phi_s^2\langle c\rangle \exp\left[\frac{\gamma_c\beta\langle\theta\rangle}{1+\beta\langle\theta\rangle}\right] \tag{5.19}$$

and

$$\frac{d\langle\theta\rangle}{dx} = \frac{Le_f}{Pe_r^2}\frac{d^2\langle\theta\rangle}{dx^2} + \phi^2\langle c\rangle \exp\left[\frac{\gamma_h\beta\langle\theta\rangle}{1+\beta\langle\theta\rangle}\right] + \phi_s^2\langle c\rangle \exp\left[\frac{\gamma_c\beta\langle\theta\rangle}{1+\beta\langle\theta\rangle}\right], \tag{5.20}$$

with

$$\begin{aligned} \frac{1}{Pe_r^2}\frac{d\langle c\rangle}{dx} &= (\langle c\rangle - 1); \qquad \frac{Le_f}{Pe_r^2}\frac{d\langle\theta\rangle}{dx} = \langle\theta\rangle \quad \text{at } x = 0 \\ \text{and } \frac{d\langle c\rangle}{dx} &= 0 = \frac{d\langle\theta\rangle}{dx} \quad \text{at } x = \frac{1}{P}. \end{aligned} \tag{5.21}$$

Here, the angular bracket denotes the cross-section averaged values. This model can be written in more familiar form by defining

$$X = xP = \frac{x'}{L} \qquad Da = \frac{\phi^2}{P} \qquad Da_s = \frac{\phi_s^2}{P} \qquad Pe = \frac{Pe_r^2}{P},$$

and dropping the angular brackets leads to the 1-D axial dispersion model with Danckwerts' boundary conditions:

$$\frac{1}{Pe}\frac{d^2c}{dX^2} - \frac{dc}{dX} - Dac\exp\left[\frac{\gamma_h\beta\theta}{1+\beta\theta}\right] - Da_sc\exp\left[\frac{\gamma_c\beta\theta}{1+\beta\theta}\right] = 0 \text{ and} \quad (5.22)$$

$$\frac{Le_f}{Pe}\frac{d^2\theta}{dX^2} - \frac{d\theta}{dX} + Dac\exp\left[\frac{\gamma_h\beta\theta}{1+\beta\theta}\right] + Da_sc\exp\left[\frac{\gamma_c\beta\theta}{1+\beta\theta}\right] = 0, \text{ with} \quad (5.23)$$

$$\begin{aligned} \frac{1}{Pe}\frac{dc}{dX} &= (c-1) \quad \text{and} \quad \frac{Le_f}{Pe}\frac{d\theta}{dX} = \theta \quad \text{at } X = 0, \\ \frac{dc}{dX} &= 0 = \frac{d\theta}{dX} \quad \text{at } X = 1. \end{aligned} \quad (5.24)$$

One limiting case of this model that is of interest is when the reactor is infinitely long. In this case, the reactor length is not appropriate for use as a characteristic length. We then choose

$$\zeta = \frac{x'\overline{u}}{D_m} = xPe_r^2 \quad (5.25)$$

for the nondimensional axial coordinate. Considering only the case of dilute reactant ($\beta \to 0$), we recast the full model as:

$$\frac{dc}{d\zeta} = \frac{d^2c}{d\zeta^2} - \Lambda c \quad , 0 < \zeta < \infty \text{ and} \quad (5.26)$$

$$\frac{d\theta}{d\zeta} = Le_f\frac{d^2\theta}{d\zeta^2} + \Lambda c \ , 0 < \zeta < \infty \quad (5.27)$$

with the inlet conditions given by

$$\frac{dc}{\partial\zeta} = c - 1 \quad \text{and} \tag{5.28}$$

$$Le_f \frac{d\theta}{d\zeta} = \theta \text{ at } \zeta = 0. \tag{5.29}$$

(The parameter $\Lambda = \frac{(k_v + \frac{k_s}{a})D_m}{\overline{u}^2}$ is the ratio of $(Da + Da_s)$ and Pe, thereby eliminating the length scale involved). It is worth noting that Λ contains the diffusivity, the reaction rate constants and the average velocity and thus, serves as a measure of relative significance of convection, diffusion and reaction. The criterion $\Lambda \gg 1$ can be thought of as defining a fast reaction in a convection-diffusion-reaction system just as $Da \gg 1$ indicates fast reaction for convection-reaction systems.

Short channel model:

When the channel length is very small compared to the spacing between the plates (as in the case of gauze or short monolith reactors), the general model can be simplified by averaging in the axial direction. This eliminates (or compresses) the axial variation of the state variables and leads to a model similar to the "short monolith model" that has been widely used in the catalytic reaction only case [Balakotaiah, et al. (2000)]. This model is given by

$$Pf(y)\,(c-1) = \frac{\partial^2 c}{\partial y^2} + \frac{1}{\alpha^2}\frac{\partial^2 c}{\partial z^2} - \phi^2 c \exp\left[\frac{\gamma_h \beta\theta}{1+\beta\theta}\right] \text{ and} \tag{5.30}$$

$$Pf(y)\theta = Le_f\left(\frac{\partial^2\theta}{\partial y^2} + \frac{1}{\alpha^2}\frac{\partial^2\theta}{\partial z^2}\right) + \phi^2 c \exp\left[\frac{\gamma_h\beta\theta}{1+\beta\theta}\right]; \tag{5.31}$$

$$-1 < y < 1, -1 < z < 1.$$

and the same transverse boundary conditions (in y and z) as the full model. The usefulness of this model lies in the fact that it simplifies the flow terms and focuses mainly on the transverse variations. For the case of catalytic reaction only, it was shown that this elliptic model has the same bifurcation features as the full 3-D model [Balakotaiah, et al. (2002)]. Again, further simplifications of the model may be formulated and these are considered in the next section.

5.3 Transport Effects on Maximum Temperature

In this section, we analyze the dilute reactant model for the 1-dimensional and 2-dimensional cases to determine the impact of transport parameters (P, Pe_r, Le_f) on the temperature and concentration fields and the maximum temperature attained in the system.

5.3.1 Long channel model

As stated in the previous section, the assumption of dilute reactant (or low adiabatic temperature rise) and the normalization of the temperature rise to unity, makes the model linear for which analytical expressions can be obtained for the 2-D (symmetric) solutions when an infinitely fast catalytic reaction is considered. Though this can be done for both parabolic and flat velocity cases, we consider here only the latter case as the resulting expression are less cumbersome and easier to analyze. For the case of a flat velocity profile, the model simplifies to

$$\frac{\partial c}{\partial x} = \frac{\partial^2 c}{\partial y^2} + \frac{1}{Pe_r^2}\frac{\partial^2 c}{\partial x^2} - \phi^2 c \quad , 0 < x < \infty,\ 0 < y < 1 \tag{5.32}$$

and

$$\frac{\partial \theta}{\partial x} = Le_f \left(\frac{\partial^2 \theta}{\partial y^2} + \frac{1}{Pe_r^2} \frac{\partial^2 \theta}{\partial x^2} \right) + \phi^2 c \ , 0 < x < \infty, 0 < y < 1 \tag{5.33}$$

with the inlet and boundary conditions given by

$$\frac{1}{Pe_r^2} \frac{\partial c}{\partial x} = c - 1 \ \text{ and} \tag{5.34}$$

$$\frac{Le_f}{Pe_r^2} \frac{\partial \theta}{\partial x} = \theta \text{ at } x = 0, \tag{5.35}$$

$$\frac{\partial c}{\partial y} = 0 \text{ and } \frac{\partial \theta}{\partial y} = 0 \text{ at } y = 0, \text{ and} \tag{5.36}$$

$$c = 0 \text{ and} \tag{5.37}$$

$$\frac{\partial \theta}{\partial y} = \frac{-1}{Le_f} \frac{\partial c}{\partial y} \text{ at } y = 1. \tag{5.38}$$

To solve this PDE system, we use the Finite Fourier Transform obtaining:

$$c(x, y) = \sum_{n=1}^{\infty} \frac{4}{(2n-1)\,\pi} \frac{(-1)^{n-1}}{\left[1 + \frac{\Lambda_n}{Pe_r^2}\right]} \exp[-\Lambda_n x] w_n(y) \tag{5.39}$$

where

$$\Lambda_n = \frac{-Pe_r^2 + \sqrt{Pe_r^4 + 4(\lambda_n + \phi^2) Pe_r^2}}{2} \tag{5.40}$$

and

$$w_n(y) = \sqrt{2} \cos\left[\frac{2n-1}{2} \pi y \right], \ \lambda_n = \left(\frac{2n-1}{2} \pi \right)^2. \tag{5.41}$$

Using the above Fourier series for $c(x, y)$, we have the following PDE for the

temperature field:

$$\frac{\partial\theta}{\partial x} = Le_f\left(\frac{\partial^2\theta}{\partial y^2}+\frac{1}{Pe_r^2}\frac{\partial^2\theta}{\partial x^2}\right) + \phi^2\sum_{n=1}^{\infty}\frac{4}{(2n-1)\,\pi}\frac{(-1)^{n-1}}{\left[1+\frac{\Lambda_n}{Pe_r^2}\right]}\exp[-\Lambda_n x]\cos[\frac{2n-1}{2}\pi y], \tag{5.42}$$

$$0 < x<\infty, 0<y<1, \tag{5.43}$$

$$\frac{Le_f}{Pe_r^2}\frac{\partial\theta}{\partial z}=\theta \text{ at } x=0, \tag{5.44}$$

$$\frac{\partial\theta}{\partial y}=0 \text{ at } y=0, \text{ and} \tag{5.45}$$

$$\frac{\partial\theta}{\partial y}=\frac{1}{Le_f}\sum_{n=1}^{\infty}\frac{2\exp[-\Lambda_n x]}{\left[1+\frac{\Lambda_n}{Pe_r^2}\right]} \text{ at } y=1. \tag{5.46}$$

This equation can also be solved by Finite Fourier Transform by employing the principle of superposition for the source terms in the governing equation and the boundary condition. The final expression for $\theta(x,y)$ is

$$\theta(x,y) = 2\sum_{n=1}^{\infty}\left(1+\frac{4\phi^2}{(2n-1)^2\,\pi^2}\right)\frac{\left[\frac{Le_f}{Pe_r^2}\Lambda_n+1\right]-\exp[-\Lambda_n x]}{\left[1+\frac{\Lambda_n}{Pe_r^2}\right]\left[\frac{Le_f}{Pe_r^2}\Lambda_n^2+\Lambda_n\right]}\psi_0(y) + 4\sum_{m,n=1}^{\infty}(-1)^m\left(1+\frac{4\phi^2}{\left((2n-1)^2-4m^2\right)\pi^2}\right)\times \frac{\left[\frac{\frac{Le_f}{Pe_r^2}\Lambda_n+1}{\frac{Le_f}{Pe_r^2}\Omega_m+1}\right]\exp[-\Omega_m x]-\exp[-\Lambda_n x]}{\left[1+\frac{\Lambda_n}{Pe_r^2}\right]\left[\frac{Le_f}{Pe_r^2}\Lambda_n^2+\Lambda_n-Le_f\mu_m\right]}\psi_m(y), \tag{5.47}$$

where

$$\Omega_m = \frac{-Pe_r^2 + \sqrt{Pe_r^4 + 4Pe_r^2 Le_f^2 \mu_m^2}}{2Le_f} \tag{5.48}$$

and

$$\begin{aligned} \psi_m(y) &= \sqrt{2}\cos[m\pi y],\ \mu_m = (m\pi)^2 \text{ when } m \geq 1 \\ &= 1,\ \mu_0 = 0 \text{ when } m = 0. \end{aligned} \tag{5.49}$$

Also the average temperature is given by

$$\langle\theta\rangle(x) = 2\sum_{n=1}^{\infty}\left(1 + \frac{4\phi^2}{(2n-1)^2\pi^2}\right)\frac{\left[\frac{Le_f}{Pe_r^2}\Lambda_n + 1\right] - \exp[-\Lambda_n x]}{\left[1 + \frac{\Lambda_n}{Pe_r^2}\right]\left[\frac{Le_f}{Pe_r^2}\Lambda_n^2 + \Lambda_n\right]} \tag{5.50}$$

while the surface and centerline temperatures are given as

$$\begin{aligned} \theta_s(x) &= \theta(y=1,x) = 2\sum_{n=1}^{\infty}\left(1 + \frac{4\phi^2}{(2n-1)^2\pi^2}\right)\frac{\left[\frac{Le_f}{Pe_r^2}\Lambda_n + 1\right] - \exp[-\Lambda_n x]}{\left[1 + \frac{\Lambda_n}{Pe_r^2}\right]\left[\frac{Le_f}{Pe_r^2}\Lambda_n^2 + \Lambda_n\right]} + \\ & 4\sum_{m,n=1}^{\infty}\left(1 + \frac{4\phi^2}{\left((2n-1)^2 - 4m^2\right)\pi^2}\right)\frac{\left[\frac{\frac{Le_f}{Pe_r^2}\Lambda_n + 1}{\frac{Le_f}{Pe_r^2}\Omega_m + 1}\right]\exp[-\Omega_m x] - \exp[-\Lambda_n x]}{\left[1 + \frac{\Lambda_n}{Pe_r^2}\right]\left[\frac{Le_f}{Pe_r^2}\Lambda_n^2 + \Lambda_n - Le_f\mu_m\right]} \end{aligned} \tag{5.51}$$

and

$$\theta_c(x) = \theta(y=0,x) = 2\sum_{n=1}^{\infty}\left(1+\frac{4\phi^2}{(2n-1)^2\pi^2}\right)\frac{\left[\frac{Le_f}{Pe_r^2}\Lambda_n+1\right]-\exp[-\Lambda_n x]}{\left[1+\frac{\Lambda_n}{Pe_r^2}\right]\left[\frac{Le_f}{Pe_r^2}\Lambda_n^2+\Lambda_n\right]} + 4\sum_{m,n=1}^{\infty}(-1)^m\left(1+\frac{4\phi^2}{\left((2n-1)^2-4m^2\right)\pi^2}\right)\times \frac{\left[\frac{\frac{Le_f}{Pe_r^2}\Lambda_n+1}{\frac{Le_f}{Pe_r^2}\Omega_m+1}\right]\exp[-\Omega_m x]-\exp[-\Lambda_n x]}{\left[1+\frac{\Lambda_n}{Pe_r^2}\right]\left[\frac{Le_f}{Pe_r^2}\Lambda_n^2+\Lambda_n-Le_f\mu_m\right]}, \tag{5.52}$$

respectively.

We now present the results for the long channel model defined by Eqs. (5.32) and (5.33) with axial diffusion/conduction terms dropped and the Danckwerts inlet conditions replaced by the Dirichlet conditions:

$$c=1,\ \theta=0 \text{ at } x=0. \tag{5.53}$$

In this case, the dimensionless concentration and temperature profiles are given by:

$$c(x,y)=\sum_{n=1}^{\infty}\frac{4(-1)^{n-1}}{(2n-1)\pi}\exp[-(\lambda_n+\phi^2)x]\cos\left[\frac{2n-1}{2}\pi y\right] \tag{5.54}$$

and

$$\begin{aligned}\theta(x,y) &= \sum_{n=1}^{\infty}\frac{2}{\lambda_n}\left(1-\exp[-(\lambda_n+\phi^2)x]\right)+ \\ &\quad 4\sum_{m,n=1}^{\infty}(-1)^m\left(1+\frac{4\phi^2}{\left((2n-1)^2-4m^2\right)\pi^2}\right)\times \\ &\quad \frac{\exp[-(\lambda_n+\phi^2)x]-\exp[-Le_f\mu_m x]}{\left[Le_f\mu_m-(\lambda_n+\phi^2)\right]}\cos[m\pi y]. \qquad (5.55)\end{aligned}$$

We note that the limiting case of no homogeneous reaction can be obtained easily by setting ϕ to zero. It may also be verified that in the limit of $Pe_r^2 \to \infty$, the model with Danckwerts inlet condition directly yields the solution of the equations with Dirichlet inlet conditions [Remark: We have excluded the case of Dirichlet boundary condition at the inlet but with axial diffusion and conduction added as this leads to physical inconsistencies as shown below for the 1-D model].

1-D model with axial gradients:

We consider only axial gradients in this subsection because we wish to investigate and isolate the effects of axial gradients on the location and magnitude of the maximum temperature. The assumption of negligible radial gradients becomes accurate if the wall reaction is sufficiently slow compared to transverse diffusion or if the channel spacing is small. These effects can be quantified in terms of Thiele modulus for the catalytic reaction and the radial Peclet number, $\phi_s^2 = \frac{k_s a}{D_m}$ and $Pe_r = \frac{\overline{u}a}{D_m}$, respectively. When ϕ_s^2 and $Pe_r \ll 1$, we can lump the transverse modes and get the homogeneous model given by eqns (5.26) and (5.27).

These equations can be readily solved to yield

$$c(\zeta) = \frac{2e^{\lambda\zeta}}{1+\sqrt{1+4\Lambda}} \tag{5.56}$$

and

$$\theta(\zeta) = \frac{2\Lambda}{\lambda\left(1+\sqrt{1+4\Lambda}\right)}\left[\frac{e^{\lambda\zeta}}{1-\lambda Le_f} - 1\right], \tag{5.57}$$

where

$$\lambda = \frac{1-\sqrt{1+4\Lambda}}{2}. \tag{5.58}$$

Then

$$\frac{d\theta}{d\zeta} = \frac{2\Lambda}{1+\sqrt{1+4\Lambda}}\left[\frac{e^{\lambda\zeta}}{1-\lambda Le_f}\right]. \tag{5.59}$$

Since $\lambda < 0$, $\frac{d\theta}{d\zeta} > 0$, which means that θ increases monotonically to its maximum value that is given by

$$\theta_{\max} = \theta(\infty) = \frac{-2\Lambda}{\lambda\left(1+\sqrt{1+4\Lambda}\right)} = 1. \tag{5.60}$$

Thus, the maximum temperature attained is the adiabatic temperature. This result is independent of the Lewis number and we conclude that the temperature in a radially lumped model with Danckwerts boundary condition can never exceed the adiabatic value.

Let us now turn to a study of the same model with Dirichlet inlet conditions given

by

$$\begin{aligned} c &= 1 \text{ and} \\ \theta &= 0 \text{ at } \zeta = 0. \end{aligned} \tag{5.61}$$

Then we obtain

$$c(\zeta) = e^{\lambda\zeta} \tag{5.62}$$

and

$$\theta(\zeta) = \frac{\Lambda}{\lambda\left(1 - \lambda Le_f\right)}\left(e^{\lambda\zeta} - 1\right). \tag{5.63}$$

Again

$$\frac{d\theta}{d\zeta} = \frac{\Lambda e^{\lambda\zeta}}{\left(1 - \lambda Le_f\right)} > 0 \tag{5.64}$$

and

$$\theta_{\max} = \theta(\infty) = \frac{\Lambda}{\lambda\left(\lambda Le_f - 1\right)} = \frac{1}{Le_f + \frac{Le_f - 1}{2\Lambda}\left(1 - \sqrt{1 + 4\Lambda}\right)}. \tag{5.65}$$

Thus, when $\Lambda \to 0$, $\theta_{\max} \to 1$, and when $\Lambda \to \infty$,

$$\theta_{\max} \approx \frac{1}{Le_f + \frac{1 - Le_f}{\sqrt{\Lambda}}} \to \frac{1}{Le_f}. \tag{5.66}$$

Thus, for infinitely fast reactions $(\Lambda \to \infty)$, the imposition of the Dirichlet boundary condition may lead to superadiabatic or subadiabatic maximum temperatures depending on the magnitude of the Lewis number, Le_f. However, the physically consistent Danckwerts boundary conditions only lead to adiabatic maximum temper-

atures. It may be shown that this conclusion also holds for the more general 1-D model defined by eqns. 5.19, 5.20 and 5.21. Thus, we conclude that deviations from the adiabatic maximum temperature are not due to axial gradients. Therefore, in the next section we study a model with transverse gradients only.

5.3.2 Short channel model

We now consider a limiting model for our homogeneous-heterogeneous reaction system where only radial gradients are present using the "short monolith model" introduced by Balakotaiah et al ([14]). We obtain this model via averaging in the axial direction when the channel length is small compared to the transverse length scale and the axial Peclet number, $Pe \ll 1$. This model is useful in proving analytical results for the temperature and the location of the hot spot in the dilute reactant case. This cannot be done with the results of the long channel model because the Fourier series solutions obtained therein converge in the L^2 norm, i.e. integrated averages of squares of the functions we evaluated converge, but the function values need not converge at every point. Also derivatives of the series need not converge rendering the determination of maximum temperature problematic. The short channel model is given by

$$\frac{1}{P}\frac{d^2c}{dy^2} - Dac = c - 1 \text{ and} \tag{5.67}$$

$$\frac{Le_f}{P}\frac{d^2\theta}{dy^2} + Dac = \theta \text{ with} \tag{5.68}$$

$$\frac{dc}{dy} = 0, \ \frac{d\theta}{dy} = 0 \qquad \text{at } y = 0 \text{ and} \tag{5.69}$$

$$\frac{dc}{dy} = -\phi_s^2 c, \quad \frac{d\theta}{dy} = \phi_s^2 c \quad \text{at } y = 1. \tag{5.70}$$

Here, P and Da are defined in the standard manner as

$$P = \frac{\overline{u}a^2}{LD_m}; \qquad Da = \frac{k_v L}{\overline{u}}. \tag{5.71}$$

This means that the Thiele modulus for the homogeneous reaction is given as

$$\phi^2 = PDa. \tag{5.72}$$

We can solve these equations in the case of flat velocity profile to obtain

$$c = \frac{P}{\psi^2}\left(1 - \frac{\cosh(\psi y)}{\cosh(\psi) + \psi\frac{\sinh(\psi)}{\phi_s^2}}\right),$$

where $\psi = \sqrt{P + \phi^2}$ and

$$\theta = \sqrt{\frac{P}{Le_f}}\frac{\tanh(\psi)}{\psi\frac{\tanh(\psi)}{\phi_s^2} + 1}\frac{\cosh\left(\sqrt{\frac{P}{Le_f}}y\right)}{\sinh\sqrt{\frac{P}{Le_f}}}\left(1 - \frac{\phi^2}{\psi^2 - \frac{P}{Le_f}}\right) + \frac{\phi^2}{\psi^2} + \frac{P}{Le_f}\frac{\phi^2}{\psi^2}\frac{\cosh(\psi y)}{\cosh(\psi)\left(\psi^2 - \frac{P}{Le_f}\right)}. \tag{5.73}$$

In this section, we are mainly interested in finding the conditions under which a "*potential temperature*" defined by the sum of dimensionless concentration and temperature exceeds 1. This potential temperature represents the hypothetical temperature that would be attained if all the available limiting reactant at any location were fully and instantly converted by the homogeneous reaction to lead to an equivalent amount

of heat generation. This is also the quantity used by Zheng and Mantzaras in their recent work ([1]). To illustrate this, we ignore the homogeneous reaction by taking $\phi^2 = 0$. We can now solve these equations and obtain

$$c(y) = \left[1 - \frac{\cosh\sqrt{P}y}{\cosh\sqrt{P} + \sqrt{P}\frac{\sinh\sqrt{P}}{\phi_s^2}}\right] \text{ and} \tag{5.74}$$

$$\theta(y) = \left[\frac{\tanh\sqrt{P}}{\sqrt{Le_f}\left(1 + \frac{\sqrt{P}}{\phi_s^2}\tanh\sqrt{P}\right)}\frac{\cosh\sqrt{\frac{P}{Le_f}}y}{\sinh\sqrt{\frac{P}{Le_f}}}\right]. \tag{5.75}$$

If we consider the catalytic reaction to be infinitely fast, we must modify the boundary conditions to

$$\frac{dc}{dy} = 0,\ \frac{d\theta}{dy} = 0 \quad \text{at } y = 0, \tag{5.76}$$

$$c = 0 \qquad \text{at } y = 1 \text{ and} \tag{5.77}$$

$$\frac{d\theta}{dy} = \frac{-1}{Le_f}\frac{dc}{dy} \qquad \text{at } y = 1. \tag{5.78}$$

This leads to the concentration profile

$$c(y) = \left[1 - \frac{\cosh\sqrt{P}y}{\cosh\sqrt{P}}\right] \tag{5.79}$$

and the temperature profile

$$\theta(y) = \left[\frac{\tanh\sqrt{P}}{\sqrt{Le_f}}\frac{\cosh\sqrt{\frac{P}{Le_f}}y}{\sinh\sqrt{\frac{P}{Le_f}}}\right]. \tag{5.80}$$

The above expressions are readily seen to be limiting solutions of (5.74) and (5.75)

when $\phi_s^2 \to \infty$. (The expressions for concentration and temperature in the system above with homogeneous reaction are easy to obtain and are given in the Appendix.) We use these results in the numerical calculations presented in the next section and also to examine the potential temperature as well as the true maximum temperature.

We can evaluate the (transverse) average values of the concentration and temperature variables, given by

$$\langle c \rangle = 1 - \frac{\tanh\sqrt{P}}{\sqrt{P}\left(1 + \frac{\sqrt{P}}{\phi_s^2}\tanh\sqrt{P}\right)} = 1 - \frac{\tanh\sqrt{P}}{\sqrt{P}} \text{ as } \phi_s^2 \to \infty \tag{5.81}$$

and

$$\langle \theta \rangle = \frac{\tanh\sqrt{P}}{\sqrt{P}\left(1 + \frac{\sqrt{P}}{\phi_s^2}\tanh\sqrt{P}\right)} = \frac{\tanh\sqrt{P}}{\sqrt{P}} \text{ as } \phi_s^2 \to \infty. \tag{5.82}$$

The expression for the average temperature is the same as the well-known result for effectiveness factor for a catalyst slab, with P taking on the role of ϕ^2. It has asymptotes given by $\frac{\tanh\sqrt{P}}{\sqrt{P}} \to 1$ as $P \to 0$ and $\frac{\tanh\sqrt{P}}{\sqrt{P}} \to \frac{1}{\sqrt{P}}$ as $P \to \infty$.

The potential temperature θ^* as defined by Zheng and Mantzaras [1] is

$$\theta^* = c + \theta. \tag{5.83}$$

We are interested in understanding when θ^* exceeds 1 at the center of the channel. To quantify this, we define an excess potential temperature θ_E :

$$\theta_E = \theta^*(0) - 1 = \frac{\tanh\sqrt{P}}{\sqrt{Le_f}} \frac{1}{\sinh\sqrt{\frac{P}{Le_f}}} - \frac{1}{\cosh\sqrt{P}}. \tag{5.84}$$

Expanding θ_E in a Taylor series in P, keeping only first order terms, we obtain

$$\theta_E = \frac{Le_f - 1}{6Le_f} P + O(P^2). \tag{5.85}$$

This means that for small values of P and $Le_f > 1$, $\theta_E > 0$. This confirms that potential temperature indeed exceeds 1 for $Le_f > 1$, but only for a limited range of P.

If we expand θ_E in a Taylor series in Le_f about $Le_f = 1$, again keeping only first order terms, we obtain

$$\theta_E = \frac{Le_f - 1}{2} \left(\frac{\sqrt{P}}{\sinh \sqrt{P}} - \frac{1}{\cosh \sqrt{P}} \right) + O\left((Le_f - 1)^2 \right). \tag{5.86}$$

For $x > 0$, we have $\frac{\tanh x}{x} < 1 \Rightarrow \frac{1}{\cosh x} < \frac{x}{\sinh x}$. Therefore $\theta_E > 0$, when $Le_f > 1$ for any P. θ_E is an increasing function of Le_f, so we consider the case when θ_E attains its maximum value for $Le_f \to \infty$. We then have $\theta_E^{\infty} = \lim_{Le_f \to \infty} \theta_E = \frac{\tanh \sqrt{P}}{\sqrt{P}} - \frac{1}{\cosh \sqrt{P}}$. This function attains a maximum value of 0.23 for $P = 7.66$. Thus the maximum possible superadiabatic temperature is 23%, which is close to the corresponding maximum excess of 20.8 % found in the numerical calculations of Zheng and Mantzaras (2014). They find the location of the excess at $x^+ = 0.0086$ where $x^+ = \frac{xD_m}{\overline{u}(4a)^2}$. This is analogous to $\frac{1}{16P}$ in our model, which comes out to be 0.00816. Thus, the short channel model yields very similar results for the potential temperature as Zheng and Mantzaras (2014).

Having shown that the short channel model retains the qualitative (and quanti-

tative) features of the full 2-D model, we have used it to examine the actual (and not the potential) peak temperature with homogeneous reaction [using the solution of Eqs.(5.67)-(5.70) presented in the Appendix]. We have found that unlike the claim of Zheng and Mantzaras (2014), the actual temperature never exceeds the adiabatic value when $Le_f > 1$ [A proof of this using the short monolith model is given in the Appendix]. The main reason for this may be explained by the fact that there cannot be instantaneous conversion of the limiting reactant without causing (infinite) temperature gradient locally. Thus, the potential temperature as defined by Zheng and Mantzaras has no relation to the actual temperature that may be attained in the system. This is further illustrated in the numerical results presented in the following section.

Although it is not the focus of this chapter, as an aside, we show how we can obtain the Sherwood number from the expressions derived in this section. We use the definition of Sherwood number, $Sh = \frac{\left(-\frac{\partial c}{\partial y}\right)_{y=1}}{c_m - c_s}$ leading to

$$Sh = \frac{\psi \tanh(\psi)}{1 - \frac{\tanh(\psi)}{\psi}}. \tag{5.87}$$

Note that this expression for the Sherwood number depends on the Thiele modulus of the homogeneous reaction simply as a modification of P to $\sqrt{P + \phi^2}$. For the catalytic

reaction to be infinitely fast, we modify the boundary conditions to

$$\begin{aligned} \frac{dc}{dy} &= 0, \ \frac{d\theta}{dy} = 0 \ \text{ at } y = 0, && (5.88) \\ c &= 0 \qquad\qquad \text{at } y = 1, \text{ and} && (5.89) \\ \frac{d\theta}{dy} &= \frac{-1}{Le_f}\frac{dc}{dy} \qquad \text{at } y = 1. && (5.90) \end{aligned}$$

The Sherwood number can be expressed again by the same formula as before because it is independent of the strength of the catalytic reaction. Explicitly, we have

$$Sh = \frac{\sqrt{P+\phi^2}}{\frac{1}{\tanh\sqrt{P+\phi^2}} - \frac{1}{\sqrt{P+\phi^2}}}. \tag{5.91}$$

It can be easily seen that this expression for the Sherwood number admits the following asymptotes:

$$\begin{aligned} Sh &\rightarrow 3 \text{ as } (P+\phi^2) \rightarrow 0 \\ Sh &\rightarrow \sqrt{P+\phi^2} \text{ as } (P+\phi^2) \rightarrow \infty. \end{aligned} \tag{5.92}$$

5.3.3 Numerical results

The analytical solutions may be used to plot the concentration and temperature fields and the impact of transport parameters on these fields. The Fourier series solutions presented above typically converged quite fast and gave us no computational difficulty. Different values of Lewis number, Peclet number and Thiele modulus yield different qualitative behavior. Figure 5-1 (top) shows a typical temperature contour

plot for the 2-D model for parallel plate reactor with a homogeneous reaction for Danckwerts inlet conditions for $\phi^2 = 3.0$, $Le_f = 1.5$ and $Pe_r = 5.0$. Next we have shown in figure 5-1, a concentration contour plot for a system with $Pe_r = 5$ and $\phi^2 = 3$ (middle), and a temperature contour plot for a system with $Pe_r = 15$, $Le_f = 2.5$ and $\phi^2 = 30$ (bottom). We note that for these values of parameters, the maximum temperature is always less than the adiabatic value represented by $\theta = 1$. Figure 5-1 (top) shows the situation where the wall is always hotter than the center while figure 5-1 (bottom) shows that the center can be hotter than the wall as well. [Remark: As Danckwerts boundary conditions allow upstream gradients, the temperature and concentration at the inlet to the channel $x = 0$ can be substantially different from the feed values]. Figure 5-2 (top) shows a temperature contour plot for Danckwerts inlet conditions with no homogeneous reaction and $Pe_r = 5.0$ for $Le_f = 1.5$ and figure 5-2 (middle) shows a concentration contour plot for this system. Again we find that the maximum temperature never exceeds the adiabatic value. However, when we plot in figure 5-2 (bottom) a dimensionless potential temperature which is the sum of θ and c, we find that the maximum (potential) temperature within the system does exceed the adiabatic value. This potential temperature corresponds to the temperature that would result if all the reactant available did indeed react, leading to the production of an equivalent amount of energy. As stated earlier, the fact that this potential temperature is never realized is due to the creation of gradients by the homogeneous reaction itself, preventing localization of energy wherever the potential temperature might have exceeded the adiabatic value. The calculations for the Dirichlet inlet condition shown in figure 5-3 give similar results. We find that the

maximum temperature never exceeds the adiabatic value for Lewis number greater than 1, unless we consider adding to the temperature variable the concentration to yield a potential temperature. Figure 5-3 shows the temperature (top), concentration (middle) and the potential temperature (bottom) for $Le_f = 1.5$ and $Pe_r = 10$, with no homogeneous reaction. [Remark: For Dirichlet boundary conditions at the inlet with no axial diffusion/conduction, we have $c(x = 0, y) = 1; \theta(x = 0, y) = 0$ for $0 \leq y < 1$. The point $x = 0$, $y = 1$ is a singularity when $\phi_s^2 \rightarrow \infty$, i.e. the wall reaction is infinitely fast.]

To gain a better understanding of the location of the hot spot, we plot the variations of the average temperature, the wall temperature and the center temperature along the length of the reactor in figures 5-4 and 5-5. These three temperatures could serve as three modes in a low-dimensional description of our system. Figure 5-4 deals with the case of $Le_f = 1.5$ and $Pe_r = 5$, with figure 5-4 (a) depicting the case of no homogeneous reaction, figure 5-4 (b) denoting a strong homogeneous reaction ($\phi^2 = 50$) and figure 5-4 (c) denoting a blown-out version of the middle figure. In this case of larger than unity Lewis number, all the temperature modes increase monotonically to the adiabatic value. Also it is evident that with increasing the strength of the homogeneous reaction, the wall temperature decreases and the difference with the centerline and wall temperatures becomes smaller. This is because the homogeneous reaction consumes the excess reactants that would otherwise have migrated to the wall. Next, we have shown in figure 5-5, the case of $Le_f = 0.5$ and $Pe_r = 5$, with figure 5-5 (a) depicting the case of no homogeneous reaction and figure 5-5 (b) denoting a strong homogeneous reaction ($\phi^2 = 50$). Here, the maximum temperature is

attained on the wall and its magnitude decreases while the location moves closer to the inlet as ϕ^2 increases.

Thus, we observe that for $Le_f < 1$, the maximum temperature is always attained at the wall. In fact, the wall temperature exceeds the adiabatic value in a small range and then dips again, finally meeting the centerline and average temperatures at the adiabatic value. When $Le_f > 1$, all three modes eventually reach the adiabatic value together, which is the maximum temperature reached everywhere. The effect of increasing the magnitude of homogeneous reaction rate is that the region of radial gradients gets compressed. The homogeneous reaction is more potent in zones of higher concentration, consuming reactants faster in these zones and leveling off gradients. We also observe that the centerline and average temperatures may exceed the wall temperature at higher values of ϕ^2, representing faster homogeneous reaction. For the sake of comparison, we show in figures 5-6 and 5-7, variations of the average temperature ($\langle\theta\rangle$), the wall temperature (θ_s) and the center temperature (θ_c) for the short channel model with the reciprocal of transverse Peclet number when (a) $\phi = 0$ and (b) $\phi^2 = 50$ for Lewis numbers of 1.5 and 0.5, respectively. These figures have been computed using the results given in the appendix. The trends observed are similar to figures 5-4 and 5-5 with all three curves asymptotically approaching 1. In figure 5-8, we have shown a contour plot for the short channel model where the reciprocal of transverse Peclet number has been taken to be analogous to the axial spatial variable. The trends are remarkably similar to plots for the 2-D model such as figure 5-2. To understand how the strength of the homogeneous reaction affects the wall and the center temperatures, figures 5-9 and 5-10 show variations of the wall

temperature (θ_s) and the center temperature (θ_c) for the short channel model with the reciprocal of transverse Peclet number when ϕ^2 is changed from 0 to 50 for Lewis numbers of 1.5 and 0.5, respectively. For both Lewis numbers, θ_c shows an increase as ϕ^2 increases, however θ_s decreases with increasing ϕ^2 when $Le_f < 1$ and increases with increasing ϕ^2 when $Le_f > 1$.

5.4 Summary and Discussion

The main goal of this chapter was to examine the impact of transport parameters on the magnitude and location of the temperature peak in coupled homogeneous-heterogeneous reaction system. Our main conclusions can be summarized as follows:

(i) Hot spot formation may be possible both near the wall and near the center, and the temperature variation in the direction transverse to flow need not be monotonic. In either case, for 2D solutions, temperature at the center never exceeds the adiabatic value for $Le_f > 1$ as claimed by Zheng and Mantzaras, (2014).

(ii) If we consider the 'potential' temperature given by the sum of the temperature and concentration, we may get superadiabatic temperatures. However, this potential temperature never corresponds to the actual temperature because the homogeneous reaction could not possibly consume instantly all the excess reactants present at a specific location such as the center and convert it to equivalent amounts of energy, as this would create an infinite local gradient.

The physical insight derived from this analysis can be useful in bifurcation studies of combustion systems in which both homogeneous and catalytic reactions can occur simultaneously. In the last two chapters, we showed that the thermally coupled

hysteresis locus is virtually unchanged from the hysteresis locus for a system with infinitely fast wall reaction. Hence, a study of homogeneous combustion with a very fast catalytic chemistry is useful to understand and compute bifurcation features of thermally coupled combustion systems. The analysis of maximum temperature in the present chapter is helpful in understanding qualitative features of the solutions of the 2-D and 3-D models.

Finally it should be pointed out that the main results of this work (especially those pertaining to the maximum temperature) are valid only for uni-directional flows with no heat recirculation within the system. In the presence of heat recirculation (or autothermal operation using heat exchange), it is well-known that superadiabatic temperatures are easily obtained irrespective of the Lewis or Peclet numbers even for ultra-lean or ultra -rich reaction mixtures (see Lovo and Balakotaiah (1992) and Schoegl and Ellzey (2007) for more details).

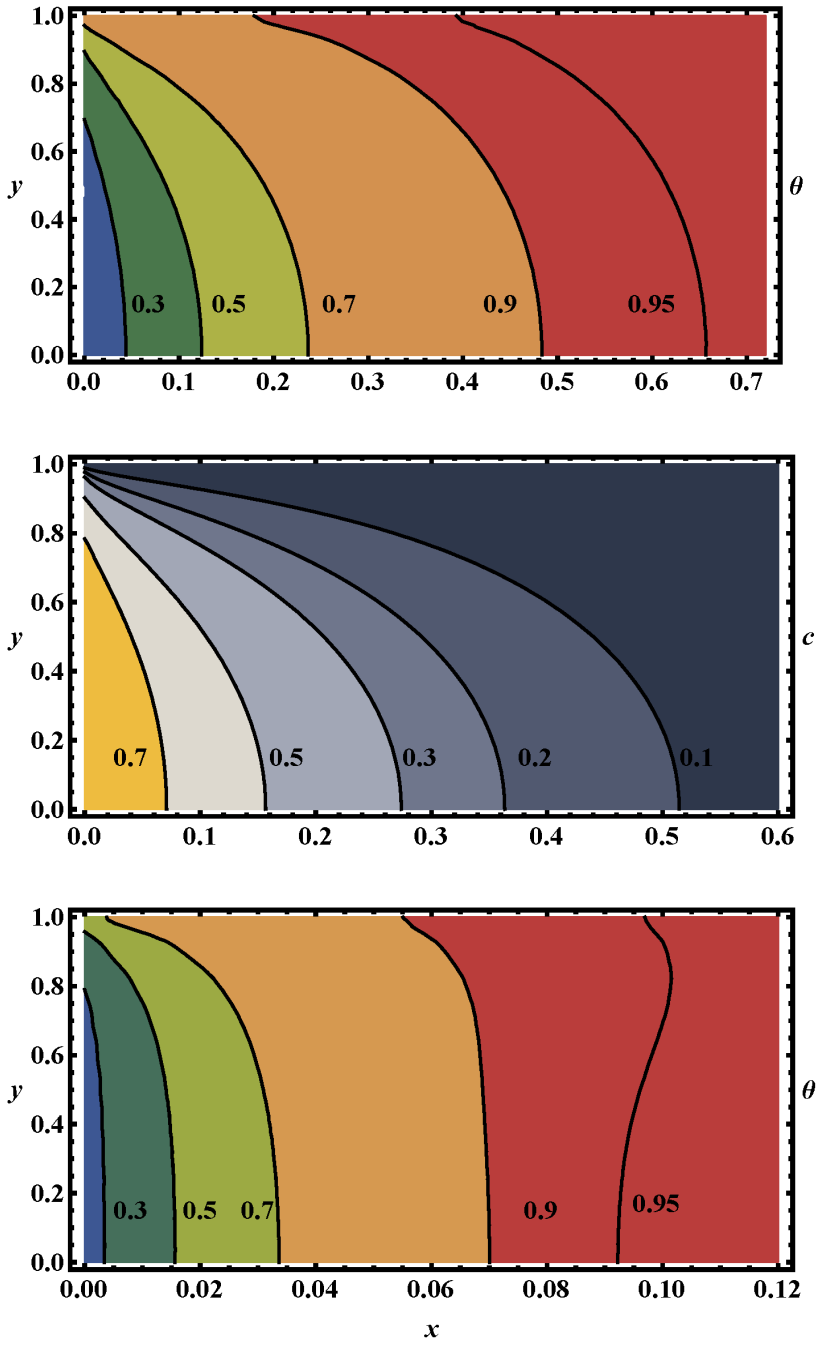

Figure 5-1: Contour plots for a 2-D parallel plate reactor model with $\phi_s^2 = \infty$ and Danckwerts inlet condition showing (top) temperature (Pe_r= 5, Le_f= 1.5, ϕ^2=3), (middle) concentration (Pe_r= 5, ϕ^2=3) and (bottom) temperature (Pe_r= 15, Le_f= 2.5, ϕ^2=30).

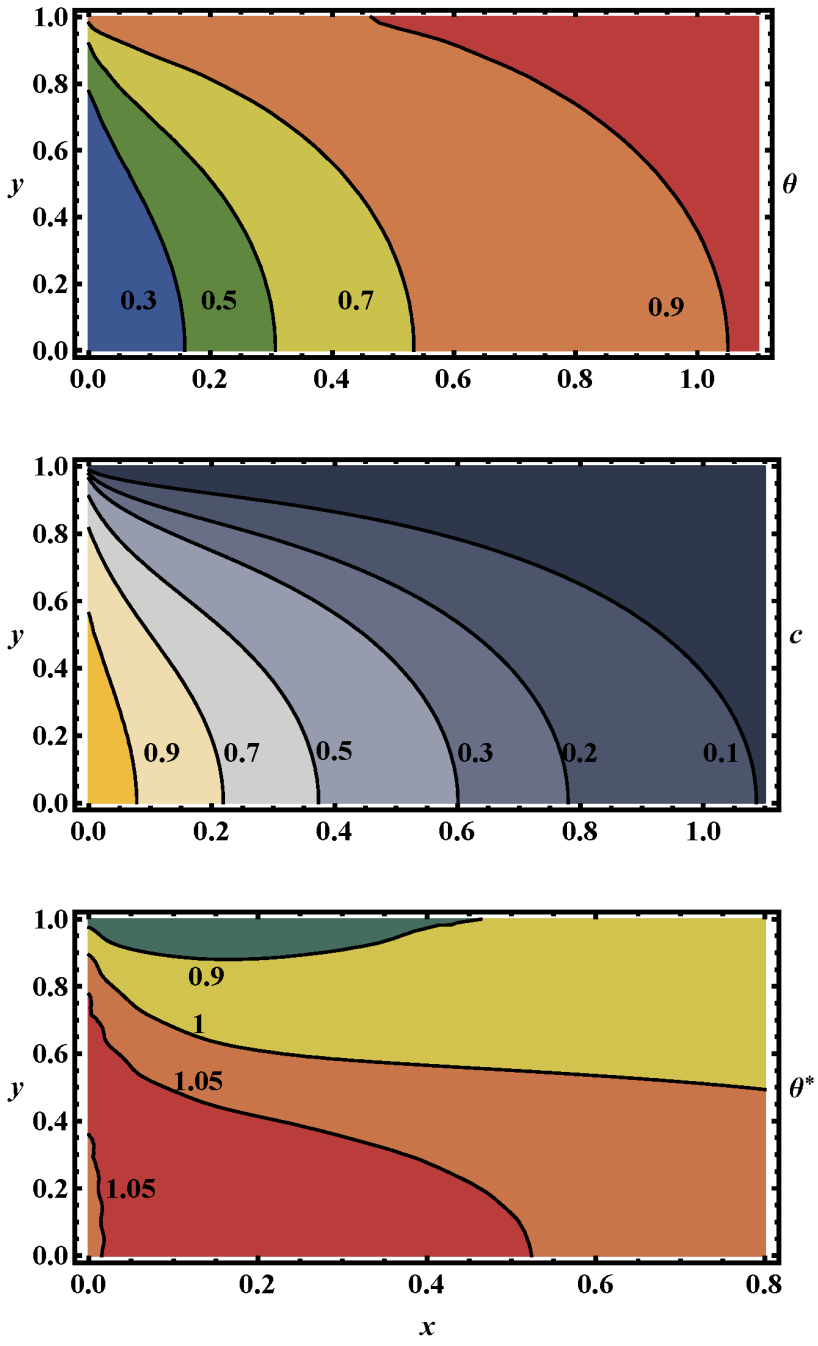

Figure 5-2: Contour plots for a 2-D parallel plate reactor model with Pe_r=10, Le_f=1.5, $\phi^2 = 0$ and $\phi_s^2 = \infty$ and Danckwerts inlet condition showing (top) temperature, (middle) concentration and (bottom) potential temperature.

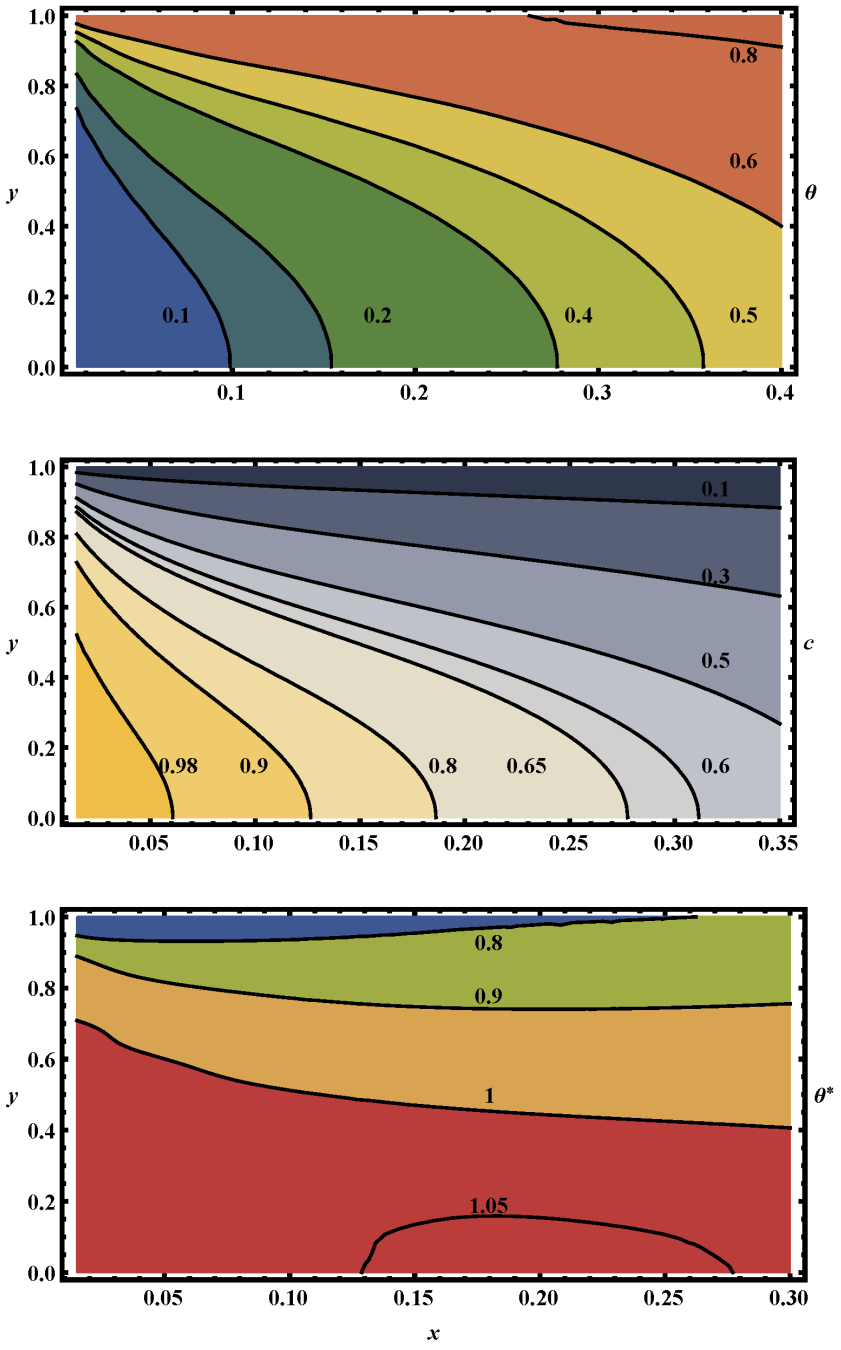

Figure 5-3: Contour plots for a parallel plate reactor with Pe_r =10, ϕ^2= 0 and $\phi_s^2 = \infty$ and Dirichlet inlet condition showing (top) temperature ($Le_f = 1.5$), (middle) concentration, and (bottom) potential temperature ($Le_f = 1.5$).

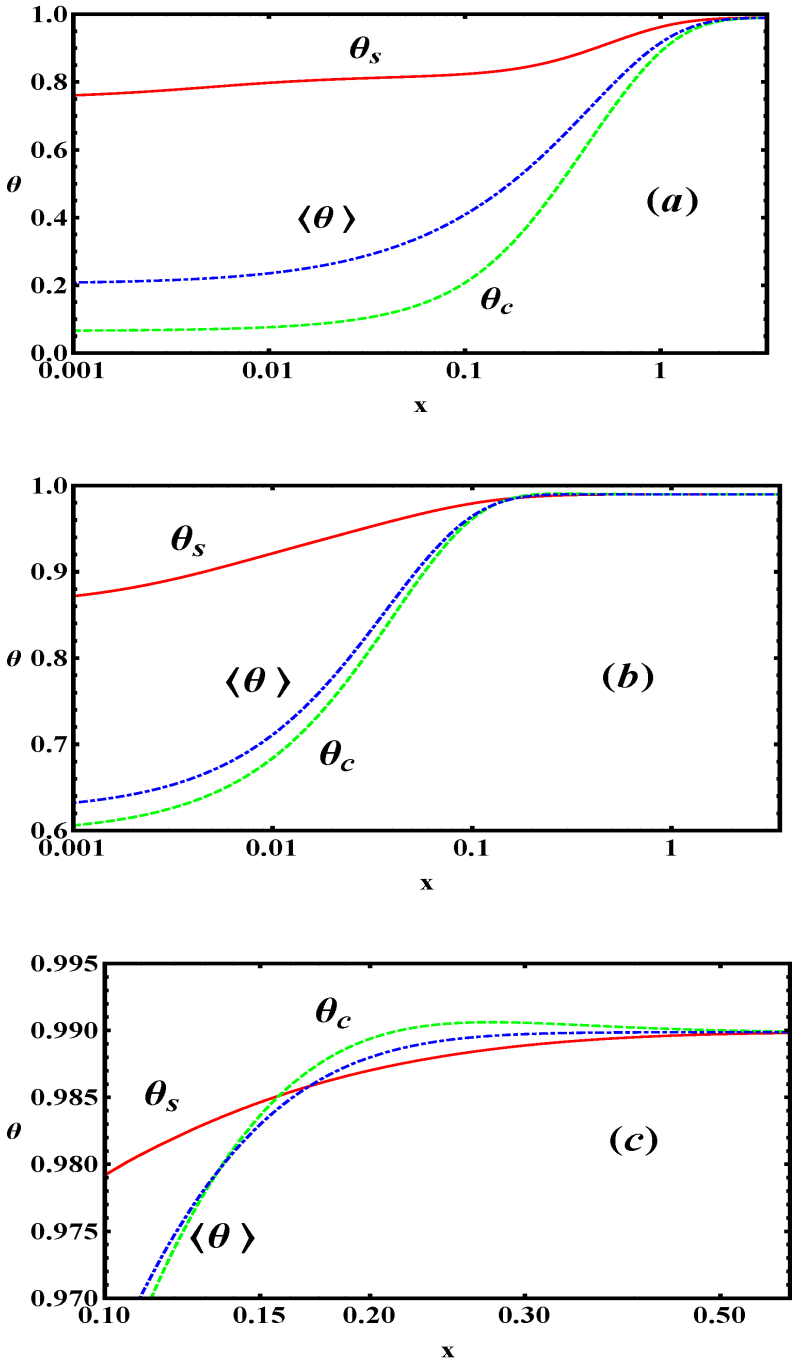

Figure 5-4: Variations of the average temperature ($\langle\theta\rangle$), the wall temperature (θ_s) and the center temperature (θ_c) along the reactor length for Le_f of 1.5 and Pe_r of 5 when $\phi_s^2 = \infty$ and (a) $\phi^2 = 0$ and (b) $\phi^2 = 50$. (c) shows a blow-up of (b).

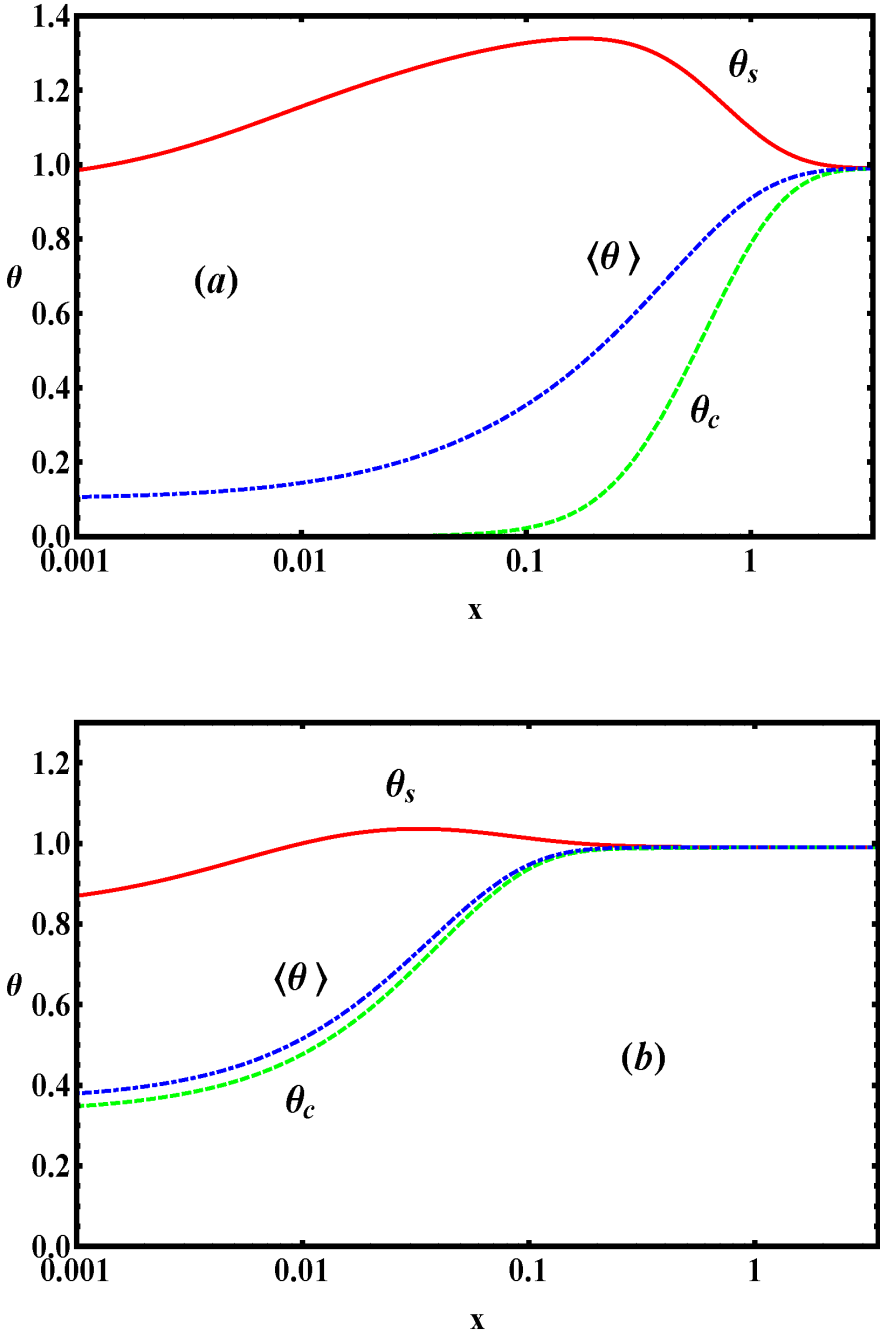

Figure 5-5: Variations of the average temperature ($\langle\theta\rangle$), the wall temperature (θ_s) and the center temperature (θ_c) along the length of the reactor for Le_f of 0.5 and radial Peclet number of 5 when $\phi_s^2 = \infty$ and (a) $\phi^2 = 0$ and (b) $\phi^2 = 50$.

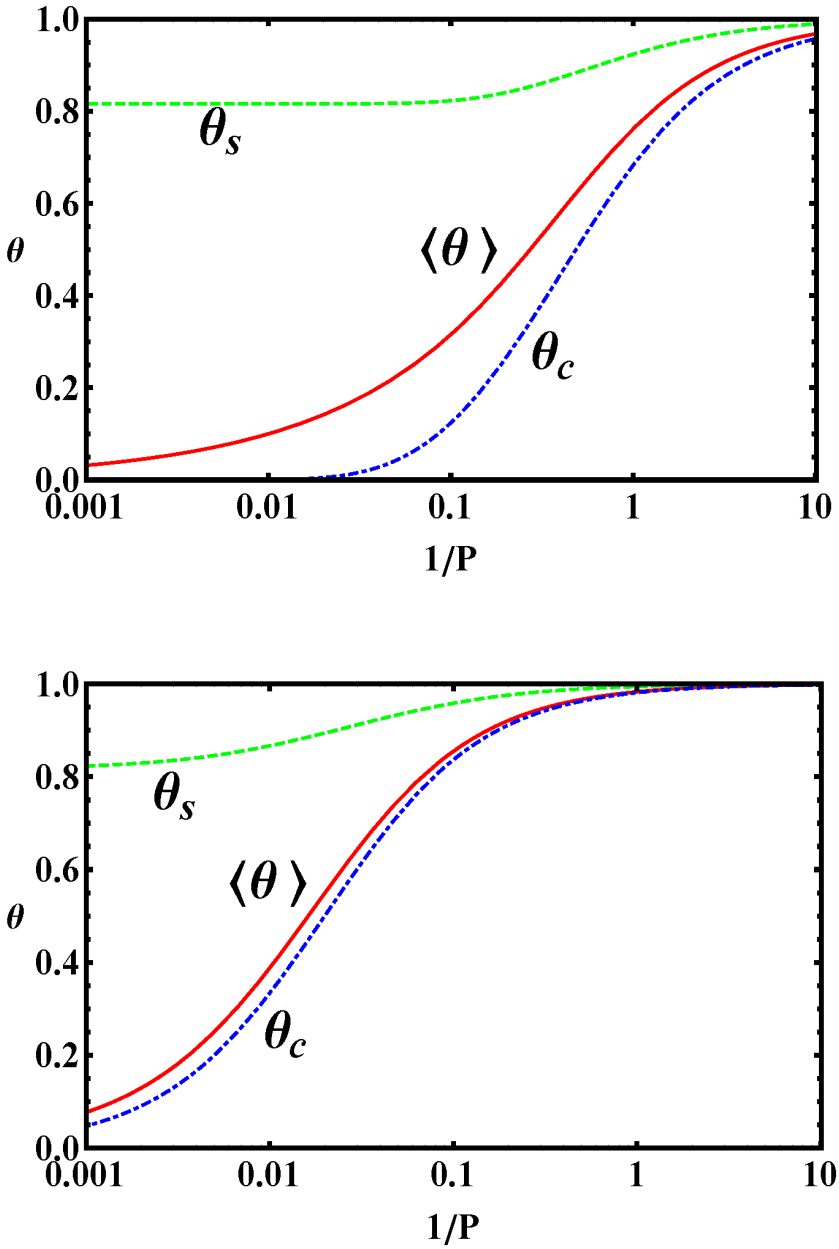

Figure 5-6: Variations of the average temperature ($\langle\theta\rangle$), the wall temperature (θ_s) and the center temperature (θ_c) for the short channel model with the transverse Peclet number for $Le_f = 1.5$ when $\phi_s^2 = \infty$ and (a) $\phi^2 = 0$ and (b) $\phi^2 = 50$.

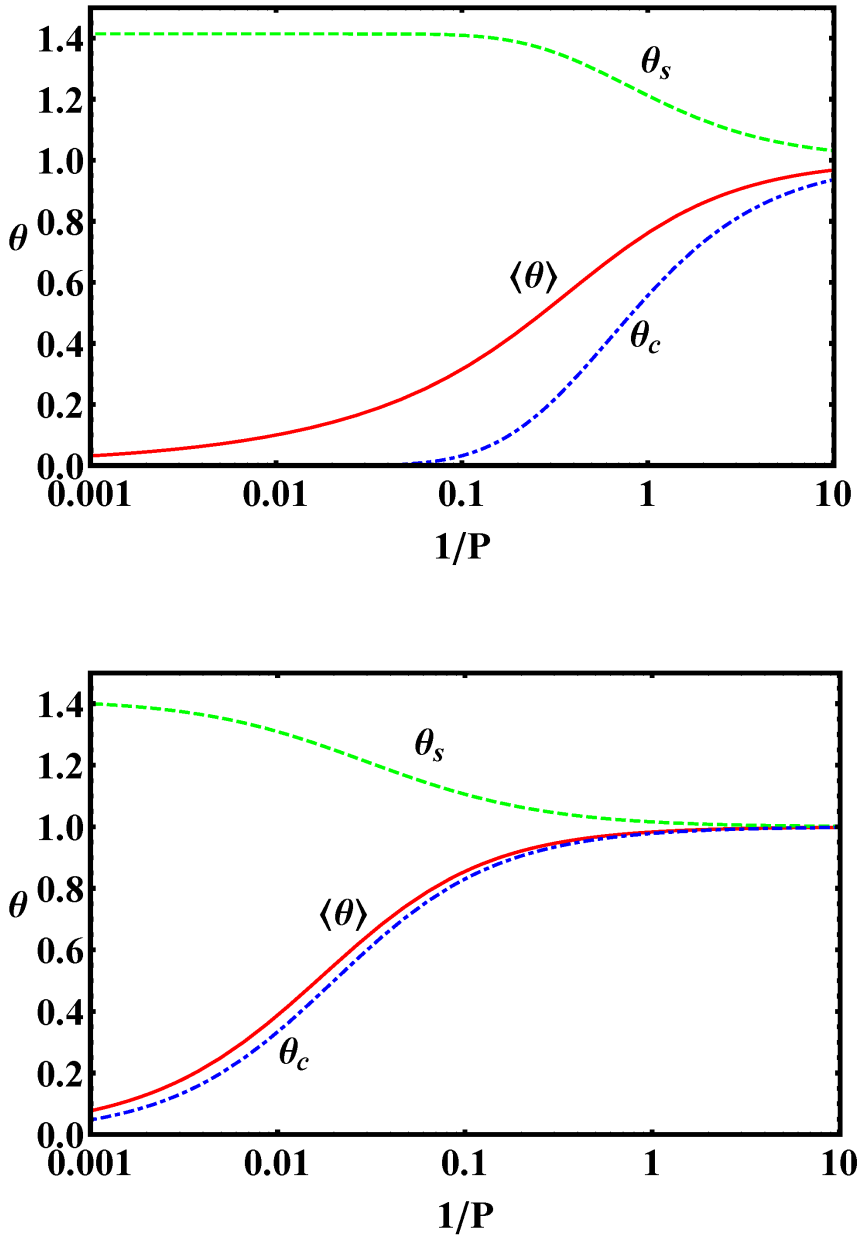

Figure 5-7: Variations of the average temperature ($\langle\theta\rangle$), the wall temperature (θ_s) and the center temperature (θ_c) for the short channel model with the transverse Peclet number for $Le_f = 0.5$ when $\phi_s^2 = \infty$ and (a) $\phi^2 = 0$ and (b) $\phi^2 = 50$.

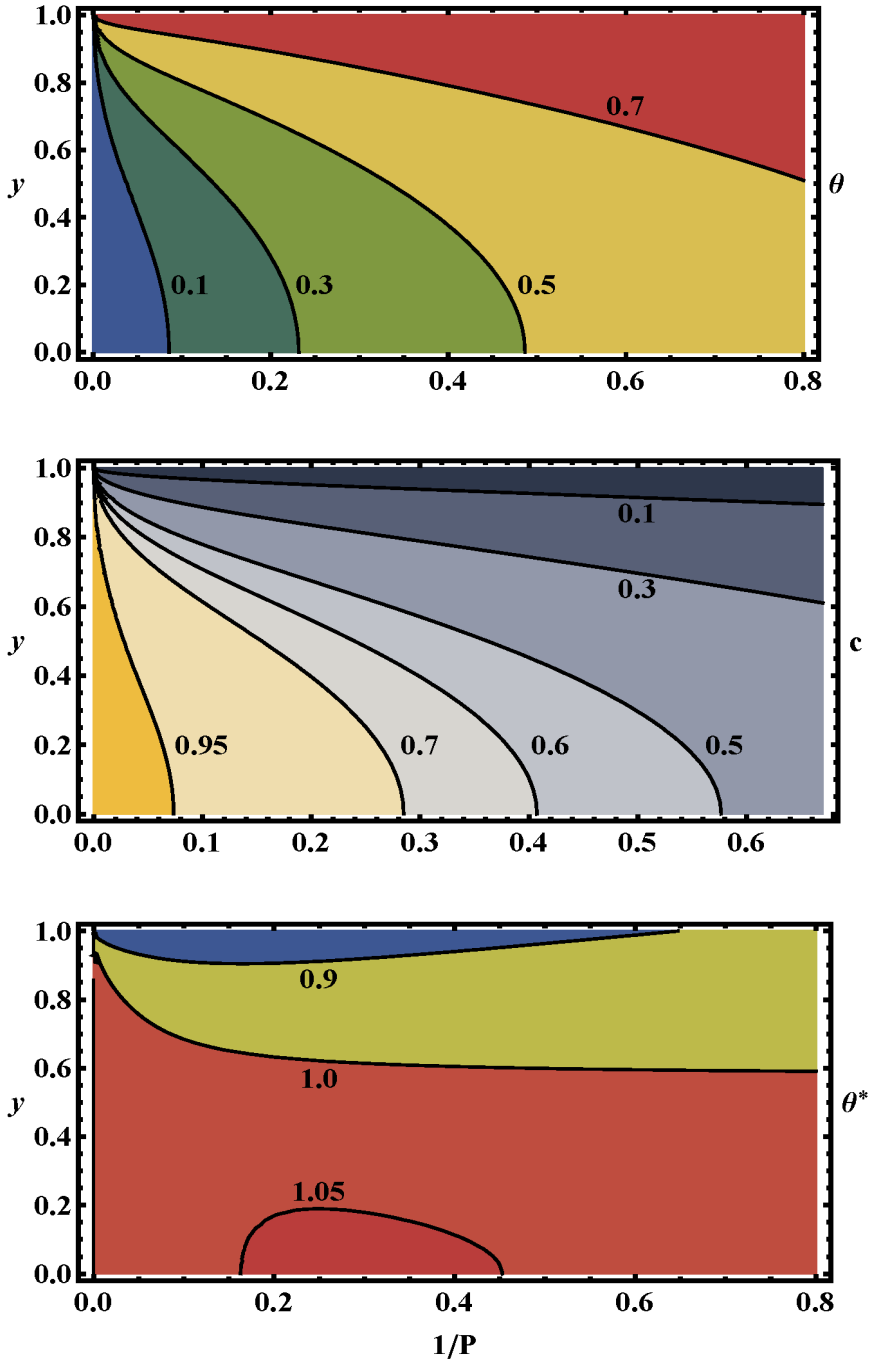

Figure 5-8: Contour plots for the short channel model for parallel plate reactor with $\phi^2 = 0$ and $\phi_s^2 = \infty$ showing (top) temperature, (middle) concentration (Le_f=1.5), and (bottom) potential temperature (Le_f=1.5).

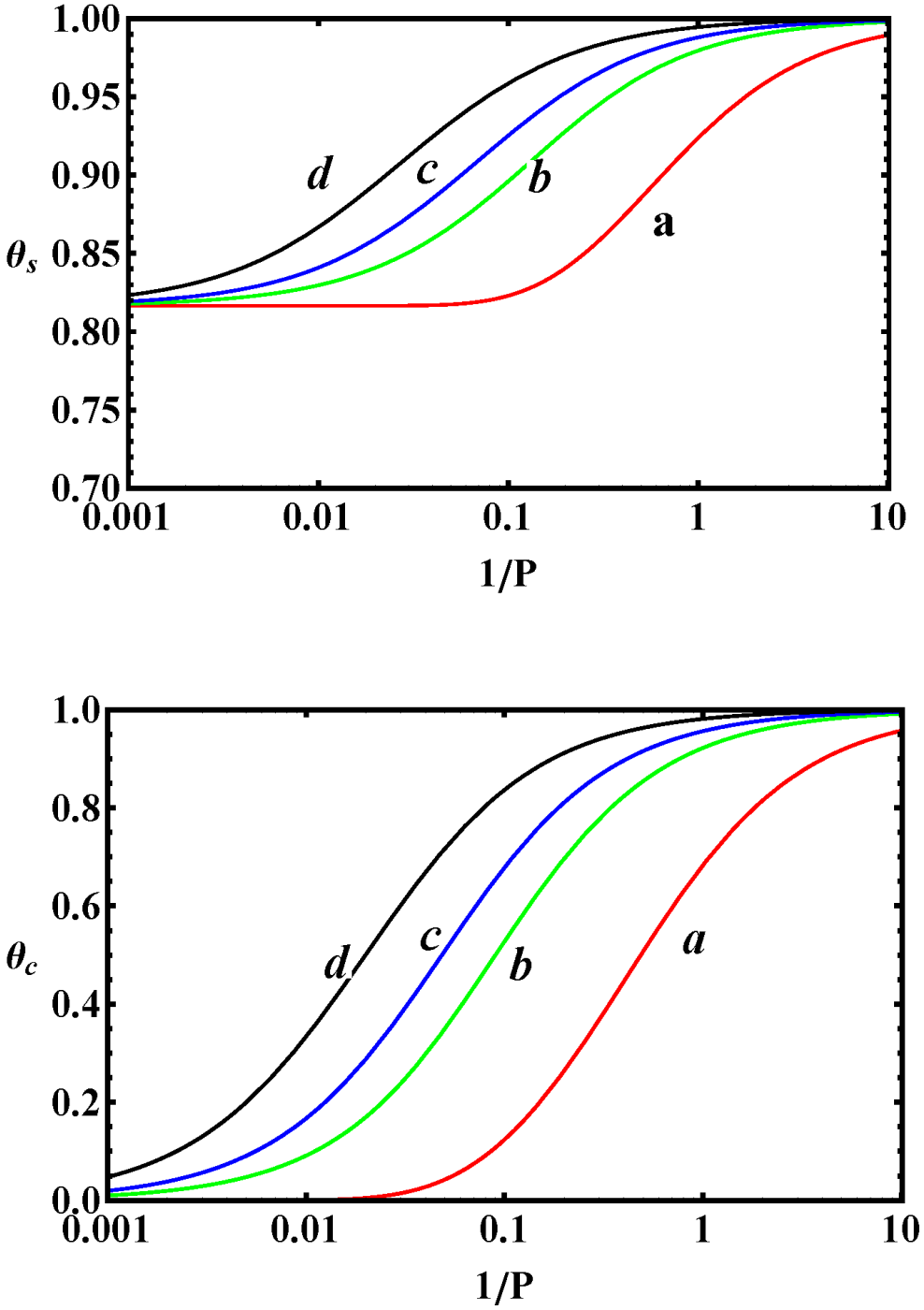

Figure 5-9: Variations of the wall temperature (θ_s) (top) and the center temperature (θ_c) (bottom) for the short channel model with the transverse Peclet number (P) for $Le_f = 1.5$ when (a) $\phi = 0$, (b) $\phi^2 = 10$, (c) $\phi^2 = 20$ and (d) $\phi^2 = 50$. $\phi_s^2 = \infty$.

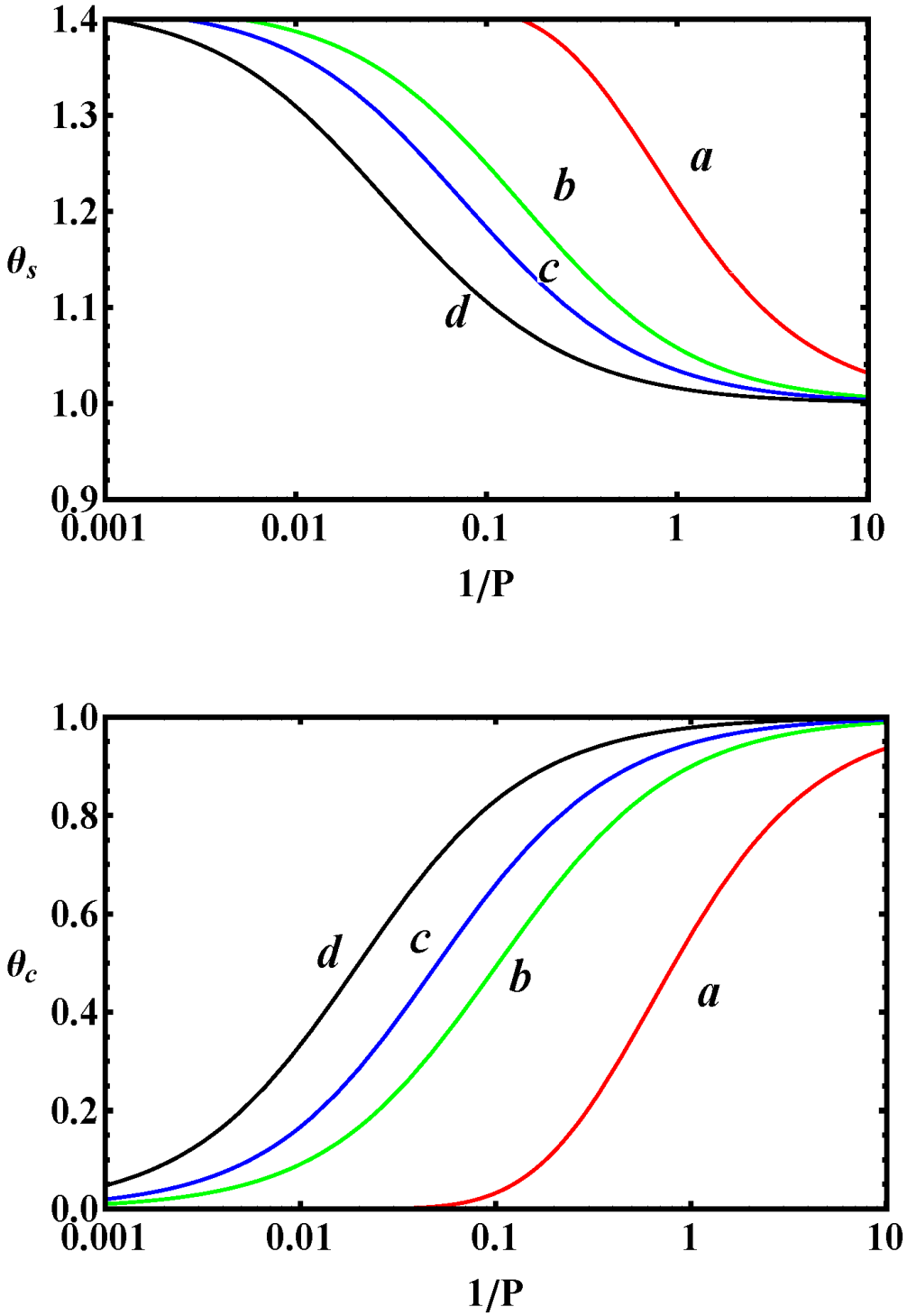

Figure 5-10: Variations of the wall temperature (θ_s) (top) and the center temperature (θ_c) (bottom) for the short channel model with the transverse Peclet number for $Le_f = 0.5$ when (a) $\phi = 0$, (b) $\phi^2 = 10$, (c) $\phi^2 = 20$ and (d) $\phi^2 = 50$. $\phi_s^2 = \infty$.

Chapter 6

Calculations of Transfer Coefficients

In this chapter we develop analytical and semi-analytical expressions for the heat and mass transfer coefficients pertinent to homogeneous-catalytic reaction systems. As the theory for heat and mass transfer coefficients for catalytic reactions is well-understood (see Gupta and Balakotaiah, 2001), we restrict ourselves to homogeneous reactions. We first show the general structure of the low-dimensional models for these systems that use the transfer coefficient concept. Then we proceed to obtain the long distance asymptotes for the transfer coefficients rigorously using the Liapunov-Schmidt reduction. These derivations ultimately reduce to solutions of certain regular perturbation problems. Subsequently, regular as well as singular perturbation methods are used to derive the short distance asymptotes for the transfer coefficients. Ultimately we make comments about the appropriate form of correlations for the transfer coefficients that take into account both these asymptotes.

6.1 Reduced order model with axial diffusion and conduction:

When a wall reaction is present, there are always transverse gradients in the concentration and temperature and hence further addition of transverse velocity gradi-

ents does not impact any of the qualitative features but changes only the quantitative features. However, when only the homogeneous reaction is present, the transverse gradients are mainly due to velocity gradients and hence the flow profile can have strong impact on the type of solutions that can exist. The full 2-D model can be averaged using the Liapunov-Schmidt reduction in the direction transverse to the flow direction if the transverse variation and the strength of the homogeneous and catalytic reactions is sufficiently small. The effect of a general velocity profile on the behavior of homogeneous-heterogeneous reactor systems using the parabolic model that ignores axial diffusion or conduction was previously shown in Alam et al., 2016. The novelty of these models is that there are two pairs of heat and mass transfer coefficients if the velocity profile is not flat.

Let us start with the 2D elliptic model:

$$f(y)\frac{\partial c}{\partial x} = \frac{1}{Pe}\frac{\partial^2 c}{\partial x^2} + \frac{1}{P}\frac{\partial^2 c}{\partial y^2} - DaR(c,\theta)$$

$$f(y)\frac{\partial \theta}{\partial x} = \frac{Le_f}{Pe}\frac{\partial^2 \theta}{\partial x^2} + \frac{Le_f}{P}\frac{\partial^2 \theta}{\partial y^2} + \beta DaR(c,\theta) \tag{6.1}$$

$$\begin{aligned} \frac{\partial c}{\partial y} &= \mp PDa_s R_c(c,\theta) \\ \frac{\partial \theta}{\partial y} &= \pm\frac{\beta}{Le_f} PDa_s R_c(c,\theta) \text{ at } y = \pm 1 \end{aligned} \tag{6.2}$$

with appropriate inlet and exit conditions. Here $R(c,\theta) := c\exp\left[\frac{\gamma_h\beta\theta}{1+\beta\theta}\right]$ and $R_c(c,\theta) := c\exp\left[\frac{\gamma_c\beta\theta}{1+\beta\theta}\right]$ are being used for notational brevity.

We wish to average the equation in the direction transverse to flow. To accomplish

this task, we express the above equation in the form:

$$\frac{\partial^2 c}{\partial y^2} = P\left(-\frac{1}{Pe}\frac{\partial^2 c}{\partial x^2} + f(y)\frac{\partial c}{\partial x} + DaR(c,\theta)\right)$$

$$\frac{\partial^2 \theta}{\partial y^2} = \frac{P}{Le_f}\left(-\frac{1}{Pe}\frac{\partial^2 \theta}{\partial x^2} + f(y)\frac{\partial \theta}{\partial x} - \beta DaR(c,\theta)\right) \tag{6.3}$$

Integrating along the y-directions leads to the following equations which we call global equations:

$$\frac{dc_m}{dx} - \frac{1}{Pe}\frac{d^2\langle c\rangle}{dx^2} = -DaR(\langle c\rangle, \langle\theta\rangle) - Da_s R_c(c_s,\theta_s)$$

$$\frac{d\theta_m}{dx} - \frac{1}{Pe}\frac{d^2\langle\theta\rangle}{dx^2} = \beta\left(DaR(\langle c\rangle, \langle\theta\rangle) + Da_s R_c(c_s,\theta_s)\right) \tag{6.4}$$

Here $\langle c\rangle$ is the transverse-averaged value of c defined as $\langle c\rangle = \frac{\int_{-1}^{1} c dy}{\int_{-1}^{1} dy}$, c_m is the cup-mixing average temperature defined as $c_m = \frac{\int_{-1}^{1} f(y) c dy}{\int_{-1}^{1} f(y) dy}$ and $c_s = c(\pm 1)$. $\langle\theta\rangle$, θ_m and θ_s are defined analogously. Now a substitution of

$$c = \langle c\rangle + Pc_1 + O(P^2) \tag{6.5}$$

$$\theta = \langle\theta\rangle + \frac{P}{Le_f}\theta_1 + O\left(\frac{P^2}{Le_f^2}\right) \tag{6.6}$$

along with the use of the zeroth order terms in the global equations leads to the following differential equation for c_1 and θ_1

$$\frac{\partial^2 c_1}{\partial y^2} = Da_s R_c(c_s,\theta_s) + (f(y)-1)\frac{dc_m}{dx} \tag{6.7}$$

$$\frac{\partial^2 \theta_1}{\partial y^2} = \beta Da_s R_c(\theta_s) + (f(y)-1)\frac{d\theta_m}{dx} \tag{6.8}$$

with appropriate boundary conditions. This yields

$$c_1 = Da_s R_c(\theta_s)\left(\frac{y^2}{2}-\frac{1}{6}\right)+\frac{dc_m}{dx}\left(\frac{y^2}{4}-\frac{y^4}{8}-\frac{7}{120}\right) \tag{6.9}$$

$$\theta_1 = \beta Da_s R_c(\theta_s)\left(\frac{y^2}{2}-\frac{1}{6}\right)+\frac{d\theta_m}{dx}\left(\frac{y^2}{4}-\frac{y^4}{8}-\frac{7}{120}\right) \tag{6.10}$$

The following equations can now be obtained in a straightforward manner.

$$c_s - c_m = P\left(-\frac{17}{35}Da_s R_c(\theta_s)-\frac{3}{35}DaR(\langle\theta\rangle)-\frac{3}{35}\frac{1}{Pe}\frac{d^2\langle c\rangle}{dx^2}\right) \tag{6.11}$$

$$\theta_s - \theta_m = \frac{P}{Le_f}\left(\frac{17}{35}\beta Da_s R_c(\theta_s)+\frac{3}{35}\beta DaR(\langle\theta\rangle)+\frac{3}{35}\frac{1}{Pe}\frac{d^2\langle\theta\rangle}{dx^2}\right) \tag{6.12}$$

$$\langle c\rangle - c_m = P\left(-\frac{3}{35}Da_s R_c(\theta_s)-\frac{2}{105}DaR(\langle\theta\rangle)-\frac{2}{105}\frac{1}{Pe}\frac{d^2\langle\theta\rangle}{dx^2}\right) \tag{6.13}$$

$$\langle\theta\rangle - \theta_m = \frac{P}{Le_f}\left(\frac{3}{35}\beta Da_s R_c(\theta_s)+\frac{2}{105}\beta DaR(\langle\theta\rangle)+\frac{2}{105}\frac{1}{Pe}\frac{d^2\langle\theta\rangle}{dx^2}\right) \tag{6.14}$$

The algebraic equations express relationships between $\langle c\rangle$, c_m and c_s ($\langle\theta\rangle$, θ_m and θ_s) and are called local equations. These different modes capture the transverse variations in the state variable across the channel. The transfer between these modes is expressed in terms of the numerical factors (asymptotic Nusselt or Sherwood numbers) appearing in the four algebraic equations. The first two algebraic equation expresses interphase mass and heat transfer, respectively. The next two algebraic equation expresses heat exchange within the fluid phase because of velocity gradients, homogeneous and catalytic reactions.

If we assume $\frac{1}{Pe}\frac{\partial^2\theta}{\partial x^2} = O(P)$, then we can ignore the terms containing $\frac{d^2\langle\theta\rangle}{dx^2}$ in the local equations while the axial diffusion term appears in the global equation as

a small perturbation. The base model for this assumption is a plug flow reactor and small radial gradients and axial diffusion appear as corrections (or mathematically, as small perturbations) to the base model. However we retain the $\frac{d^2\langle\theta\rangle}{dx^2}$ containing terms if we consider $\frac{1}{Pe}\frac{d^2\langle\theta\rangle}{dx^2} = O(1)$, in which case even the scenario of small axial gradients (base model of an ideal CSTR) can be considered within the framework of the above derivation.

6.1.1 Models without axial diffusion/conduction: Reduction to Index-infinity DAEs

When the axial conduction terms are ignored, we get systems of differential- algebraic equations instead of boundary value problems. For instance, for the 2D convection dominated model, the averaged model for the case of unit Lewis number is found to be of the following form:

$$\frac{d\theta_m}{dx} = DaR(\langle\theta\rangle) + Da_s R_c(\theta_s), 0 < X < 1 \tag{6.15}$$

$$\theta_s - \theta_m = P\left(\frac{1}{Nu_\infty} Da_s R_c(\theta_s) + \frac{1}{\widehat{Nu_\infty}} DaR(\langle\theta\rangle)\right) \tag{6.16}$$

$$\langle\theta\rangle - \theta_m = P\left(\frac{1}{\widehat{Nu_\infty}} Da_s R_c(\theta_s) + \frac{1}{Nu_{i,\infty}} DaR(\langle\theta\rangle)\right) \tag{6.17}$$

$$\theta_m = 0 \text{ at } X = 0$$

In classical settings, the terms involving $\widehat{Nu_\infty}$ do not appear, but for a system with

coupled homogeneous-heterogeneous reactions, the homogeneous reaction affects the heat transfer between the phases and the catalytic reaction affects the heat transfer within the gas phase. To a first order in P, these two effects are the same and therefore we have the same heat transfer coefficient $\widehat{Nu_\infty}$ in both local equations. For a fully developed (laminar) velocity profile and a parallel plate geometry, we have $Nu_\infty = 35/17$, $Nu_{i,\infty} = 105/2$ and $\widehat{Nu_\infty} = 35/3$ while for the circular geometry, $Nu_\infty = 48/11$, $Nu_{i,\infty} = 48$ and $\widehat{Nu_\infty} = 16$. [For flat velocity profile, $Nu_{i,\infty} = \widehat{Nu_\infty} = \infty$ and $\langle\theta\rangle = \theta_m$]. Hence, we have for the parallel plate case:

$$\theta_m - \langle\theta\rangle = P\left(\frac{-3}{35}Da_s R_c(\theta_s) - \frac{2}{105}DaR(\langle\theta\rangle)\right)$$

$$\theta_m - \theta_s = P\left(\frac{-17}{35}Da_s R_c(\theta_s) - \frac{3}{35}DaR(\langle\theta\rangle)\right) \tag{6.18}$$

Remark: The modeling of the above infinite index DAE system is often erroneously done using IVP methods, ignoring the possible hysteresis type behavior and calculating only one out of infinitely many possible solutions. This also leads to numerical issues such as Gibbs phenomena. We refer the reader to Ratnakar and Balakotaiah, 2016 for more exposition on such models.

6.2 Short distance asymptotes for parabolic velocity profiles

The derivation of transfer coefficients for systems with parabolic velocity profiles is much more involved than that for the case of flat velocity. Despite the existence

of analytical expressions for transfer coefficients in terms of special functions (Graetz eigenfunctions and parabolic cylinder functions for long channel and short channel models respectively, see Abramowitz and Stegun, [9]), such expressions are of little use from a practical standpoint. In this section we outline the development of expressions using perturbation methods and numerical calculations for the transfer coefficients in forms that are amenable to bifurcation calculations

Homogeneous reaction systems

We start with the problem

$$\begin{aligned} \frac{d^2c}{dy^2} &= P(1.5\left(1-y^2\right))(c-c_{in}) + \phi^2 c \\ 0 &< y < 1 \\ \frac{dc}{dy} &= 0 \text{ at } y = 0 \text{ and } 1 \end{aligned} \tag{6.19}$$

We are interested in finding the following Sherwood numbers defined as

$$\widehat{Sh} = \frac{\phi^2 \langle c \rangle}{c_m - c_s} \tag{6.20}$$

and

$$Sh_i = \frac{\phi^2 \langle c \rangle}{c_m - \langle c \rangle} \tag{6.21}$$

We concentrate here on the large P (i.e. short distance) asymptotes in this section because the small P asymptotes can be easily determined using regular perturbation. [Remark: it is the small P asymptote that are obtained by employing the Liapunov-

Schmidt reduction.] Let us begin by deriving the asymptotic dependence of $\widehat{Sh}$ on P for large P. In this case, to obtain c_s, we make a standard boundary layer approximation near $y = 1$ and replace the parabolic velocity profile with a linear one, i.e. $1.5\,(1-y^2) = 1.5(1+y)(1-y) \approx 3(1-y)$. This is a valid assumption because the boundary layer is thin near the inlet for a short channel reactor.

Let us define

$$\begin{aligned}
\beta &= \frac{\phi^2}{(3P)^{2/3}} = \frac{DaP^{1/3}}{3^{2/3}} \\
\chi &= \frac{c_{in} - c}{c_{in}} \\
\eta &= \frac{\phi^2}{(3P)^{2/3}} + (3P)^{1/3}\,(1-y) \\
&= \beta + (3P)^{1/3}\,(1-y)
\end{aligned}$$

We are interested in P sufficiently large so that $\phi^2 \ll (3P)^{2/3}$ or $\beta \ll 1$. The reason we are interested in this limit is because then $\frac{1}{\phi} \gg \frac{1}{P^{1/3}}$, meaning the reaction zone thickness is larger than that of the boundary layer and it, therefore, makes sense to calculate the effects of the boundary layer on the species transfer. We can now reformulate the species balance in near the wall as

$$\begin{aligned}
\frac{d^2\chi}{d\eta^2} &= \eta\chi - \beta \\
0 &< \eta < \infty \\
\frac{d\chi}{d\eta} &= 0 \text{ at } \eta = \beta \\
\chi \text{ is finite as } \eta &\to \infty
\end{aligned}$$

The general solution of this equation can be written using Airy and Scorer functions as

$$\chi(\eta) = A_1 Ai(\eta) + A_2 Bi(\eta) + \pi\beta Gi(\eta) \tag{6.22}$$

Here, A_1 and A_2 are constants. To ensure finiteness, we must have $A_2 = 0$ while from the boundary condition at $\eta = \beta$ we obtain $A_1 = \frac{-\pi\beta Gi'(\beta)}{Ai'(\beta)}$. Thus

$$\chi(\eta) = \pi\beta \left(Gi(\eta) - \frac{Gi'(\beta)}{Ai'(\beta)} Ai(\eta) \right)$$

We want to evaluate $\chi(\eta)$ at $\eta = \beta$, i.e. $y = 1$ in original coordinates. Then

$$\begin{aligned} Ai(\beta) &= Ai(0) + \beta Ai'(0) + O\left(\beta^2\right) \\ Gi(\beta) &= Gi(0) + \beta Gi'(0) + O\left(\beta^2\right) \\ &= \frac{1}{\sqrt{3}} Ai(0) - \frac{1}{\sqrt{3}} \beta Ai'(0) + O\left(\beta^2\right) \end{aligned}$$

using known relationships between Airy and Scorer functions. Thus for small β, retaining only $O(1)$ terms of $\left(Gi(\beta) - \frac{Gi'(\beta)}{Ai'(\beta)} Ai(\beta) \right)$, we get

$$\begin{aligned} \chi(\beta) &= \frac{c_{in} - c_s}{c_{in}} = \pi\beta \frac{2}{3^{5/6}\Gamma(2/3)} + O\left(\beta^2\right) \\ &\approx 1.857\beta = 1.857 \frac{\phi^2}{(3P)^{2/3}} \end{aligned}$$

Thus $\frac{c_{in} - c_s}{c_{in}} = O\left(\frac{\phi^2}{(3P)^{2/3}} \right) = O\left(P^{1/3} Da \right)$ .The bulk conversion represented by $\frac{c_{in} - c_m}{c_{in}}$

is very close to that for flat velocity as $O\left(\frac{\phi^2}{P}\right) = O\left(Da\right)$.Thus

$$\begin{aligned}\widehat{Sh} &= \frac{\phi^2 \langle c \rangle}{c_m - c_s} = \frac{\phi^2}{\chi_s - \chi_m} \\ &= O\left(\frac{PDa}{P^{1/3}Da}\right) = O\left(P^{2/3}\right) \text{ when } P \gg 1.\end{aligned}$$

To study the Sherwood number $Sh_i = \frac{\phi^2 \langle c \rangle}{c_m - \langle c \rangle}$ for the problem

$$\begin{aligned}\frac{1}{P}\frac{d^2c}{dy^2} &= (1.5\left(1-y^2\right))(c - c_{in}) + Dac \\ 0 &< y < 1 \\ \frac{dc}{dy} &= 0 \text{ at } y = 0 \text{ and } 1 \qquad (6.23)\end{aligned}$$

for small values of Da, we choose to do a regular perturbation expansion in Da as $c = 1 - Dac_1 + O(Da^2)$, leading to the boundary value problem:

$$\begin{aligned}\frac{1}{P}\frac{d^2c_1}{dy^2} &= (1.5\left(1-y^2\right))c_1 - 1 \qquad (6.24) \\ 0 &< y < 1 \\ \frac{dc_1}{dy} &= 0 \text{ at } y = 0 \text{ and } 1 \qquad (6.25)\end{aligned}$$

For large values of P, this is a singular perturbation problem and an inspection quickly reveals a boundary layer next to $y = 1$. Outside the boundary layer, the solution can be expressed by a regular perturbation expansion in $1/P$. Keeping only

the leading order term c_{10}, we find

$$c_{10} = \frac{1}{f(y)} = \frac{1}{1.5\,(1-y^2)} \tag{6.26}$$

c_{10} is the solution when the $\frac{1}{P}\frac{d^2c_1}{dy^2}$ term is small but within the boundary layer, $\frac{d^2c_1}{dy^2}$ is sufficiently large that $\frac{1}{P}\frac{d^2c_1}{dy^2}$ balances 1. If we approximate c_{10} near the wall as $\frac{1}{1.5(1-y)(1+y)} \approx \frac{1}{3(1-y)}$, then $\frac{d^2c_{10}}{dy^2} \approx \frac{2}{3(1-y)^3}$. This means that within the boundary layer,

$$\frac{1}{P}\frac{2}{3(1-y)^3} = O(1)$$

or

$$1 - y = O(P^{-1/3})$$

Also, we can estimate c_{10} near the beginning of the boundary layer as $\frac{1}{3(1-y)} \approx O(P^{1/3})$.

Let us now re-express Sh_i as $Sh_i = \frac{P}{\langle c_1\rangle - c_{1,m}}$. We can immediately see that $c_{1,m} = 1$ upon integrating the 6.24. Thus in order to calculate Sh_i, we need to calculate $\langle c_1\rangle$. To leading order, the average of c_1 in the boundary layer is $O(1)$ (c_{10} is $O(P^{1/3})$ while the boundary layer thickness is $O(P^{-1/3})$). Thus

$\langle c_1\rangle \sim \int_0^{1-P^{-1/3}} \frac{dy}{1.5(1-y^2)} + O(1) = \frac{1}{3}\ln\left[\frac{1+y}{1-y}\right]|_{y=0}^{y=1-P^{-1/3}} + O(1) = \frac{1}{3}\ln\left[\frac{2-P^{-1/3}}{P^{-1/3}}\right] + O(1) \approx \frac{1}{3}\ln 2 - \frac{1}{3}\ln P^{-1/3} \approx \frac{1}{9}\ln P$.

$\ln P$ supersedes $O(1)$ terms for very large P, and then $Sh_i = O(\frac{P}{\ln P})$. It is quite difficult to obtain this asymptotic relation by numerical calculations, because $\ln P$, despite being an increasing function of P, increases quite slowly.

We note that although the short distance asymptote varies as $O(\frac{P}{\ln P})$, this exact dependence is not useful for numerical calculations. What matters is that the Sherwood number becomes very large for large values of P. We find by numerical bifurcation calculations in the next section that an increasing function of P such as $P^{2/3}$ works very well as far as bifurcation analysis is concerned.

We now proceed to the case of very fast reaction, *i.e.* $Da \to \infty$ while $P \to \infty$ as well. In this case as well, the solution outside the boundary layer dictates the bulk average quantities such as c_m and $\langle c \rangle$. This outer solution is given by

$$c_\infty = \frac{f(y)}{Da + f(y)} \tag{6.27}$$

$$\approx \frac{f(y)}{Da} \text{ for } Da \gg 1 \tag{6.28}$$

This immediately yields for $f(y) = 1.5\,(1 - y^2)\,, \langle c \rangle = \frac{1}{Da}$ and $c_m = \frac{6}{5Da}$ leading to $Sh_i = 5PDa$.

We can verify these results numerically. To do so, we solve the 1D model with transverse gradients with an isothermal first order reaction and then use these calculations to evaluate $c_m, \langle c \rangle$ and c_s.Then using the various definitions of the Sherwood numbers, we can plot the numbers as functions of the transverse Peclet number. From these plots, we can verify the long distance asymptote and the dependence on P can be seen through the slopes of the plot for large P. We have shown these plots in figures 6-1, 6-2 and 6-3.

Hence the following expressions for the Sherwood numbers are useful to obtain

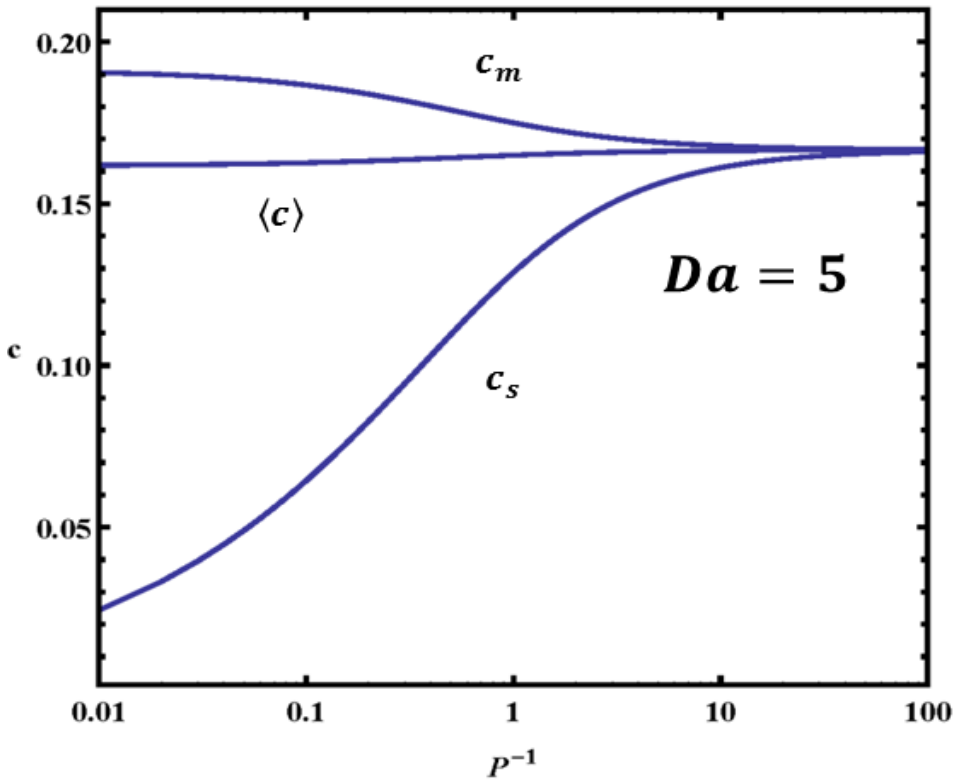

Figure 6-1: Plot of the average, cup-mixing average and surface concentration modes as transverse Peclet number is changed for a 1D model with transverse gradients and a first order isothermal reaction.

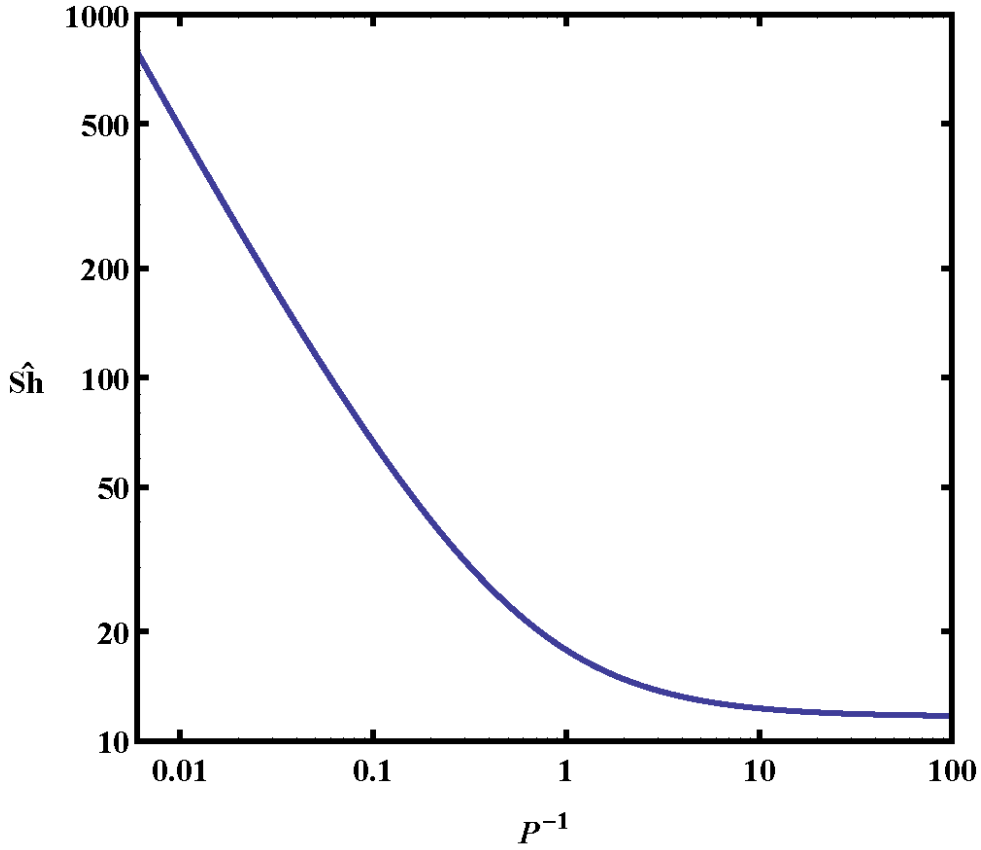

Figure 6-2: Homogeneous reaction Sherwood number based on wall flux.

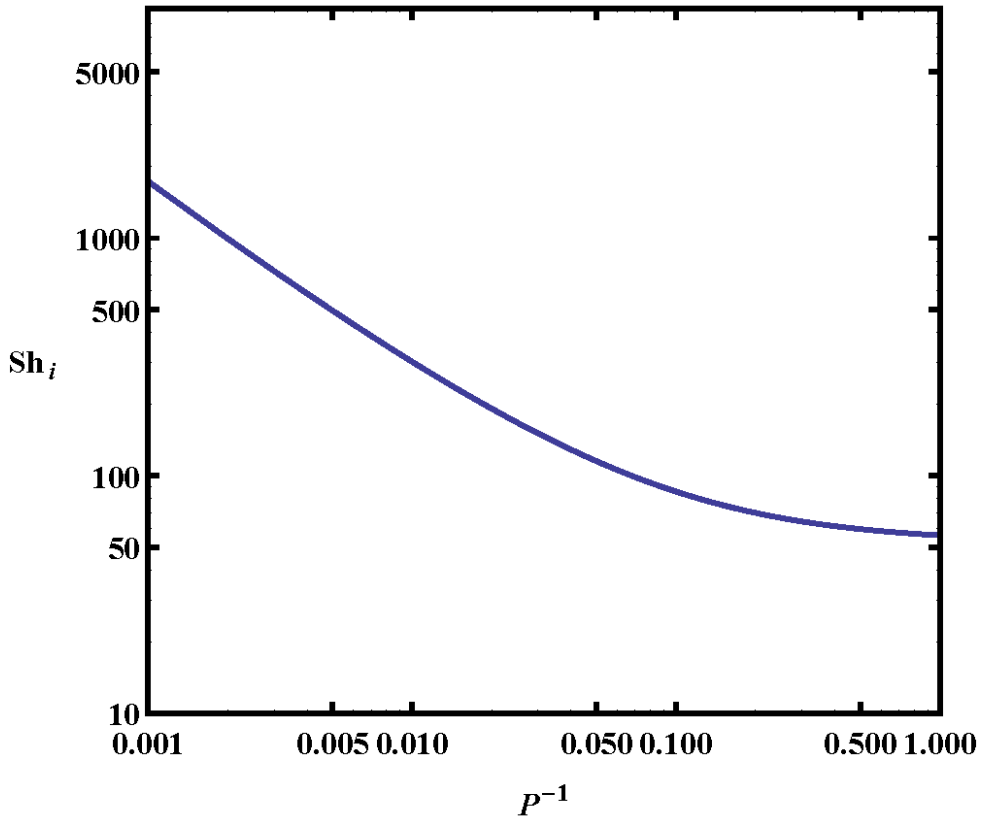

Figure 6-3: Homogeneous reaction internal Sherwood number for low values of Damkohler numbers.

low-dimensional models:

$$\widehat{Sh} = \widehat{Sh}_{\infty}(1 + P^{2/3}) \tag{6.29}$$

$$Sh_i = Sh_{i\infty}(1 + P^{2/3}) \tag{6.30}$$

and

$$Sh = Sh_{\infty}(1 + P^{1/3})$$

Here, the subscript ∞ denotes long distance asymptotes. The Nusselt numbers are similarly expressed by replacing P by $\frac{P}{Le_f}$.

Chapter 7

Transport Effects on the Formation of Patterns

7.1 Patterned States and 3-D Solutions

As stated in chapter 5, most literature studies of coupled homogeneous-heterogeneous reaction considered only 2-D solutions and ignored the stability of two-dimensional solutions to 3-D perturbations. For the case of catalytic reaction in a tube, Balakotaiah et al. (2002) have shown that transport limited patterns and hence 3-D solutions can exist, irrespective of the value of the Lewis number. In this case, the azimuthally symmetric solutions can coexist with asymmetric solutions, i.e. there is a region of parameters in which both 2-D and 3-D solutions can exist or when $Le_f < 1$, only 3-D solutions can exist.

In the previous chapters, we ignored the z-dependence of the solutions and considered only 2-D solutions. However, when thermal effects are significant ($\gamma\beta \gg 1$) and there are transport limitations, patterns may be formed leading to 3-dimensional solutions. In this chapter, we examine the conditions under which the concentration and temperature fields can be 3-dimensional for the case of coupled homogeneous-

heterogeneous reactions. For simplicity of analysis, we choose the short channel model, as the reciprocal of the transverse Peclet number can be interpreted as the axial length. Further, we examine below only the case of either homogeneous or catalytic reaction only for the simple reason that if patterns are formed in either limiting case, then they also exist when both chemistries operate side by side. We find that the homogeneous reaction by itself can lead to the formation of Turing patterns, where despite the absence of catalytic reaction that typically causes transverse gradients the different rates of heat and species diffusion across the channel can produce nonuniform solutions. These patterns have not been studied in detail before and have a bearing on the maximum temperature attained in a reactor system. Some of these solutions may have zones where the temperature exceeds the adiabatic value, though this may be possible only in a small range of parameters.

7.1.1 Turing Patterns

We consider the short channel model when only the homogeneous reaction is occurring. In this case, there is no *a priori* reason for the existence of a nonuniform state. Intuitively, the absence of the catalytic reaction and a flat incoming velocity may lead one to think that inhomogeneous solutions would not exist. Ignoring the transverse gradients in the short channel model leads to the following lumped model:

$$1 - c = DaR(c, \theta)$$

$$\theta = DaR(c, \theta)$$

which can have up to three solutions for some range of Da values. However, as is well-known from the literature on Turing patterns [Segel and Jackson (1972) , Muzika and Schreiber (2013), Ševčíková, et al (1996), Trávníčková et al (2009), Gupta and Chakraborty (2009)], this spatially homogeneous state can lose stability if the thermal and mass diffusivities are different in a way that allows for more dispersion of the stabilizing variable (the concentration variable) than the destabilizing variable (the temperature variable). This is the situation when $Le_f < 1$. We can analyze this loss of stability by considering the evolution of small spatial perturbations from the homogeneous state. Let us denote the homogeneous state by (c_0, θ_0),and define the perturbations as

$$c_1 = c - c_0 \text{ and}$$

$$\theta_1 = \theta - \theta_0.$$

Linearizing the short channel model about (c_0, θ_0) yields

$$\frac{1}{P}\left(\frac{\partial^2 c_1}{\partial y^2} + \frac{1}{\alpha^2}\frac{\partial^2 c_1}{\partial z^2}\right) = a_{11}c_1 + a_{12}\theta_1 \text{ and} \tag{7.1}$$

$$\frac{Le_f}{P}\left(\frac{\partial^2 \theta_1}{\partial y^2} + \frac{1}{\alpha^2}\frac{\partial^2 \theta_1}{\partial z^2}\right) = a_{21}c_1 + a_{22}\theta_1. \tag{7.2}$$

Here, the constants a_{11}, a_{12}, a_{21} and a_{22} are defined as

$$a_{11} = \frac{\partial}{\partial c}\left[Dac\exp\left[\frac{\gamma_h \beta\theta}{1+\beta\theta}\right] - (1-c)\right]|_{(c_0,\theta_0)} = 1 + Da\exp\left[\frac{\gamma_h\beta\theta_0}{1+\beta\theta_0}\right],$$

$$a_{12} = \frac{\partial}{\partial\theta}\left[Dac\exp\left[\frac{\gamma_h\beta\theta}{1+\beta\theta}\right] - (1-c)\right]|_{(c_0,\theta_0)} = \gamma_h\beta Da\exp\left[\frac{\gamma_h\beta\theta_0}{1+\beta\theta_0}\right]\left(\frac{1}{1+\beta\theta_0}\right)^2,$$

$$a_{21} = \frac{\partial}{\partial c}\left[-Dac\exp\left[\frac{\gamma_h\beta\theta}{1+\beta\theta}\right] + \theta\right]|_{(c_0,\theta_0)} = -Da\exp\left[\frac{\gamma_h\beta\theta_0}{1+\beta\theta_0}\right] \text{ and}$$

$$a_{22} = \frac{\partial}{\partial\theta}\left[-Dac\exp\left[\frac{\gamma_h\beta\theta}{1+\beta\theta}\right] + \theta\right]|_{(c_0,\theta_0)} = 1-\gamma_h\beta Dac_0\exp\left[\frac{\gamma_h\beta\theta_0}{1+\beta\theta_0}\right]\left(\frac{1}{1+\beta\theta_0}\right)^2.$$

Assuming the perturbation functions are sufficiently smooth, we can decompose them into Fourier modes. We then obtain the following set of homogeneous equations for the amplitudes $(\widehat{c_1}, \widehat{\theta_1})$:

$$\begin{aligned}(a_{11} + \frac{k^2}{P})\widehat{c_1} + a_{12}\widehat{\theta_1} &= 0 \text{ and} \\ a_{21}\widehat{c_1} + a_{22}(\theta_1 Le_f\frac{k^2}{P})\widehat{\theta_1} &= 0; \quad k^2 = m^2\pi^2 + \frac{n^2\pi^2}{\alpha^2}. \end{aligned} \tag{7.3}$$

The condition for pattern formation is that the determinant for the above system be < 0. The stable homogeneous states and patterned states are separated by the curve defined by the vanishing of this determinant. This condition turns out to be $1+ Da\exp\left[\frac{\gamma_h\beta\theta_0}{1+\beta\theta_0}\right]\left(1-\frac{\gamma_h\beta c_0}{(1+\beta\theta_0)^2}\right)+Le_f\frac{k^2}{P}\left(1+Da\exp\left[\frac{\gamma_h\beta\theta_0}{1+\beta\theta_0}\right]\right)+\frac{k^2}{P}\left(1-Da\frac{\gamma_h\beta c_0}{(1+\beta\theta_0)^2}\exp\left[\frac{\gamma_h\beta\theta_0}{1+\beta\theta_0}\right]\right)+ Le_f\frac{k^4}{P^2} = 0$, which is linear in $\gamma_h\beta$. We must also satisfy the following steady state equation for the uniform state:

$$\frac{\theta_0}{1-\theta_0} = Da\exp\left[\frac{\gamma_h\beta\theta_0}{1+\beta\theta_0}\right].$$

Using the conversion, $\chi = 1- \theta_0$ as a parameter, we can express these two equa-

tions in the parametric form:

$$\begin{aligned} \gamma_h\beta &= \frac{(1+\beta\chi)^2}{\chi(1-\chi)}\frac{(1+Le_f k^2)(1+k^2(1-\chi))}{1+k^2} \text{ and} \\ Da &= \frac{\chi}{(1-\chi)}\exp\left[\frac{(1+\beta\chi)}{(1-\chi)}\frac{(1+Le_f k^2)(1+k^2(1-\chi))}{1+k^2}\right]. \end{aligned} \tag{7.4}$$

Varying χ between 0 and 1, we can trace out the entire neutral stability curve [Here, k is the wave number with m and n representing the transverse mode numbers; α is the aspect ratio] . We have shown in figure 6-1, the bifurcation set for the homogeneous state along with neutral stability curves for first several modes for $\alpha = 1$, namely the cases of $m = 1, n = 0$ (or equivalently $m = 0, n = 1$); $m = 1, n = 1$ and $m = 2, n = 0$ (or equivalently $m = 0, n = 2$). When $Le_f \geq 1$, the bifurcating patterned states emerge from the unstable homogeneous branch and hence are unstable but when $Le_f < 1$, stable patterns can be found even when the corresponding homogeneous solution is unique. This is consistent with the understanding of Turing patterns for $Le_f < 1$ in literature (as summarized in Segel and Jackson, 1972 and mentioned above).

Though we have focused on the steady state behavior in this work, it must be pointed out that many reactor systems with exothermic reaction exhibit oscillatory dynamics when subjected to time-dependent perturbations. Thus, the formation of Turing patterns may be accompanied with dynamically unstable patterns which may subsequently stabilize via a Hopf or saddle-node bifurcation. For an illustration of these bifurcations, we refer the reader to the work of Hadač, et al. (2015).

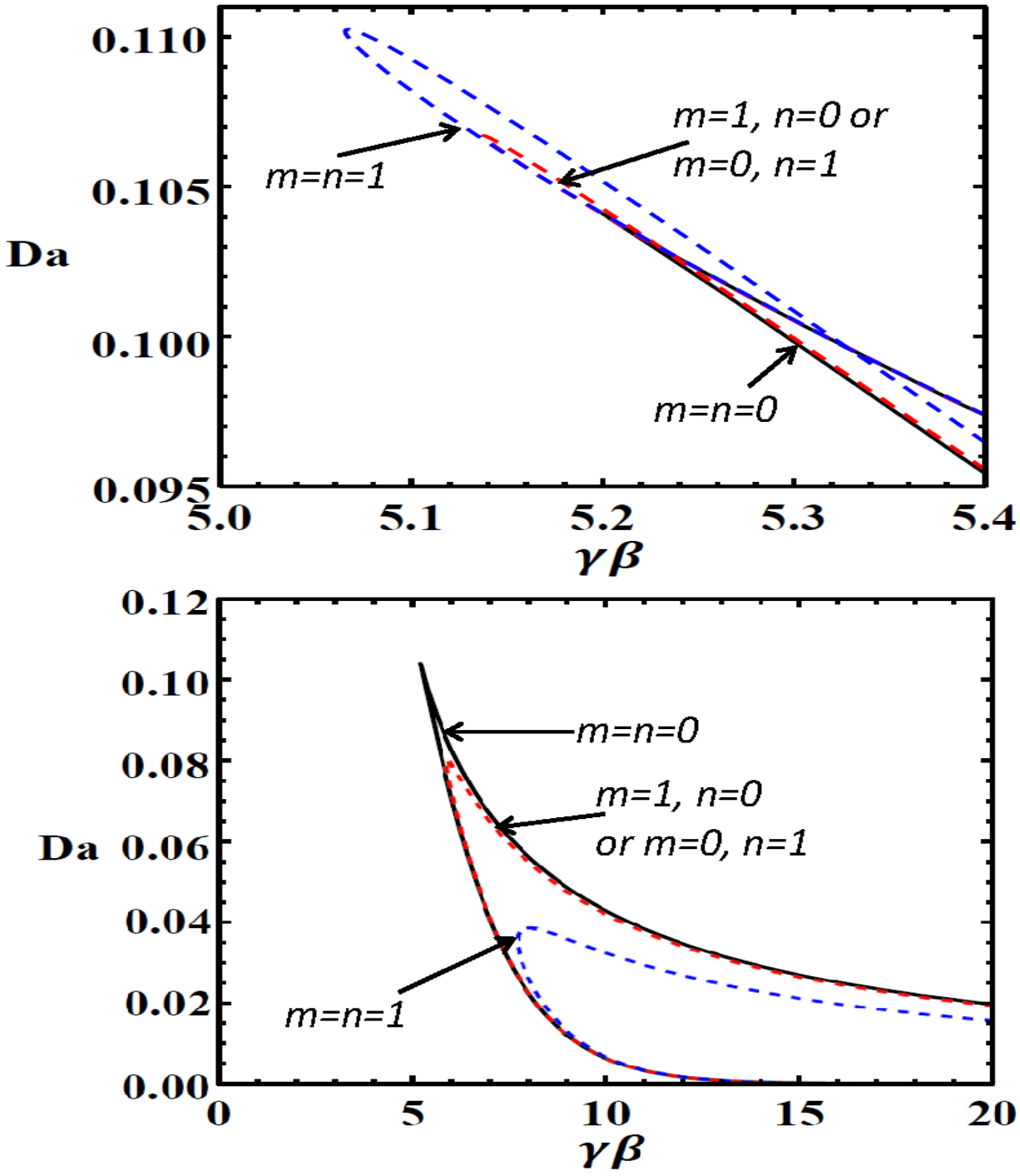

Figure 7-1: Neutral Stability curves and bifurcation set for homogeneous reaction only case with $Le_f = 0.3$, $P = 30$ and $\beta = 0.3$ (top) and $Le_f = 1.3$, $P = 25$ and $\beta = 0.3$ (bottom).

7.1.2 Transport Limited Patterns

The short channel model may also be used to examine the stability of the 2-D solutions to 3-D perturbations. We consider the 2-D short channel model with no homogeneous reaction given below:

$$\frac{1}{P}\left(\frac{\partial^2 c}{\partial y^2}+\frac{1}{\alpha^2}\frac{\partial^2 c}{\partial z^2}\right)+(1-c) = 0, \text{ and} \tag{7.5}$$

$$\frac{Le_f}{P}\left(\frac{\partial^2 \theta}{\partial y^2}+\frac{1}{\alpha^2}\frac{\partial^2 \theta}{\partial z^2}\right)-\theta = 0 \text{ with} \tag{7.6}$$

$$\frac{\partial c}{\partial y} = -\phi_s^2 c \exp\left[\frac{\gamma_s \beta\theta}{1+\beta\theta}\right] \text{ at } y=1, \tag{7.7}$$

$$\frac{\partial c}{\partial y} = \phi_s^2 c \exp\left[\frac{\gamma_s \beta\theta}{1+\beta\theta}\right] \text{ at } y=-1, \tag{7.8}$$

$$Le_f\frac{\partial \theta}{\partial y} = \phi_s^2 c \exp\left[\frac{\gamma_s \beta\theta}{1+\beta\theta}\right] \text{ at } y=1, \tag{7.9}$$

$$Le_f\frac{\partial \theta}{\partial y} = -\phi_s^2 c \exp\left[\frac{\gamma_s \beta\theta}{1+\beta\theta}\right] \text{ at } y=-1, \tag{7.10}$$

$$c(x,y,-1)=c(x,y,1) \text{ and } \theta(x,y,-1)=\theta(x,y,1). \tag{7.11}$$

We first consider the $z-$independent solution to the above model which is given by

$$c_0 = 1-\sqrt{Le_f}\theta_s\frac{\tanh\left[\sqrt{\frac{P}{Le_f}}\right]\cosh\left[\sqrt{P}y\right]}{\sinh\sqrt{P}} \text{ and} \tag{7.12}$$

$$\theta_0 = \theta_s\frac{\cosh\left[\sqrt{\frac{P}{Le_f}}y\right]}{\cosh\left[\sqrt{\frac{P}{Le_f}}\right]}, \tag{7.13}$$

where the surface temperature $\theta_s = \theta(\pm 1)$ can be found by solving the following nonlinear algebraic equation:

$$a_0\theta_s = \phi_s^2 \exp\left[\frac{\gamma_s\beta\theta}{1+\beta\theta}\right](1 - b_0\theta_s)\,, \tag{7.14}$$

where

$$a_0 = \sqrt{Le_f P}\tanh\left[\sqrt{\frac{P}{Le_f}}\right]$$

and

$$b_0 = \sqrt{Le_f}\frac{\tanh\left[\sqrt{\frac{P}{Le_f}}\right]}{\tanh\sqrt{P}}.$$

For simplicity, we use the positive exponential approximation. This approximation is valid when β is small but γ_s is sufficiently large to render $\gamma_s\beta$ finite. Thus, the model is still nonlinear, but the calculations become more tractable. Setting the above equation as well as its first two derivatives with respect to θ_s to zero, we obtain the hysteresis locus given by

$$\gamma_s\beta = 4b_0.$$

Similarly the bifurcation set can be obtained in a parametric form by simultaneously solving the equation and its first derivative with respect to θ_s as

$$\gamma_s\beta = \frac{1}{\theta_s(1 - b_0\theta_s)} \tag{7.15}$$

and

$$\phi_s^2 = \frac{a_0\theta_s}{(1 - b_0\theta_s)}\exp\left[-\gamma_s\beta\theta_s\right] \tag{7.16}$$

with $0 < \theta_s < b_0^{-1}$.

To study the patterned states, we linearize the model about (c_0, θ_0) and define the perturbation functions:

$$\omega_1 = c - c_0 \text{ and}$$

$$\omega_2 = \theta - \theta_0.$$

We get the following linearized BC's:

$$\begin{aligned} \frac{\partial \omega_1}{\partial y} &= -\phi_s^2 \left[\exp\left[\gamma_s \beta \theta\right] \omega_1 + c_0 \gamma_s \beta \exp\left[\gamma_s \beta \theta\right] \omega_2\right] \quad \text{at } y = 1, \\ Le_f \frac{\partial \omega_2}{\partial y} &= \phi_s^2 \left[\exp\left[\gamma_s \beta \theta\right] \omega_1 + c_0 \gamma_s \beta \exp\left[\gamma_s \beta \theta\right] \omega_2\right] \quad \text{at } y = 1, \end{aligned} \tag{7.17}$$

$$\begin{aligned} \omega_1(z &= -1, y) = \omega_1(z = 1, y), \text{ and} \\ \omega_2(z &= -1, y) = \omega_2(z = 1, y). \end{aligned} \tag{7.18}$$

We can decompose the solution of the linear PDE into components corresponding to various Fourier modes. The solution for the $m - th$ mode is given as

$$\omega_{1m} = C_m \cosh\left(\zeta_m y\right) \cos\left(2\pi m z + \psi\right) \text{ and}$$

$$\omega_{2m} = D_m \cosh\left(\chi_m y\right) \cos\left(2\pi m z + \psi\right),$$

where

$$\zeta_m = \sqrt{P + \frac{4\pi^2 m^2}{\alpha^2}}, \tag{7.19}$$

$$\chi_m = \sqrt{\frac{P}{Le_f} + \frac{4\pi^2 m^2}{\alpha^2}}, \tag{7.20}$$

and C_m and D_m are constants. We pick $\psi = 0$, pinning the solution down to a particular phase angle. To calculate the neutral stability curves, we use the boundary conditions to a get a pair of homogeneous equations:

$$\begin{aligned} C_m \left[\zeta_m \sinh(\zeta_m) + \phi_s^2 \cosh(\zeta_m) \exp\left[\gamma_s \beta \theta\right]\right] + D_m c_0 \gamma_s \phi_s^2 \beta \exp\left[\gamma_s \beta \theta_0\right] \cosh(\chi_m) &= 0 \\ C_m \left[-\phi_s^2 \cosh(\zeta_m) \exp\left[\gamma_s \beta \theta\right]\right] + D_m \left[Le_f \chi_m \sinh(\chi_m) - c_0 \gamma_s \phi_s^2 \beta \exp\left[\gamma_s \beta \theta_0\right] \cosh(\chi_m)\right] &= 0. \end{aligned}$$

The neutral stability curves are found by setting the determinant of the above system to be zero, leading to the following equation:

$$Le_f \chi_m \zeta_m = \phi_s^2 \left[c_0 \gamma_s \beta \coth(\chi_m) \zeta_m - Le_f \chi_m \coth(\zeta_m)\right].$$

For defining the neutral stability curves, this equation has to be satisfied along with eqn (7.16) yielding the following parametric form of the neutral stability curves:

$$\gamma_s \beta = Le_f \chi_m \frac{\coth(\zeta_m) + \frac{\zeta_m (1 - b_0 \theta_s)}{a_0 \theta_s}}{\zeta_m \coth(\chi_m) (1 - b_0 \theta_s)} \text{ and} \tag{7.21}$$

$$\phi_s^2 = \frac{a_0 \theta_s}{(1 - b_0 \theta_s)} \exp\left[-\gamma_s \beta \theta_s\right], \tag{7.22}$$

where $0 < \theta_s < b_0^{-1}$.

For $P >> 1$, $\gamma_s\beta = Le_f\chi_m \frac{\coth(\zeta_m)+\frac{\zeta_m(1-b_0\theta_s)}{a_0\theta_s}}{\zeta_m \coth(\chi_m)(1-b_0\theta_s)} \approx \frac{1}{\theta_s\left(1-\sqrt{Le_f}\theta_s\right)}$ and as $b_0 \approx \sqrt{Le_f}$ in this limit, we conclude that at high values of P, the neutral stability curves coincide with the bifurcation set of the z-uniform states. This means that for high P (large transverse gradients or near the inlet to a channel), patterns corresponding to all the modes are possible. We show the bifurcation set for the $z-$uniform state as well as the neutral stability curve for the first two modes in figure 6-2. We again find that neutral stability curves stay enclosed inside the bifurcation set when $Le_f \geq 1$, but when $Le_f < 1$ one can obtain patterns even in the region of unique solution for the uniform system.

The codimension-1 loci for the patterned states corresponding to different modes can be obtained by differentiating (7.21) w.r.t. θ_s and setting the resulting equation to zero. We can then eliminate θ_s using (7.21). This finally yields the following parametric form for $\gamma_s\beta$:

$$\gamma_s\beta = \frac{Le_f\chi_m}{a_0 b_0 \coth(\chi_m)} \frac{\left(a_0\coth(\zeta_m) - b_0\zeta_m\right)^2}{\zeta_m^2\left(\sqrt{1+\frac{a_0\coth(\zeta_m)-b_0\zeta_m}{b_0\zeta_m}}-1\right)^2}. \tag{7.23}$$

This locus gives us the minimum value of $\gamma_s\beta$ for which patterns can be found. For $P >> 1$, $\gamma_s\beta = \frac{Le_f\chi_m}{a_0 b_0 \coth(\chi_m)} \frac{(a_0\coth(\zeta_m)-b_0\zeta_m)^2}{\zeta_m^2\left(\sqrt{1+\frac{a_0\coth(\zeta_m)-b_0\zeta_m}{b_0\zeta_m}}-1\right)^2} \approx \frac{1}{P\sqrt{Le_f}} \frac{(a_0\coth(\zeta_m)-b_0\zeta_m)^2}{\left(\sqrt{1+\frac{a_0\coth(\zeta_m)-b_0\zeta_m}{b_0\zeta_m}}-1\right)^2} \approx \frac{4Le_f P}{P\sqrt{Le_f}} = 4\sqrt{Le_f}$. This means that the codimesnion-1 loci coincide with the hysteresis locus for the 2-D solutions when $P >> 1$. Also when $P \ll 1$, $\gamma_s\beta = \frac{Le_f}{P} \frac{\sqrt{\frac{4\pi^2m^2}{\alpha}}\tanh\left(\sqrt{\frac{4\pi^2m^2}{\alpha}}\right)}{\left(\frac{\tanh\left(\sqrt{\frac{P}{Le_f}}\right)}{\sqrt{\frac{P}{Le_f}}}\right)}$. This implies that the minimum $\gamma_s\beta$ for pattern formation, and

hence the region of patterns decreases with increasing Le_f and increases with increasing P. In figure 6-3, we have shown codimension 1 and hysteresis loci for Lewis numbers of 0.3 and 2. It is clear that 3-D patterns can be formed even when there is no steady state multiplicity.

We do not undertake the task of computing 3-D solutions in this work. However we note that when $Le_f < 1$, 3-D solutions bifurcate super-critically and hence are stable. Further, the maximum temperature can certainly exceed the adiabatic temperature. For $Le_f \geq 1$, the 3-D solutions bifurcate from the unstable 2-D branches. They may gain stability through a limit point bifurcation (see Balakotaiah et al, (2002)).

7.2 Summary and Discussion

The main goal of this chapter was to examine the impact of transport parameters to identify the different types of solutions that could exist and the region of parameters in which 3-D solutions exist. We examined the stability of 1-D/2-D solutions to 3-D perturbations and discussed the various types of solutions that could exist or coexist in the system. The main results of this chapter related to these objectives may be summarized as follows:

(i) We find that 3-D solutions can exist in systems where only the catalytic and/or the homogeneous reaction take place. The region of parameter values in which these 3-D solutions exist increases with the transverse Peclet number (or inversely with the distance from inlet) and also increases with decreasing Lewis number.

(ii) When $Le_f < 1$, 3-D patterned states can exist even when there are no multiple (homogeneous or 2-D) solutions. However, when $Le_f \geq 1$, it is possible for the 3-D

states to exist only in the region of multiple 1-D/2-D solutions.

The results on pattern formation presented here have implications on the modeling of combustion systems so that uniformity is not erroneously assumed in the model when patterns exist. A bifurcation analysis for 2-D and 3-D reactor models of heterogeneous-homogeneous combustion would be an appropriate testing ground for ideas presented in this work. This is a subject for future investigation.

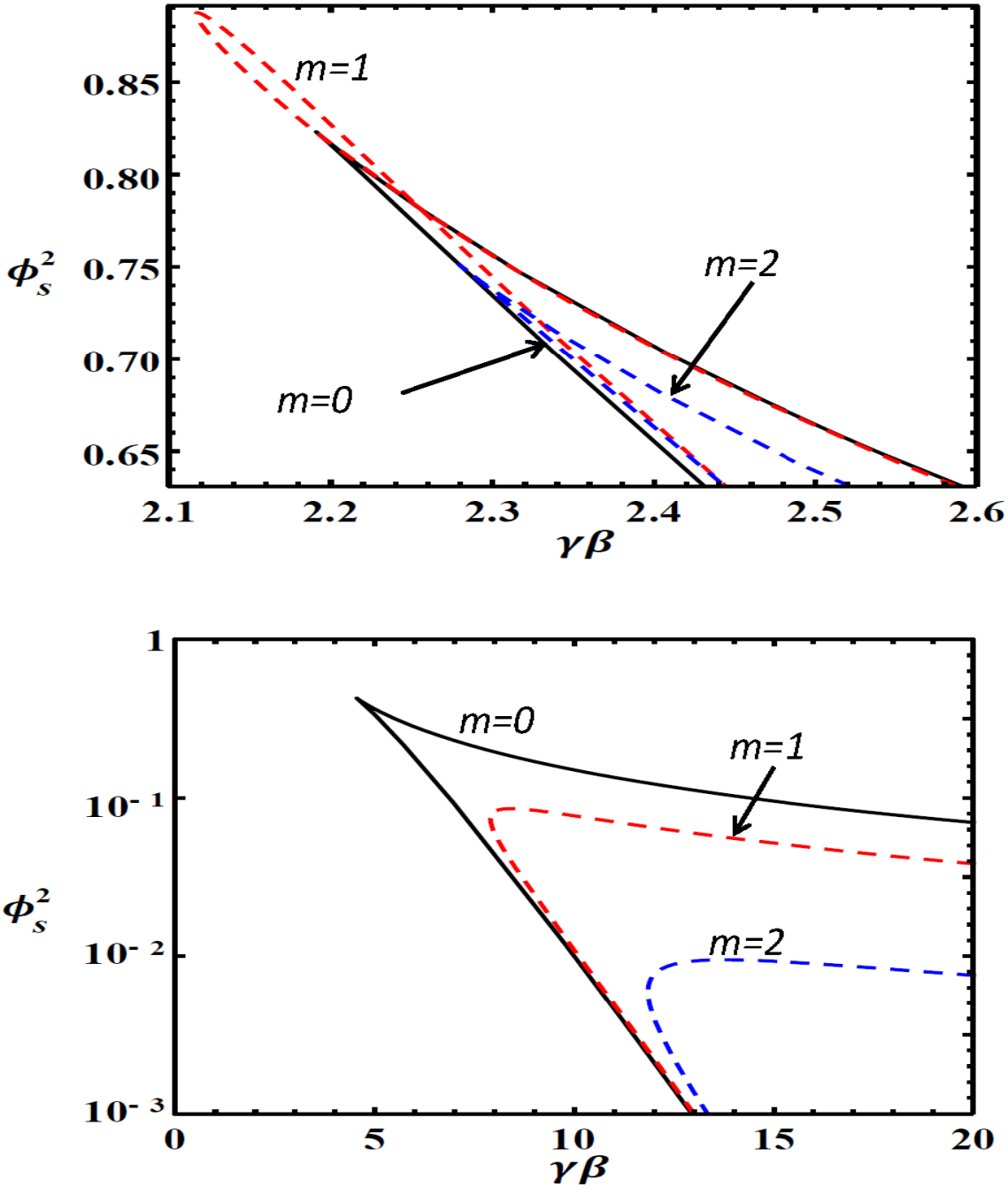

Figure 7-2: 3D Neutral Stability curves and 2D bifurcation set for $Le_f = 0.3$, $P = 37$ and $\alpha = 1$ (top) and for $Le_f = 1.3$, $P = 10$ and $\alpha = 1$ (bottom) .

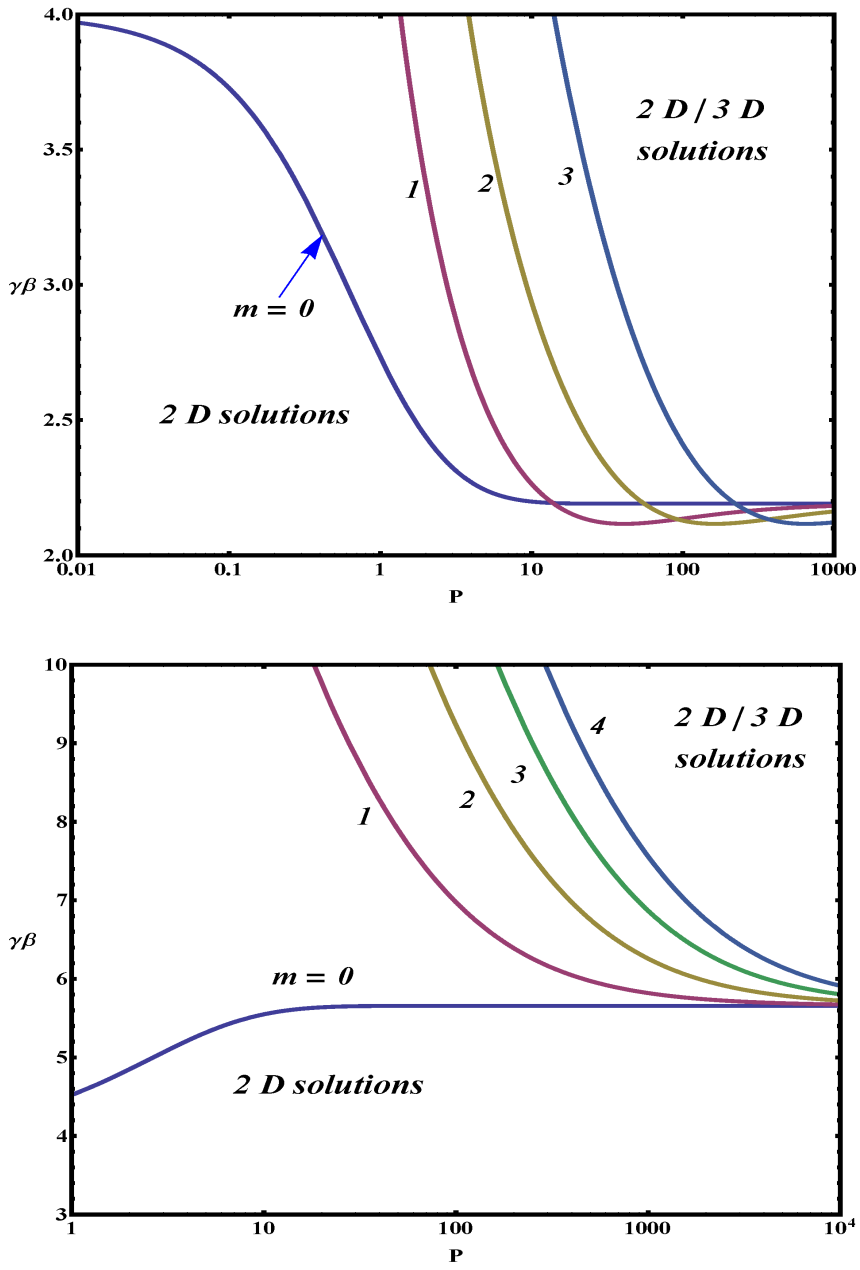

Figure 7-3: Hysteresis locus and codimension 1 loci for $Le_f = 0.3$ and $\alpha = 1$ (top) and for $Le_f = 2$ and $\alpha = 1$ (bottom) .

Chapter 8

Conclusions and Recommendations for future work

The main contribution of this thesis is the presentation of a comprehensive bifurcation analysis of the thermally coupled homogeneous-heterogeneous combustion process in short monolith, fibermat or gauze type reactors. The simple lumped model or 1D model with transverse gradients to describe these systems display a rich bifurcation behavior. In prior work (Balakotaiah, Gupta and West, 2000), it was shown that the aforementioned models have the same qualitative features as the more complex 2-D elliptic models provided the axial Peclet numbers are not large. Thus, the bifurcations predicted by these models will also be present in the more detailed models. The coarse map of various bifurcations observed in this model can be used as a guide to explore the more detailed models with multi-step chemistry. Further, while we focused on the oxidation of propane and methane, our procedure is general enough to be applicable to other systems of reactions that include complex feeds (which could be lean or rich) with various hydrocarbons and possibly CO and H_2.

Our analysis of propane oxidation on platinum with stoichiometric feed shows that for propane mole fractions below about 2.5% and channel hydraulic diameters

below about 1mm, the ignition-extinction behavior of the coupled system is primarily determined by the catalytic reaction, with the homogeneous reaction playing no role in the ignition behavior but assisting in the late stages of the fuel conversion. In this region of parameters, catalytic ignition always precedes homogeneous ignition and the homogeneous chemistry is activated (further downstream or) at higher values of residence times where the fluid phase temperature increases sufficiently for the homogeneous rate to be significant. Finally, we note that the phenomenon of quenching of homogeneous reactions in microburners reported by several investigators, may be due to the dominance of catalytic reaction over homogenous reaction, in addition to (or instead of) the quenching of free radicals.

The coupled homogeneous-heterogeneous portion of the propane hysteresis loci shows that as the channel hydraulic radius increases, the region where both chemistries interact moves to lower values of fuel mole fractions. For sufficiently high values of R_Ω, the homogeneous ignition could precede the catalytic ignition, but for the kinetics used in our study, this occurs at unrealistically high values of R_Ω and also at high fuel inlet mole fractions that lead to very high gas and solid temperatures. However, if the catalyst reaction rate (per unit volume) is lowered by about two orders of magnitude, it is possible to find operating conditions that lead to homogeneous chemistry dominance. It is worth noting that varying the catalyst activity and changing the hydraulic radius are both important ways employing which the desired ignition-extinction behavior can be controlled. As mentioned above, for reacting flows in monoliths (or fibermat or gauze type reactors) when catalytic reaction dominates, the exit conversion admits the asymptotes $\chi = 1$ for $P << 1$ and $\chi \approx \epsilon_f / P^{1/2}$ for

$P >> 1$ with the transition around $P = 1$. Thus, if P is small (for large residence times or small channel diameters, say), the system jumps to the high temperature (and high conversion) ignited branch due to catalytic reaction alone. If $P \gg 1$, then the catalytic reaction leads to some intermediate conversion, after which the homogenous and catalytic reactions interact and could lead to a second ignition. As shown in this work, the parameter space where the hysteresis diagrams for propane oxidation admit a parabola-shaped branch of hysteresis locus corresponds to $P > 1$.

In chapter 4, we presented bifurcation diagrams for lean oxidation of methane using pressure as the bifurcation parameter. The predicted ignition locus compares favorably with experimental data and computational results. Our analysis also shows that lean oxidation of methane is also catalytically dominant and the channel hydraulic diameter can be increased by a factor of ten or more without any significant change in the ignition (or operating pressure) or inlet temperature or methane conversion.

The work on Maximum Temperatures presented in Chapter 5 discusses that in the case of $Le_f > 1$, the peak temperature within the reactor never exceeds the adiabatic value although it can be non-monotonic in the direction transverse to flow. Also if the homogeneous reaction is sufficiently strong, the center of the reactor may be hotter than the wall for the case of $Le_f > 1$. This is contrary to some results in recent literature and the work described in Chapter 5 aims to clarify these conceptual issues. To describe such solutions, reduced order models require at least three temperature modes for their analysis (the natural choice for the three modes is the average gas phase temperature, the cup-mixing average temperature and the solid phase temper-

ature, see Chakraborty and Balakotaiah, 2004). We continue the exploration of the impact of various transport parameters such as Le_f and P on the qualitative features of solutions in Chapter 7. We find that stable patterns are possible for $Le_f < 1$ and that patterned states can exist even when there is no multiplicity of solutions. These results show that that 3D solution structure is expected for the case of low Lewis numbers and high transverse Peclet numbers, necessitating bifurcation studies on 3-D models in such cases.

We now discuss some limitations and extensions of the work presented here.

(i) We considered only adiabatic systems. While the adiabatic case provides some insight, heat losses are important especially in order to compare to experiments.

(ii) At high temperatures, radiation heat losses become important and must be included in the mathematical model.

(iii) We have restricted ourselves to steady state bifurcations, but the transient behavior of the model can be rich, displaying a variety of dynamic bifurcations.

The bifurcation analysis of models that include heat losses, radiation heat transfer and possibility of time-dependent phenomena is obviously more complex but as stated earlier, all the features of the adiabatic model will still be retained, and can serve as a starting point for the numerical investigation of the features of such systems. However, additional bifurcation phenomena may be observed, complicating the phase diagrams. Such models as well as more detailed two- and three- dimensional models are topics for future investigations.

References

1. J. Zaman, Oxidative processes in natural gas conversion, Fuel Processing Technology 58 (1999) 61.

2. A. Holmen, Direct conversion of methane to fuels and chemicals, Catalysis Today 141 (2009) 2.

3. S. S. Bharadwaj and L. D. Schmidt, Catalytic partial oxidation of natural gas to syngas, Fuel Processing Technology 42 (1995) 109.

4. L. D. Pfefferle and W. C. Pfefferle, Catalysis in combustion, Catal. Rev.- Sci. Eng. 29 (1987) 219.

5. L. D. Pfefferle, Heterogeneous/ homogeneous reactions and transport coupling for catalytic combustion systems: a review of model alternatives, Catalysis Today 26 (1995) 255.

6. X. Song, W. R.Williams, L. D. Schmidt and R. Aris, Bifurcation Behavior in Homogeneous-Heterogeneous Combustion: II. Computations for Stagnation-Point Flow, Combustion and Flame 84 (1991) 292.

7. X. Song, L. D. Schmidt and R. Aris, Steady States and Oscillations in Homogeneous-Heterogeneous Reaction Systems, Chem. Eng. Sci. 46 (1991) 1203.

8. X. Song, L. D. Schmidt and R. Aris,The ignition criteria for Stagnation-point flow: Semenov-Frank-Kamenetski or van't Hoff, Combust. Sci. Technol. 75 (1991).

9. D. G. Vlachos, L. D. Schmidt and R. Aris, Ignition and Extinction of Flames near Surfaces: combustion of CH_4 in air, AIChE J 40 (1994) 1005.

10. G. L. Landi, A. Di Benedetto, P. S. Barbato, G. Russo and V. Di Sarli, Transient Behavior of Structured $LaMnO_3$ catalyst during methane combustion at high pressure, Chem. Eng. Sci. 116 (2014) 350.

11. S. Karagiannidis and J. Mantzaras, Numerical Investigation on the start-up of methane fueled catalytic microreactors, Comb. Flame 157 (2010) 1400.

12. O. Deutschmann, F. Behrendt and J. Warnatz, Formal treatment of catalytic conversion and combustion of methane, Catal. Today 46 (1998) 155.

13. O. Deutschmann and L. D. Schmidt, Modeling the partial oxidation of methane in a short-contact-time reactor, AiChE J 44 (1998) 2465.

14. R. Quiceno, J. Perez-Ramirez, J. Warnatz and O. Deutschmann, Modeling the high temperature catalytic partial oxidation of methane over platinum gauze: Detailed gas-phase and surface chemistries coupled with 3D flow field simulations, Applied Catal. A: general 303 (2006) 166.

15. S. Karagiannidis, J. Mantzaras, G. Jackson and K. Boulouchos, Hetero-/ homogeneous combustion and stability maps in methane-fueled catalytic microreactors, Proceedings of the Combustion Institute 31 (2007) 3309.

16. S. Karagiannidis, J. Mantzaras and K. Boulouchos, Stability of hetero-/ homogeneous combustion in propane and methane-fueled catalytic microreactors:

Channel confinement and molecular transport efffects, Proceedings of the Combustion Institute 33 (2011) 3241.

17. G. Pizza, J. Mantzaras, C. E. Frouzakis, A. G. Tomboulides and K. Boulouchos, Suppression of combustion instabilities of premixed hydrogen/air flames in microchannels using heterogeneous reactions, Proceedings of the Combustion Institute 32 (2009) 3051.

18. G. Pizza, J. Mantzaras, C. E. Frouzakis, Flame dynamics in catalytic and non-catalytic mesoscale microreactors, Catalysis Today 155 (2010) 123.

19. G. Stefanidis and D. G. Vlachos, Controlling homogeneous chemistry in homogeneous-heterogeneous reactors: Application to propane combustion, Ind. Eng. Chem. Res. 48 (2009) 5962.

20. S. Chattopadhyay and G. Veser, Heterogeneous-homogeneous interactions in catalytic microchannel reactors, AIChE J. 52 (2006) 6.

21. C. Van Heerden, Autothermic processes. Industrial & Engineering Chemistry, 45(1953), 1242-1247.

22. O. Bilous & N. R. Amundson, Chemical reactor stability and sensitivity. AIChE Journal (1955)., 1(4), 513-521.

23. R. Aris, The mathematical theory of diffusion and reaction in permeable catalyts, volumes 1 and 2 (1975), Oxford University Press, London.

24. R. A. Schmitz, Multiplicity, stability, and sensitivity of states in chemically reacting systems—a review (1975) 156-211.

25. V. Hlaváček & P. van Rompay, Current problems of multiplicity, stability and sensitivity of states in chemically reacting systems. Chemical Engineering Science, 36 (1981), 1587-1597.

26. V. Hlaváček, Dynamics of nonlinear systems. CRC Press; 1986.

27. D. Luss, Steady-State Multiplicity Features of Chemically Reacting Systems. Chemical Engineering Education (1986), 20(1).

28. M. Kubicek & M. Marek, Computational methods in bifurcation theory and dissipative structures (2012), Springer Science & Business Media.

29. M. Marek & I. Schreiber, Chaotic behaviour of deterministic dissipative systems(1995), Cambridge University Press.

30. E. L. Allgower & K. Georg, Numerical continuation methods: an introduction (2012), Springer Science & Business Media.

31. A. Uppal, W. H. Ray & A. B. Poore, On the dynamic behavior of continuous stirred tank reactors, Chemical Engineering Science, 29 (1974), 967-985.

32. V. Balakotaiah & D. Luss, Structure of the steady-state solutions of lumped-parameter chemically reacting systems. Chemical Engineering Science, 37 (1982), 1611-1623.

33. V. Balakotaiah & D. Luss, Multiplicity features of reacting systems: dependence of the steady-states of a CSTR on the residence time. Chemical Engineering Science, 38 (1983), 1709-1721.

34. V. Balakotaiah & D.Luss, Global analysis of the multiplicity features of multi-reaction lumped-parameter systems. Chemical Engineering Science, 39 (1984), 865-881.

35. V. Balakotaiah, D. Luss, & B. L. Keyfitz, Steady state multiplicity analysis of lumped-parameter systems described by a set of algebraic equations. Chemical engineering communications, 36 (1985), 121-147.

36. W. W.Farr & R. Aris, (1986). "Yet who would have thought the old man to have had so much blood in him?"—Reflections on the multiplicity of steady states of the stirred tank reactor. Chemical engineering science, 41(6), 1385-1402.

37. K. F. Jensen & W. H. Ray, The bifurcation behavior of tubular reactors. Chemical Engineering Science, 37 (1982), 199-222.

38. G. Nicolis & I. Prigogine, Self-organization in nonequilibrium systems (1977), Wiley, New York.

39. V. Balakotaiah and D. H. West, Thermal effects and bifurcations in gas phase catalytic partial oxidations, Current Opinions in Chemical Engineering 5 (2014) 68.

40. M. P. Harold & D. Luss, Use of multiplicity features for kinetic modeling: car-

bon monoxide oxidation on platinum/alumina. Industrial & engineering chemistry research, 26 (1987)., 2099-2106.

41. S. V. Sotirchos, & N. R. Amundson, Diffusion and reaction in a char particle and in the surrounding gas phase. A continuous model. Industrial & engineering chemistry fundamentals, 23 (1984), 191-201.

42. S. V. Sotirchos & N. R. Amundsen, Diffusion and reaction in a char particle and in the surrounding gas phase. Two limiting models. Industrial & engineering chemistry fundamentals, 23 (1984), 180-191.

43. P. H. Nielsen & J. Villadsen, An analysis of the multiplicity pattern of models for simultaneous diffusion, chemical reaction and absorption. Chemical engineering science, 40 (1985)., 571-587.

44. M. Golubitsky and D.G. Schaeffer, Singularities and Groups in Bifurcation Theory, Vol. 1 (1985), Springer-Verlag.

45. G. Veser, M. Ziauddin, and L. D. Schmidt, Ignition in alkane oxidation on noble-metal catalysts, Catalysis Today 47 (1999) 219.

46. O. Deutschmann, and L. D. Schmidt, Modeling the partial oxidation of methane in a short-contact-time reactor, AIChE Journal 44 (1998) 2465.

47. D. K. Zerkle, M. D. Allendorf, M. Wolf and O. Deutschmann, Understanding homogeneous and heterogeneous contributions to the platinum-catalyzed partial oxidation of ethane in a short-contact-time reactor, Journal of Catalysis, 196 (2000) 18.

48. A. Di Benedetto, G. Landi, V. Di Sarli, P.S.Barbato, R. Pirone and G. Russo, Methane catalytic combustion under pressure, Catalysis Today 197 (2012) 206.

49. P.S. Barbato, A. Di Benedetto, V. Di Sarli, G. Landi and R.Pirone, High-Pressure Combustion over a Perovskyte catalyst, Ind. Eng. Chem. Res. 51 (2012) 7547.

50. R. E. Hayes and S.T. Kolaczkowski. Introduction to catalytic combustion (1998) CRC Press.

51. I. Alam, D. H. West, V. Balakotaiah, Bifurcation analysis of thermally coupled homogeneous-heterogeneous combustion, Chem. Eng. Journal 280 (2015) 293.

52. V. Balakotaiah, N. Gupta and D. H. West, A simplified model for analyzing catalytic reactions in short monoliths, Chem Eng Sci 55 (2000) 53.

53. N. Gupta and V. Balakotaiah, Bifurcation analysis of a two-dimensional catalytic monolith reactor model, Chem Eng Sci 56 (2000) 4771.

54. D. Bhatia, M. P. Harold and V. Balakotaiah, Kinetic and bifurcation analysis of the cooxidation of CO and H2 in catalytic monolith reactors, Chem Eng Sci 64 (2009) 1544.

55. S. Chakraborty and V. Balakotaiah, Multimode low dimensional models for non-isothermal homogeneous and catalytic reactors, Chem Eng Sci. 64 (2004) 3695.

56. N. Gupta and V. Balakotaiah, Heat and mass transfer coefficients in catalytic monoliths, Chem Eng Sci. 56 (2001) 4771.

57. S. R. Gundlapally and V. Balakotaiah, Heat and mass transfer correlations and bifurcation analysis of catalytic monoliths with developing flows, Chem. Engng. Sci. 66 (2011) 1879.

58. R. Agrawal, D. H.West and V. Balakotaiah, Modeling and Analysis of Local Hot Spot Formation in down-flow adiabatic packed-bed reactors, Chem. Engng. Sci. 62 (2007) 4926.

59. R. R. Ratnakar, M. Bhattacharya and V. Balakotaiah, Reduced order models for describing dispersion and reaction in monoliths, Chem. Engng. Sci. 83 (2012) 77.

60. V. Balakotaiah, Structural stability of nonlinear convection-reaction models, Chem Eng Edu, fall issue (1996).

61. S.M.S. Dometti and V. Balakotaiah, On the limits of validity of effective dispersion for bulk reactions, Chem. Engng. Sci. 55 (2000) 6169.

62. N. Gupta, V. Balakotaiah and D. H. West, Transport limited patterns in catalytic reactors, Chem Eng Sci 57 (2002) 435.

63. C. K. Wesbrook and F.L. Dryer, Chemical kinetic modeling of hydrocarbon combustion, Combust. Sci. Tech. 27 (1981) 31.

64. L. Hiam, H. Wise and S. Chaikin, Catalytic oxidation of hydrocarbons on platinum, J. Catal. 10 (1968) 272.

65. I. A. Zeldovich, G. I. Barenblatt and V. B. Librovich, The mathematical theory of combustion and explosions, Consultants Bureau, New York (1985).

66. K. Ramanathan, V. Balakotaiah and D. H. West, Light-off criterion and transient analysis of catalytic monoliths, Chem Eng Sci 58 (2003) 1381.

67. V. Balakotaiah, D. Kodra, and D. Nguyen, Runaway limits for homogeneous and catalytic reactors. Chem. Eng. Sci. 50 (1995) 1149

68. X. Zheng and J. Mantzaras, An analytical and numerical investigation of hetero-/homogeneous combustion with deficient reactatnts having larger than unity Lewis numbers, Combustion and Flame 161 (2014) 1911.

69. P. T. Coffee, On simplified reaction mechanisms by oxidation of hydrocarbon fuels in flames by C.K. Westbrook and F.L. Dryer, Combust. Sci. Tech. 43 (1985) 333.

70. A. Di Benedetto, G. Landi, V. Di Sarli, P.S.Barabato, R. Pirone and G. Russo, Methane catalytic combustion under pressure, Catalysis Today 197 (2012) 206.

71. P.S. Barabato, A. Di Benedetto, V. Di Sarli, G. Landi and R.Pirone, High-Pressure Combustion over a Perovskyte catalyst, Ind. Eng. Chem. Res. 51 (2012) 7547.

72. C. N. Satterfield, H. Resnick, and R. L. Wentworth, Simultaneous heat and

mass transfer in a diffusion-controlled chemical reaction - Part I: Studies in a tubular reactor, Chem. Eng. Prog., 50, (1954) 460-466.

73. L. L. Hegedus, Temperature Excursions in Catalytic Monoliths, AIChE J. 21(1975) 849.

74. L. D. Pfefferle, and W. C. Pfefferle, Catalysis in combustion, Catalysis Reviews Science and Engineering, 29 (1987) 219.

75. P.A. Bui, D.G. Vlachos, P.R. Westmoreland, Homogeneous ignition of hydrogen/air mixtures over platinum, Proc Combust Inst 26 (1996) 1763.

76. M. Lovo and V. Balakotaiah, Multiplicity features of adiabatic autothermal reactors, AIChE J. 38 (1992) 101.

77. I. Schoegl and J. L. Ellzey, Superadiabatic combustion in conducting tubes and heat exchangers of finite length, Combustion and Flame 151(2007) 142.

78. L. A. Segel, J. L. Jackson, Dissipative structure: An explanation and an ecological example, Journal of Theoretical Biology 37 (1972) 545.

79. F. Muzika and I. Schreiber, Control of Turing patterns and their usage as sensors, memory arrays, and logic gates, The Journal of chemical physics 139 (2013) 164108.

80. H. Ševčíková, I. Schreiber and M. Marek, Dynamics of oxidation Belousov-Zhabotinsky waves in an electric field, The Journal of Physical Chemistry 100 (1996) 19153.

81. T. Trávníčková, M. Kohout, I. Schreiber and M. Kubíček, Front waves and complex spatiotemporal patterns in a reaction-diffusion-convection system with thermokinetic autocatalysis. Chaos 19 (2009), 043125.

82. A. Gupta and S. Chakraborty, Linear stability analysis of high-and low-dimensional models for describing mixing-limited pattern formation in homogeneous autocatalytic reactors, Chem. Eng. Journal 145 (2009) 399.

83. O. Hadač, M. Kohout, J. Havlica, I. Schreiber, Oscillations and patterns in a model of simultaneous CO and C_2H_2 oxidation and NO_x reduction in a cross-flow reactor, Physical Chemistry Chemical Physics, 17(2015), 6458.

Appendix

Analysis of the peak temperature using the Short Channel model

In this appendix, we analyze the peak temperature for the case of infinitely fast catalytic reaction using the short channel model. We start with equations eqs.(5.67)-(5.69) where eqn (5.70) replaced by the conditions for infinitely fast catalytic reaction: eqs.(5.77)-(5.78). We can solve for c to obtain $c = \frac{P}{\psi^2}\left(1 - \frac{\cosh(\psi y)}{\cosh(\psi)}\right)$, where $\psi = \sqrt{P + \phi^2}$. Now θ must satisfy

$$\begin{aligned} \frac{d^2\theta}{dy^2} - \frac{P}{Le_f}\theta &= -\frac{\phi^2}{Le_f}\frac{P}{\psi^2}\left(1 - \frac{\cosh(\psi y)}{\cosh(\psi)}\right),\ 0 < y < 1 \\ \text{with } \frac{d\theta}{dy} &= 0 \text{ at } y = 0 \\ \text{and } \frac{d\theta}{dy} &= \frac{P}{Le_f}\frac{\tanh(\psi)}{\psi} \text{ at } y = 1. \end{aligned}$$

From this equation we obtain

$$\theta = \sqrt{\frac{P}{Le_f}}\frac{\tanh(\psi)}{\psi}\frac{\cosh\left(\sqrt{\frac{P}{Le_f}}y\right)}{\sinh\sqrt{\frac{P}{Le_f}}}\left(1 - \frac{\phi^2}{\psi^2 - \frac{P}{Le_f}}\right) + \frac{\phi^2}{\psi^2} + \frac{P}{Le_f}\frac{\phi^2}{\psi^2}\frac{\cosh(\psi y)}{\cosh(\psi)\left(\psi^2 - \frac{P}{Le_f}\right)}. \tag{8.1}$$

When $Le_f > 1$, θ is an increasing function of y, attaining its maximum at $y = 1$. Thus, to prove boundedness of solution it is sufficient to consider only the wall temperature, $\theta(1)$. It is given by

$$\theta(1) = \frac{\phi^2}{\phi^2 + P\left(1 - \frac{1}{Le_f}\right)} + \sqrt{\frac{P}{Le_f}}\left(\frac{P\left(1 - \frac{1}{Le_f}\right)}{\phi^2 + P\left(1 - \frac{1}{Le_f}\right)}\right)\frac{\tanh\left(\sqrt{P + \phi^2}\right)}{\sqrt{P + \phi^2}}\coth\left(\sqrt{\frac{P}{Le_f}}\right). \tag{8.2}$$

For transparency of the ensuing proof, let us define $\lambda := \sqrt{\frac{P}{Le_f}}$. Then we can express $\theta(1)$ as

$$\theta(1) = \frac{\lambda}{\psi}\frac{\tanh\psi}{\tanh\lambda} + \frac{\phi^2}{\psi^2 - \lambda^2}\left(1 - \frac{\lambda}{\psi}\frac{\tanh\psi}{\tanh\lambda}\right). \tag{8.3}$$

When $P = 0$, $\theta(1) = 1$. For $P > 0$ and $Le_f > 1, \psi^2 - \lambda^2 = \phi^2 + P\left(1 - \frac{1}{Le_f}\right) > \phi^2$, i.e. $\frac{\phi^2}{\psi^2 - \lambda^2} < 1$. Thus

$$\theta(1) < \frac{\lambda}{\psi}\frac{\tanh\psi}{\tanh\lambda} + 1.\left(1 - \frac{\lambda}{\psi}\frac{\tanh\psi}{\tanh\lambda}\right) = 1. \tag{8.4}$$

Thus, θ is always bounded by 1 for $Le_f > 1$ and in this case, the actual temperature never exceeds the adiabatic value.